AL/AO-TR-1995-0051

ARMSTRONG LABORATORY

DEVELOPMENT OF A TUNABLE MODE-LOCKED TITANIUM SAPPHIRE LASER

Odis P. McDuff

Electrical Engineering Department
The University of Alabama
Tuscaloosa, Alabama 35487

AEROSPACE MEDICINE DIRECTORATE
CLINICAL SCIENCES DIVISION
OPHTHALMOLOGY BRANCH
2507 Kennedy Circle
Brooks Air Force Base, TX 78235-5117

November 1995

Final Technical Report for period October 1989 – October 1992

Approved for public release; distribution is unlimited.

AIR FORCE MATERIEL COMMAND
BROOKS AIR FORCE BASE, TEXAS

NOTICES

When Government drawings, specifications, or other data are used for any purpose other than in connection with a definitely Government-related procurement, the United States Government incurs no responsibility or any obligation whatsoever. The fact that the Government may have formulated or in any way supplied the said drawings, specifications, or other data, is not to be regarded by implication, or otherwise in any manner construed, as licensing the holder, or any other person or corporation; or as conveying any rights or permission to manufacture, use, or sell any patented invention that may in any way be related thereto.

The Office of Public Affairs has reviewed this technical report, and it is releasable to the National Technical Information Service, where it will be available to the general public, including foreign nationals.

This technical report has been reviewed and is approved for publication.

John Taboada

JOHN TABOADA, Ph.D.
Contract Monitor

Joe E Burton

JOE EDWARD BURTON, Colonel, USAF, MC, CFS
Chief, Clinical Sciences Division

REPORT DOCUMENTATION PAGE

Form Approved
OMB No. 0704-0188

1. AGENCY USE ONLY (Leave blank)	2. REPORT DATE	3. REPORT TYPE AND DATES COVERED
	November 1995	Final Report–October 1989–October 1992

4. TITLE AND SUBTITLE
Development of a Tunable Mode-Locked Titanium Sapphire Laser

5. FUNDING NUMBERS
PE – 62202F
PR – 7755
TA – 24
WU – 21

6. AUTHOR(S)
Odis P. McDuff

7. PERFORMING ORGANIZATION NAME(S) AND ADDRESS(ES)
Electrical Engineering Department
The University of Alabama
Tuscaloosa, Alabama 35487

8. PERFORMING ORGANIZATION REPORT NUMBER

9. SPONSORING/MONITORING AGENCY NAMES(S) AND ADDRESS(ES)
Armstrong Laboratory (AFMC)
Aerospace Medicine Directorate
Clinical Sciences Division, Ophthalmology Branch
2507 Kennedy Circle
Brooks Air Force Base, TX 78235-5117

10. SPONSORING/MONITORING AGENCY REPORT NUMBER
AL/AO-TR-1995-0051

11. SUPPLEMENTARY NOTES
Armstrong Laboratory Technical Monitor: Dr. John Taboada, (210) 536-2857

12a. DISTRIBUTION/AVAILABILITY STATEMENT
Approved for public release; distribution is unlimited.

12b. DISTRIBUTION CODE

13. ABSTRACT (Maximum 200 words)

The objective of this project was to develop, fabricate, and deliver a computer-controlled acousto-optically mode locked Titanium Sapphire laser for the Vision Biophysics Function of the Clinical Sciences Division of the USAF School of Aerospace Medicine (USAFSAM). The mode-locking pulse rate was to be synchronized to the pulse rate of a Nd:YAG mode-locked laser at the Vision Function. The frequency-doubled output of the USAFSAM Nd:YAG laser is to serve as a pump for the Titanium Sapphire laser.

14. SUBJECT TERMS
Fiber-Optic
Medical Imaging
Nd-Yag Laser
Picosecond

15. NUMBER OF PAGES
132

16. PRICE CODE

17. SECURITY CLASSIFICATION OF REPORT	18. SECURITY CLASSIFICATION OF THIS PAGE	19. SECURITY CLASSIFICATION OF ABSTRACT	20. LIMITATION OF ABSTRACT
Unclassified	Unclassified	Unclassified	UL

NSN 7540-01-280-5500

Standard Form 298 (Rev. 2-89)
Prescribed by ANSI Std. Z39-18
298-102

Table of Contents

List of Tables

List of Figures

Page

Page

Development of a Tunable Mode-Locked Titanium Sapphire Laser

Final Technical Report
Subcontract No. B-10-A08-S1

by Odis P. McDuff
Professor of Electrical Engineering
The University of Alabama

Subcontract Director

I. Introduction

The objective of this project was to develop, fabricate, and deliver a computer-controlled acousto-optically mode locked Titanium Sapphire laser for the Vision Biophysics Function of the Clinical Sciences Division of the USAF School of Aerospace Medicine (USAFSAM). The mode-locking pulse rate was to be synchronized to the pulse rate of a Nd:YAG mode-locked laser at the Vision Function. The frequency-doubled output of the USAFSAM Nd:YAG laser is to serve as a pump for the Titanium Sapphire laser.

The first step of the work was to make analyses of the transient effects of the Q-switched mode-locked pumping. This involved some computer generated curves of the inversion buildup in the Titanium Sapphire. Gain analyses were made to determine the interrelationships of cavity loss, output coupling, and pumping level. The purpose was to determine, first of all, the desired Titanium Sapphire crystal parameters, so that optimum performance could be obtained with the pump available at the USAF School of Aerospace Medicine. The starting point for this gain analysis was the work of Alfrey (Reference 1). The initial

analyses assumed low level pumping and considered threshold problems. These were then extended to high level pumping. Optimum operating points were obtained and then the mode-locked performance calculated using the previously developed techniques of the Principal Investigator, et.al. (References 2, 3).

The next step in the work was to select the cavity configuration, analyze its performance dependence upon the various parameters, and to select the design parameters. This involved a classic stability analysis of a folded, tightly focused, astignatically compensated, longitudinally pumped cavity. The cavity was then constructed and experimentally optimized. The cavity components included purchased items within the contract budget and items furnished by the School of Aerospace Medicine.

II. Effective Pumping Level with Mode-Locked Pump

The pump will consist of bursts of mode-locked pulses, each burst occuring during the Q-switched pulse. Since the effective upper level lifetime of the laser transition in Titanium Sapphire is rather long, with a generally accepted figure of 3.2 μs, the response of the population to the time varying pump is of fundamental importance.

A. Before Laser Oscillation Starts

We first look at the build up of the population inversion immediately after a burst of mode-locked pump pulses is applied, and before the titanium sapphire laser

reaches threshold. As shown in Figure 1, at the beginning of a mode-locked pump pulse, the population increases exponentially with a time constant τ, the lifetime of the laser transition upper level.* In Figure 1 t_m^{-1} is the repetition rate of the mode-locked pump, i.e.

$$t_m = \frac{2L}{c} , \tag{1}$$

t_{ps} is the width of the pump mode-locked pulse, and n is the normalized population inversion

$$n = \frac{N}{N_p} . \tag{2}$$

In equation (2) N_p is the peak inversion toward which N is headed,

$$N_p = R\tau , \tag{3}$$

where R is the peak pump rate and τ is the upper level lifetime, τ = 3.2 μs. In the case of the USAFSAM pump, L = 1 m and hence t_m = 6.67 ns. Also, the value of t_{ps} is $\approx$ 100 ps. The population grows exponentially toward n=1 while the mode-locked pump pulse is present,

$$n = n_i + (1-n_i)(1-e^{-t/\tau}) . \tag{4}$$

* The numbered figures appear at the end of the report.

During the interval t_{ps} this grows to the value

$$n\Big|_{t_{ps}} = n_i + (1-n_i)(1-e^{-t_{ps}/\tau}) \quad . \qquad (5)$$

Then while the mode-locked pump pulse is absent, the inversion decays toward zero according to

$$n = n\Big|_{t_{ps}} e^{-t/\tau} \qquad (6)$$

which stops when the next mode-locked pump pulse arrives. We call this value n_i'

$$n_i' = n\Big|_{t_{ps}} e^{-\frac{t_m - t_{ps}}{\tau}} \qquad (7)$$

or, substituting equation (5),

$$n_i' = [n_i + (1-n_i)(1-e^{-t_{ps}/\tau}] \; e^{-\frac{t_m - t_{ps}}{\tau}} \quad . \qquad (8)$$

Equation (8) was plotted using the computer, plotting n_N, the inversion at the end of N cycles of the mode-locked pump, versus N. The result is shown in Figure 2. The apparent exponential growth of this curve led to additional investigation of the solution of equation (8).

If we identify as follows:

$$A = e^{-t_m/\tau}$$

$$B = e^{t_{ps}/\tau} \qquad (9)$$

$$C = A(B-1) \ ,$$

Then equation (8) is of the form

$$n_i' = A\, n_i + C \ , \qquad (10)$$

or in other words we have a difference equation of the form

$$n_{N+1} = A\, n_N + C \ . \qquad (11)$$

This equation has a solution

$$n_N = C \sum_{p=0}^{p=N-1} A^p \qquad (12)$$

If the growth is permitted to continue, as N --> ∞ we reach a steady state value

$$n_\infty = C \sum_{p=0}^{\infty} A^p \qquad (13)$$

which has a known sum

$$n_\infty = \frac{C}{1-A} \quad . \tag{14}$$

Substituting the values of A, B, and C

$$n_\infty = \frac{e^{-t_m/\tau}\ (e^{t_{ps}/\tau}-1)}{1 - e^{-t_m/\tau}} \quad , \tag{15}$$

or considering the relative magnitudes of t_m, t_{ps}, τ, we have

$$\begin{aligned} n_\infty &\approx \frac{t_{ps}}{t_m}\ (1 - t_m/\tau) \\ &\approx \frac{t_{ps}}{t_m} \quad . \end{aligned} \tag{16}$$

or

$$N_\infty = \frac{t_{ps}}{t_m}\ N_p \quad . \tag{17}$$

The effective population is equal to the average of the mode-locked pulsed variation of population that we would have had if the inversion could have followed the pump pulsation.

This means that the population does not respond to the mode-locked variation in pump pulses because $\tau >> t_{ps}$ and $\tau >> t_m$.

Continuing, equation (12) can be summed for any value N, to give

$$n_N = \frac{C(1-A^N)}{1-A} \tag{18}$$

which gives, when we substitute the values of A, B, C,

$$n_N = n_\infty \left(1 - e^{\frac{-t_m N}{\tau}}\right) . \tag{19}$$

But, since $N = t/t_m$, we have

$$n_N = n_\infty \left(1 - e^{-t/\tau}\right) . \tag{20}$$

We are sampling the population at the beginning of each mode-locked pump pulse, and we have a classic exponential growth with time constant τ. However, instead of growing to the peak of the mode-locked pulses, it grows to the average. This is shown qualitatively below.

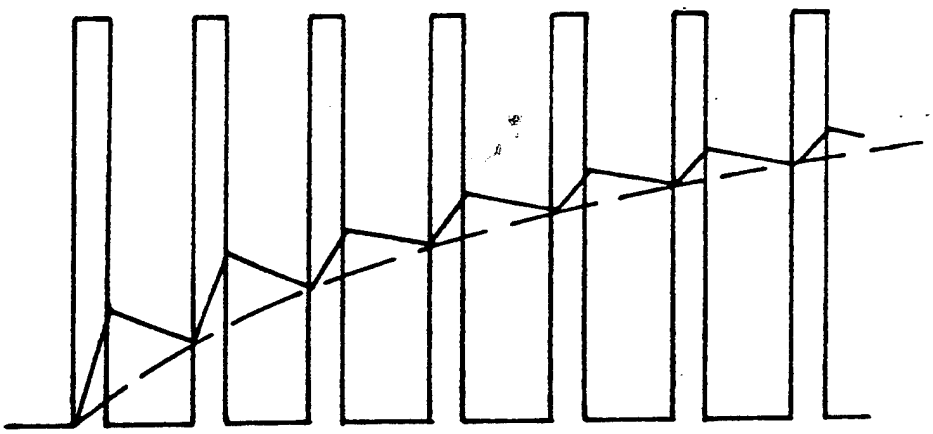

From the computer plot in Figure 2 we get by graphical construction a time constant of $\approx$ 3.2 μs, the value of τ.

Since the gain is directly proportional to the inversion N, the gain follows the same type curve as it rises to meet the loss threshold during the Q-switched pulse. For a given peak pumping level and hence effective (average) pump, the time for the laser to begin oscillating can be determined. If the Q-switched pump pulse is not long enough for the population to reach threshold, for a given peak and hence average value, oscillation will never start.

In a paper on synchronous mode locking of titanium sapphire (Reference 4), the authors said oscillation started ≈ 100 ns after the Q-switched pulse started. In the curve in Figure 2 that would correspond to N = 100/6.7 = 15. At that point

$$n_N\Big|_{N=15} = n_\infty(1 - e^{-t/\tau}) \qquad (21)$$

$$= 0.031\ n_\infty\ ,$$

or the threshold was at 0.031 of the average of the mode-locked unsaturated gain. The pump energy was ≈ 6 mJ per Q-switched pump pulse and the Q-switch pulse width was ≈175ns. This would give an <u>average</u> (averaged over the mode-locked pump pulses) pump power level during the Q-switched pulse of ≈ 34 KW. If we say this power level would have given an average gain exponent (unsaturated) of 25, then the threshold gain was (0.031)(25) = 0.775 or ≈ 77.5% round-trip

gain at threshold. This means the total round trip loss was $\approx 77.5\%$.

As stated above, our concern will be that we reach oscillation threshold during the Q-switched pump pulse.

B. Effect of Oscillation

Now, to obtain the actual inversion level while the titanium-sapphire laser is oscillating, we must include the effect of photon density upon the effective lifetime or time constant of the growth.

For the sake of simplicity, let us say that the titanium sapphire laser is lasing with "perfect" mode locked pulses (here, we are saying rectangular pulses are "perfect") which are occuring exactly at the same time that the pump pulses are present. We note that this exact synchronism of pulse presence is <u>not necessary</u> as far as the titanium sapphire laser is concerned, if the laser is being actively locked with a mode locker. We also say for simplicity that the width of the titanium-sapphire laser mode-locked pulse is the same as the pump mode-locked pulse.

The effect will be simply that the effective laser lifetime during the perfect pulse will be reduced to the value (see any standard laser text)

$$\frac{1}{\tau_{eff}} = \frac{1}{\tau}\,(1 + I_U/I_S) \qquad (22)$$

where I_ν is the peak intensity of the laser pulse and I_s is the saturation intensity of titanium-sapphire (which is $\approx 2.6 \times 10^9$ W/m^2). Then, we get a modified version of equation (8) which has τ_{eff} during the build-up but still has τ during the decay, i.e.

$$n_i' = [n_i + (1-n_i)(1-e^{-t_{ps}/\tau_{eff}})]\, e^{-\frac{(t_m-t_{ps})}{\tau}} \quad . \quad (23)$$

We can't use equation (23) for the build-up to threshold but we can use it to get the variation at steady-state oscillation, saying we already have reached steady state during the Q-switched pulse. A sketch is below.

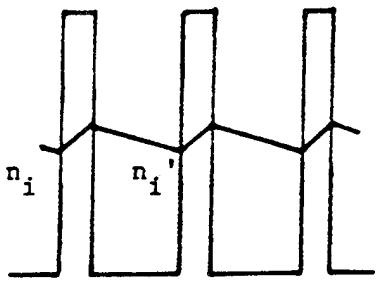

at steady state $n_i = n_i'$

After manipulation, equation (23) gives

$$n = n_\infty \frac{1}{1 + n_\infty \frac{I_\nu}{I_s}} \quad (24)$$

where n_∞ is as defined previously in equations (16).

Thus, the saturated n is given by

$$n_{saturated} = \frac{t_{ps}}{t_m} \frac{1}{1 + \frac{t_{ps}}{t_m} \frac{I_v}{I_s}} \tag{25}$$

This says simply that the average intensity $(t_{ps}/t_m)\ I_v$ is what is effective in producing the average saturation (remember I_v is the peak intensity of the mode-locked laser pulse). If the laser were oscillating "cw" during the Q-switched pulse, one would get simply

$$n = \frac{1}{1 + I_v/I_s} \quad . \tag{26}$$

III. Effective Pumping Level -- Q-Switched Pump

Now we consider the build up of the inversion during the Q-switched pulse. In Figure 3 we see the pertinent parameters labeled.

The same type of equation applies here as in the consideration of the mode-locking effects,

$$n'_{Ni} = [n_{Ni} + (n_p - n_{Ni})(1 - e^{-\tau_p/\tau})]\ e^{-\frac{(t_q - \tau_p)}{\tau}} \quad . \tag{27}$$

With the numbers $\tau_p \approx 100$ ns, $t_q \approx 0.5$ ms, $\tau \approx 3.2\ \mu$s, we get a steady state value

$$(n'_{Ni})_{ss} \approx 0 \ . \tag{28}$$

This simply means that the inversion dies away to ≈ 0 between the Q-switched pump pulses.

Then we simply ask, if $n_{Ni} = 0$, what is the value of n_{Nf}? We have

$$n_{Nf} = n_\infty(1-e^{-\tau p/\tau}) \approx \frac{\tau p}{\tau} n_\infty \ . \tag{29}$$

Now from the Q-switching effect itself, the average of the Q-switched population inversion pulses is

$$n_{avg} = \frac{\tau p}{t_q} (n_\infty) \tag{30}$$

(this is the average inversion if there were no transient effects, i.e. the system could follow the pump perfectly). Thus we have

$$n_{Nf} = \frac{\tau p}{\tau} \frac{\tau q}{\tau p} n_{avg} \ . \tag{31}$$

With the numbers used above,

$$n_{Nf} = (156) \ n_{avg} \ , \tag{32}$$

or the effective pumping level at the trailing edge of the Q-switched pulse is

$$P_f = 156\ P_{avg} \cdot \qquad (33)$$

The sketch below shows the results of these assumed numbers, saying P_{avg} = 400 mw.

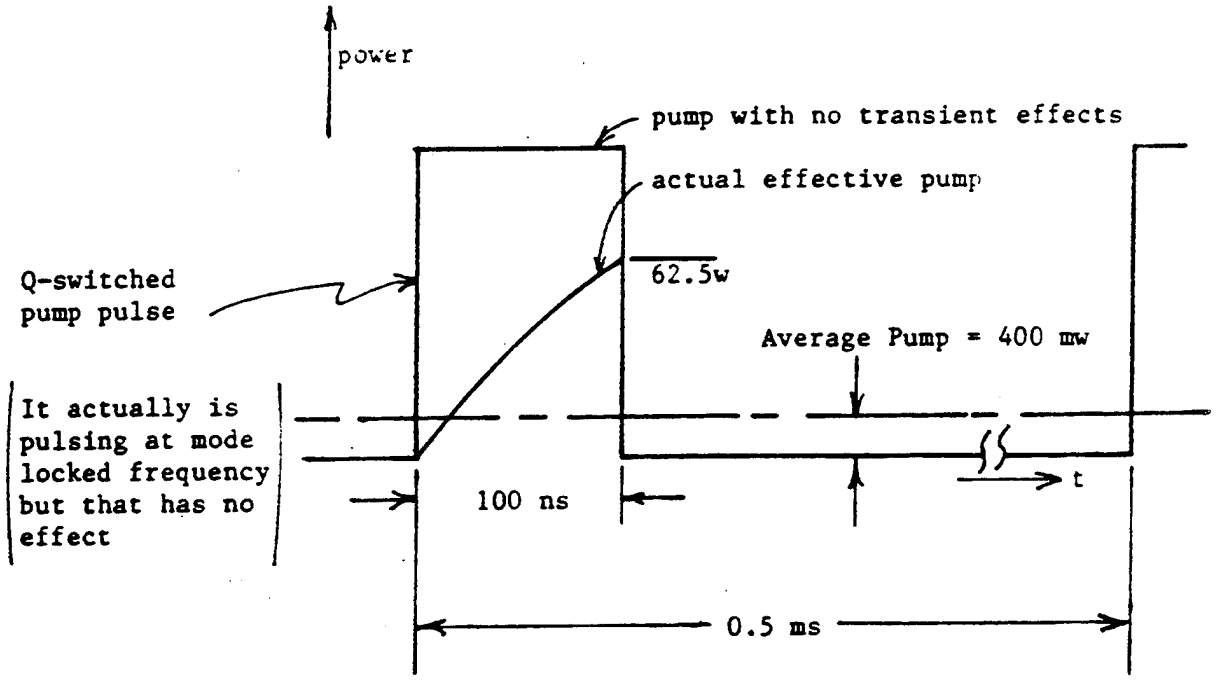

As will be seen from the work in the following sections, a reasonable cw pump power at threshold might be as low as 1-2 watts, although most of the results reported in the literature give somewhat higher pump power thresholds.

IV. Gain Considerations -- Threshold and Power Output

In this section we will consider the inter-relationships of the cavity loss, pumping level, and laser crystal parameters.

A. Basic Equations for the Low Gain/Low Loss Case

The analysis is somewhat simpler if the gains and losses involved are small enough that exponentials can be approximated by

$$e^G \approx 1 + G \ . \tag{34}$$

In this case

$$\text{Percent Gain} = \left(\frac{I_{out} - I_{in}}{I_{in}}\right) 100$$

$$= (e^G - 1)\ 100$$

$$\approx (G)(100) \ , \tag{35}$$

or the gain exponent is approximately the percent gain. This approximation is good for gains (losses) up to ≈ 35%.

The analysis of a Titanium Sapphire laser is somewhat different from many lasers because the laser crystal itself has absorption at the lasing frequency which may be non-negligible. This is expressed in terms of the figure of merit (FOM) of the crystal

$$\text{FOM} = \frac{\alpha_{pump}}{\alpha_{laser}} \ . \tag{36}$$

In this work we will assume that the pump is at doubled Nd:YAG output (530 nm) and will assume that the laser is at

800 nm. Thus the commonly published values of FOM will be closely applicable to our analysis.

An expression for the unsaturated (small signal) gain coefficient of a Titanium Sapphire crystal (round trip) is given by Alfrey (Reference 1) with some modification here as

$$g_o = \frac{2\ P_p}{\pi\ W^2}\ \frac{\lambda_p}{\lambda}\ \frac{1}{I_s}\ (1 - e^{-\alpha_m d})\ , \qquad (37)$$

where

P_p = pump power

W = radius of pump Gaussian beam

λ_p = pump wavelength (taken as 530 nm)

λ = lasing wavelength (taken as 800 nm)

α_m = crystal absorption coefficient at λ_p

d = length of laser crystal .

This equation gives the gain coefficient at a point in the crystal. The equation can be used over the whole length of the crystal without integration if the crystal is not too long compared to the confocal length of the pump beam (i.e. the spot sizes do not change significantly throughout the gain medium).

In addition the round trip loss coefficient in the laser is given by

$$\text{Loss} = T + L_i + \frac{\alpha_m d}{\text{FOM}/2} \qquad (38)$$

where L_i is the round trip loss coefficient for cavity losses other than the laser crystal and output coupler, T is the fractional transmission of the output mirror, and $(\alpha_m d)/(FOM/2)$ is the round trip loss in the crystal at the laser frequency.

If $T > \approx 0.35$, then we must use $-\ell n(1-T)$ in the equation (38) instead of T, because then the small gain/small loss approximation becomes innacurate.

The pump threshold is obtained by setting the small signal gain g_o equal to the loss,

$$g_o = \text{Loss}$$

which gives the pump threshold

$$P_{th} = \frac{\pi W^2}{2} \frac{\lambda}{\lambda_p} I_s \frac{(T + L_i + \frac{\alpha_m d}{FOM/2}}{1 - e^{-\alpha_m d}} . \qquad (39)$$

When the pump power is greater than P_{th}, the power output is determined by solving for that power level that saturates the gain to where it is equal to loss. This gives a cavity power

$$P_C = \frac{1}{2} \frac{\lambda_p}{\lambda} P_p(1 - e^{-\alpha_m d}) \frac{1}{T + L_i + \frac{\alpha_m d}{FOM/2}} - \frac{\pi W^2 I_s}{4} . \qquad (40)$$

Then the laser power output is

$$P_{out} = T\, P_c \tag{41}$$

which gives

$$P_{out} = \frac{1}{2}\frac{\lambda_p}{\lambda} P_p(1 - e^{-\alpha_m d}) \frac{T}{T + L_i + \frac{\alpha_m d}{FOM/2}} - \frac{\pi W^2}{4} I_s T. \tag{42}$$

The pump threshold power of equation (39) makes the $P_{out} = 0$.

Since the crystal absorption appears both in the numerator (pumping efficiency) and in the denominator (cavity efficiency) of equation (42), it is not immediately obvious what would be the desired value of crystal $\alpha_m d$.

B. Pump Threshold--Low Gain/Low Loss Case

If the pump level is going to be a possible limiting factor, we need to look at the expected pump threshold and the effects of the laser-rod losses upon that threshold value.

Alfrey says that $W \approx 25\text{-}50\ \mu m$ is the smallest that one can expect to have and maintain alignment of the pump and laser beams. Since several parameters are involved in the determination of pump threshold, it is desirable to present several curves showing the effects of the parameters.

Figures 4-9 show plots of P_{th} versus $\alpha_m d$ with the static cavity loss $T + L_i$ as a parameter. Curves are plotted at W = 50 μm and at FOM = 100, 200, 300 and at W = 25 μm with the same values of FOM. The losses $T + L_i$ are "small", as would be appropriate if one is seeking to have a low pump threshold power. A somewhat gradual dependence of P_{th} upon $\alpha_m d$, other conditions the same, is noted. Also, the range of P_{th} in the various curves is from less than 100 mw to slightly less than 600 mw. Most of the published work has been at higher loss cavities and pump threshold powers have been higher than these values.

The value of $\alpha_m d$ that determines the minimum pump power threshold was determined analytically by setting

$$\frac{d\ P_{th}}{d(\alpha_m d)} = 0 \tag{43}$$

and solving for $\alpha_m d$. The resulting equation for $\alpha_m d$ that gives the lowest threshold power is

$$(FOM/2)\ (T + L_i) = e^{\alpha_m d} - 1 - \alpha_m d \tag{44}$$

First, a generalized curve of $\alpha_m d$ for lowest threshold power versus $FOM(T + L_i)$ can be plotted from equation (44). The resulting curve is shown in Figure 10. Curves for $\alpha_m d$ for lowest threshold power are shown versus $T + L_i$ in Figures 11-13 for specific values of FOM.

If equation (44) is substituted back into the pump threshold equation (39), one obtains an equation for pump threshold power at the value $\alpha_m d$ that minimizes threshold,

$$(P_{th})_{\substack{\text{optimum} \\ \alpha_m d}} = \frac{\pi W^2}{FOM} \frac{\lambda}{\lambda_p} I_s e^{\alpha_m d} \qquad (45)$$

Figures 14-19 show the pump power threshold at optimum $\alpha_m d$ versus the cold cavity loss $T + L_i$ at the various combinations of FOM and W used above. This is done by going to Figures 11-13 to get the relationship between $\alpha_m d$ and $T + L_i$.

From the curves shown so far one can select $\alpha_m d$ for given values of cavity loss, FOM, and spot size if pump threshold is the principal criterion. This would be the situation if one barely has enough pump power available.

C. Power Output -- Low Gain/Low Loss Case When $\alpha_m d$ Selected to Minimize P_{th}

If one has available more than marginal pump power, then threshold and slope efficiency determine the power output. The slope efficiency η_s is given by (in fractional form rather than percent)

$$\eta_s = \frac{d\ P_{out}}{d\ P_p}$$

Using equation (42) then, the slope efficiency is given by

$$\eta_s = \frac{1}{2}\frac{\lambda_p}{\lambda}\left(1 - e^{-\alpha_m d}\right)\frac{(FOM/2)(T)}{(FOM/2)(T + L_i) + \alpha_m d} \qquad (46)$$

The slope efficiency was plotted versus cold cavity loss, $T + L_i$, assuming $T = L_i$ and that $\alpha_m d$ was the value that minimized P_{th} at each value of $T + L_i$. Again, the relationship between $\alpha_m d$ and $T + L_i$ comes from the curves of Figures 11-13. The slope efficiency is shown in Figure 20 in generalized form, η_s vs $FOM(T + L_i)$, and then in Figures 21-23 for the specific FOM's used above. Finally, actual power output curves, P_{out} vs P_p, are shown in Figures 24-29 for the various FOM's and spot sizes used above, and with $\alpha_m d$ as a parameter. Again, Figures 24-29 have $T = L_i$ and $T + L_i$ equal to the value that goes with the $\alpha_m d$ for lowest P_{th} (Figures 11-13).

From Figures 24-29, one can determine the value of $\alpha_m d$ that will maximize power output at a given pump level, under the conditions that $T = L_i$ and that $T + L_i$ is at the value giving the lowest threshold for the given $\alpha_m d$.

D. Power Output -- Low Gain/Low Loss Case When Adjusted for Optimum Output Coupling

If the pump level is sufficienty high that reaching threshold is not a problem, then one would be more interested in choosing the coupling T to maximize output power at a given L_i and $\alpha_m d$. The optimum coupling can be found by differentiating the output power expression, equation (42), with respect to T, setting the derivative

equal to zero, and solving for T_{opt}. The result is (for "low" coupling)

$$T_{opt} = -L_i - \frac{\alpha_m d}{FOM/2} + \sqrt{\frac{2}{\pi W^2 I_s}\frac{\lambda_p}{\lambda}(1-e^{-\alpha_m d})(L_i + \frac{\alpha_m d}{FOM/2})P_p} \quad (47)$$

Then the output power at this T_{opt} can be calculated using equation (42). Rather than write an analytical expression for P_{out} at optimum coupling (by combining equations (46) and (47), we simply show the results of various numerical calculations.

Figures 30-32 show the values of T_{opt} under a variety of low level operating conditions having pump power of 400 mw (cw power or the power during a Q-switched pump pulse). Figures 33-35 show the power output at the optimum coupling conditions of Figures 30-32. Figures 36-38 show the values of T_{opt} under a variety of conditions having pump power of 600 mw. Figures 39-41 show the power output corresponding to the optimum coupling in Figures 36-38.

From the figures above one can see what values of $\alpha_m d$ would be preferable at given values of FOM, W, and L_i.

V. Expected Mode-Locked Performance with Low Level Pumping

Using the previously developed techniques of the Principal Investigator, et.al. (References 2,3) which came from earlier work (References 5,6) of the Principal

Investigator and S.E. Harris, the mode-locked performance was studied numerically.

A. The Coupling-Mode Differential Equations

The starting point was the coupled-mode differential equations developed earlier. The symbols in this section will be those used in References 2 and 3. As shown in the references one can express the total electromagnetic field in the laser cavity as a sum of normal mode eigen functions.

$$E(z,t) = \sum_n E_n(t) \cos [\nu_n t + \phi_n(t)] U_n(z) , \qquad (48)$$

where $U_n(z) = \sin (n_o + n) \pi z/L$. The $E_n(t)$ and $\phi_n(t)$ are the slowly time varying amplitude and phase of the nth mode, ν_n is its frequency,* L is the cavity length, and n_o is the number of spatial variations of some central mode whose frequency is chosen to be closest to the center of the atomic fluorescence line. Starting with Lamb's self consistency equations (Reference 7) and including the effects of atomic polarization and the parametric polarization due to the loss modulator, one obtains coupled first order differential equations as follows.

$$(\dot{\phi}_n - n\Delta\nu + \frac{c}{2L} \psi_n) E_n =$$

$$\frac{-c\alpha_c}{2L} [E_{n+1} \sin(\phi_{n+1} - \phi_n) - E_{n-1} \sin(\phi_n - \phi_{n-1})] \qquad (49)$$

* In this discussion all symbols for frequencies will denote circular frequencies unless otherwise noted.

$$\dot{E} + \frac{c}{2L}\alpha_n E_n - \frac{c}{2L} G_n E_n = \frac{-c\alpha_a}{2L} E_n$$

$$\frac{-c\alpha_c}{2L} [E_{n+1} \cos(\phi_{n+1} - \phi_n) - E_{n-1} \cos(\phi_n - \phi_{n-1})] \quad (50)$$

B. Discussion of Parameters

In equations (48), (49) and (50) the frequency ν_n of the nth mode has been expressed in terms of the detuning $\Delta\nu$ of the modulator drive frequency ν_m from the axial mode spacing, i.e., $\Delta\nu = \Delta\Omega - \nu_m$, such that

$$\Omega_n - \nu_n = n\Delta\nu \ . \quad (51)$$

The parameter Ω_n is the frequency of the nth cavity resonance and is given by

$$\Omega_n = \Omega_o + (n\pi c)/L \ , \quad (52)$$

where Ω_o is the frequency of some center mode. Also $\Delta\Omega$ is the frequency interval between axial resonances ($\Delta\Omega = \pi c/L$).

The atomic contribution to the polarization of the nth mode is introduced by means of macroscopic quadrature and in-phase components of susceptibility, denoted by χ_n'' and χ_n', respectively. Then an optical signal propagating through a length L of the cavity undergoes additional phase retardation $\nu L\chi_n'/2c$ because of the presence of the atomic

medium. At the same time, the output optical intensity is increased by an amount equal to exp $(-\upsilon L\chi_n'')2c)$. It is useful to define a factor G_n such that

$$G_n = -\frac{\upsilon L}{c}\chi_n'' \quad . \tag{53}$$

Thus the fractional single pass power gain of the nth mode is given by

$$\text{Single Pass Power Gain}\Big|_{\text{nth mode}} = \frac{I_{out} - I_{in}}{I_{in}}\Big|_{\text{nth mode}} = e^{G_n - 1} \quad . \tag{54}$$

As noted in previous sections of the report, at small gains, $e^{G_n} \approx 1 + G_n$ and therefore G_n is approximately equal to the fractional single pass power gain. The parameter G_n depends nonlinearly upon frequency and power level. Similarly, it is useful to define a phase retardation ψ_n such that

$$\psi_n = \frac{\upsilon L}{c}\chi_n' \quad , \tag{55}$$

where ψ_n is the additional round trip phase retardation which is seen by the nth mode as a result of the insertion of the atomic medium. This also depends nonlinearly upon frequency and power level. In the computer simulation a specific dependence upon frequency and power level must be assumed for G_n and ψ_n. These differ for inhomogeneous and

homogeneous broadening and are considered in detail later. The unsaturated, or "small signal," value of G_n will be equal to one-half the unsaturated round trip gain g_o calculated earlier in equation (37).

The quantity α_n is defined in terms of Q_n of the nth mode by the expressions

$$\alpha_n = \frac{\nu L}{c} \frac{1}{Q_n} \tag{56}$$

and includes both dissipative loss and output coupling loss (mirror transmission). If the loss is small, α_n is approximately equal to the fractional single pass power loss of the nth mode (i.e., $e^{\alpha_n} \approx 1 + \alpha_n$). In typical cases α_n is independent of n. Comparing to the previous symbols

$$\alpha_n = T + \frac{L_i}{2} + \frac{\alpha_m d}{FOM} \tag{57}$$

In practice the perturbing element or modulator extends over a short distance in the axial, or z direction and usually will have no significant spatial variation over its length in that direction. The expression for the attenuation through a loss modulator perturbing element, per pass through the element, can be written

$$\alpha(t) = \alpha_M(1 + \cos \nu_m t) \ . \tag{58}$$

As previously, if the loss is small, $e^{\alpha_M} \approx 1 + \alpha_M$ and therefore α_M is approximately the average single pass loss through the perturbing element.

This yields the cross coupling term α_c which is given by the expression

$$\alpha_c = \frac{L}{\ell} \frac{\alpha_M}{\pi} \sin \frac{\pi \ell}{2L} \cos \frac{z_0 \pi}{L} \quad , \tag{59}$$

where ℓ is the axial length of the modulator centered at z_0. For $\ell << L$, equation (59) becomes approximately

$$\alpha_c = \frac{\alpha_M}{2} \cos \frac{z_0 \pi}{L} \quad . \tag{60}$$

The cross coupling loss term α_c is maximized by making z_0 small and then becomes

$$\alpha_c = \frac{\alpha_M}{2} \quad . \tag{61}$$

The self-coupling term

$$\alpha_a = \alpha_M \tag{62}$$

and therefore is equal to the average loss per pass through the modulator.

Several loss terms have been defined in this section and are summarized as follows:* α_n, the single pass power loss of the nth mode with is usually independent of n; α_M, the average loss per pass through the perturbing element; a self-coupling term α_a which is equal to α_M; and a cross-coupling term α_c which is approximately equal to one half of this average loss, α_M.

1) Inhomogeneous Saturation

It remains to give the form of G_n and ψ_n depending on the particular type of line broadening or saturation. For the inhomogeneous cause the principal features of the problem are considered to be treated adequately by assuming a Doppler broadened Gaussian atomic line with the homogeneous linewidth much smaller than both the axial mode interval $\Delta\Omega$ and the Doppler linewidth. For these cases the gain is expressed as

$$G_n = \frac{g_n/2}{\sqrt{1 + K\, E_n^2}} \quad , \tag{63}$$

where g_n is the unsaturated round trip fractional power gain of the nth mode and K is the saturation parameter. For the Doppler broadened Gaussian line them, g_n is given by

* These descriptions are applicable to the low loss case, otherwise the terms should more correctly be called attenuation constants.

$$g_n = g_o \frac{Z_i\left(\frac{\nu_n - \nu_o}{Ku}\right)}{Z_i(0)} \qquad (64)$$

and corresponding to this, ψ_n is taken to be

$$\psi_n = g_o \frac{Z_r\left(\frac{\nu_n - \nu_o}{Ku}\right)}{Z_i(0)} \quad , \qquad (65)$$

where power dependent mode pulling and pushing effects have been neglected. In (64) and (65) g_o is the unsaturated "line-center" power gain (the "line shape" may actually be due to an intracavity filter) and Z_r and Z_i are the real and imaginary parts of the plasma dispersion function, as described by Lamb (Reference 7). For vanishingly small homogeneous linewidth, (64) and (65) become g_o times the normalized Gaussian and Hilbert transform of the Gaussian, respectively. In equations (64) and (65) the parameter ν_o is the center frequency of the atomic line. Ku has units of angular frequency and equals 0.6 times the half power Doppler linewidth. It often is convenient to express the axial mode interval in terms of Ku and thus make use of the tables of Fried and Conte (Reference 8).

2) Homogeneous Saturation

In the case of homogeneous line broadening the gain is expressed as (Reference 2)

$$G_n = g_o \frac{\pi}{2} \Delta\nu_L \frac{g_L(\nu_n)}{1 + K \frac{\pi}{2} \Delta\nu_L \sum_m E_m^2 g_L(\nu_m)} , \qquad (66)$$

where g_o is the unsaturated line-center power gain, $g_L(\nu)$ is the Lorentzian line shape function.

$$g_L(\nu) = \frac{1}{\pi} \frac{\Delta\nu_L/2}{(\nu_o - \nu)^2 + (\frac{\Delta\nu_L}{2})^2} , \qquad (67)$$

and again K is a saturation parameter.

C. Digital Computer Solution

Equations (49) and (50) were solved on a digital computer for various operating conditions (both an IBM 3081D and CRAY X-MP/24 were used, as appropriate). The differential equations were started on the computer, after selecting initial mode amplitudes and phases and the laser parameters, and permitted to run until a steady state condition was reached (all $\dot{E}_n = 0$ and $\dot{\phi} = 0$ to 3 decimal places). The n = 0 mode was generally taken at line center, with a frequency $\nu_o = \Omega_o$. The solution gives all the mode amplitudes E_n and mode phases ϕ_o. Thus, one could say that the output is in the frequency domain in polar form

$$E(\omega)_n = E_n \underline{/\phi_n} . \qquad (68)$$

From a Fourier analysis point of view, these are samples of the Fourier spectrum. It is a simple discrete Fourier transform problem then to find the function in the time domain.

A standard Fourier transform computer program was used. First equation (68) was changed to rectangular form,

$$E(\omega)_n = E_n \cos \phi_n + j\, E_n \sin \phi_n \,, \tag{69}$$

and then the standard program was used to obtain real and imaginary parts in time, $x(t) + j\, y(t)$, so that then, with the notation,

$$E(t) \cos[\Omega_o t + \theta(t)] = \sum_n E_n \cos[(\Omega_o + n\omega_m)t + \phi_n]. \tag{70}$$

One has

$$E(t) = \sqrt{x^2(t) + y^2(t)} \tag{71}$$

$$\theta(t) = \tan^{-1} \frac{y(t)}{x(t)} \,. \tag{72}$$

In this procedure, Ω_o is the arbitrarily selected center frequency which in our case was selected to be at the atomic line-center frequency. It is of no important consequence here if the center mode resonance is not exactly at line

center. Furthermore, Ω_o could also be at the center of an intracavity tuner response curve.

Thus, the shape of the output pulse is given by E(t) and its instantaneous optical frequency is given by the time derivative of $\theta(t)$,

$$\omega(t) = \Omega_o + d\theta/dt \ . \qquad (73)$$

If $d\theta/dt$ is time varying the pulse has chirp but, with loss modulation as is being considered here, the chirp is usually negligible. The output power would have the shape of $|E(t)|^2$ and would be equal to $(T)(P_{cavity})$.

D. Specific Laser Simulations

Several low-pumping-level computer simulation runs at different mode locker losses α_c were made using the above equations.

The assumed laser parameters were as follows:

FOM	= 200
W	= 25 μm
$\alpha_m d$	= 1.5
L_i	= 0.005
P_{pump}	= 400 mW (average of mode-locked pulses during Q-switched pulse)
λ_p	= 530 nm
λ_{laser}	= 800 nm
g_o	= 0.0806 (calculated from equation (37))

Detuning $\Delta\nu = 0$

Linewidth of tuner (FWHM) = 0.1 mn (46.9 GHz)

c/2L = 150 MHz

Free Running Laser Power = 26.5 mW (calculated for one free running mode as would be for homogeneous saturation).

Figure 42 shows the mode amplitudes, effective unsaturated gain, and loss in arbitrary units versus mode number n for $\alpha_c = 0.053$. Figure 43 shows the resultant shape of P_{out}. The pulse peak power is 1.04 W, the average power is 25.8 mW, and the intensity pulse FWHM is 107 ps.

Figures 44 and 45 show similar results for $\alpha_c = 0.107$, Figures 46 and 47 show results for $\alpha_c = 0.269$, and Figures 48 and 49 show results for $\alpha_c = 0.54$. The latter value, $\alpha_c = 0.54$, is near the maximum value that one could expect from a practical acousto-optic mode locker.

Many of the details of the computer simulation technique also are included in Reference 9.

One sees from the Figures 42-49 the effects of increasing the mode-locker diffraction loss. The mode-locked pulses become shorter and the peak power increases. The bandwidth of the tuner will have a very large effect, with a broader response curve permitting a wider mode spectrum and a shorter pulse. If the response curve becomes too broad, however, the mode locking becomes unstable.

VI. Design of the Laser Cavity

As shown in section IV it is necessary for the pump and laser spot size to be small inside the Titanium Sapphire rod. Therefore most workers have used cavities with internal focusing elements to obtain small spot size and to decrease the stability sensitivity to length adjustment. Since low-loss mirrors are more practical than low-loss lenses, folded cavities have been used in which concave mirrors at oblique incidence are used for the focusing. Furthermore, this permits compensation for the astignatism present in laser rods cut with Brewster angle ends similar to the case in dye lasers (Reference 10).

The 2-folding-mirror cavities sketched in Figure 50 were considered. The ring cavity in Figure 50(a) was not chosen because of the need for an extra cavity element ot make it unidirectional. Furthermore, the wavelength selection was to be accomplished by a reflection grating furnished by USAFSAM. The layout in Figure 50(c) was chosen because it would give a long, narrow overall laser shape (the overall cavity length had to be $\approx$ 1 meter to match the c/2L requirement of USAFSAM.).

A. Cavity Stability

First the fundamental question of stability of a cavity with a tight focusing section will be considered. A later section will consider the effects of the folding.

Without the folding, the cavity can be modeled as a straight cavity with a tightly focused lensed section. For symplicity, symmetry is assumed as sketched:

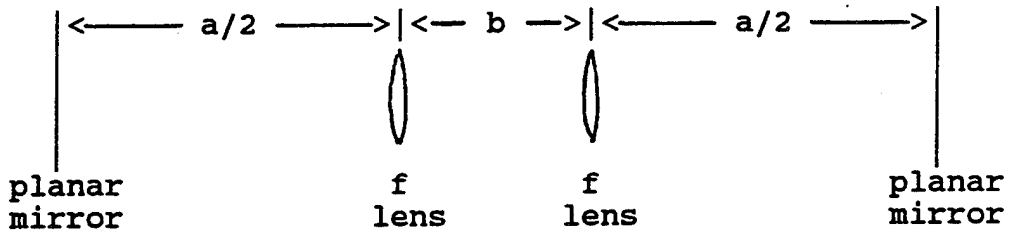

Since the behavior at the point half-way between the lenses (the tightly focused point) is desired, a ray-matrix unit cell with the input at that point was chosen. This involves the matrix multiplication

$$\begin{pmatrix} A & B \\ C & D \end{pmatrix} = \begin{pmatrix} 1 & b/2 \\ 0 & 1 \end{pmatrix} \begin{pmatrix} 1 & 0 \\ -1/f & 1 \end{pmatrix} \begin{pmatrix} 1 & a \\ 0 & 1 \end{pmatrix} \begin{pmatrix} 1 & 0 \\ -1/f & 1 \end{pmatrix} \begin{pmatrix} 1 & b/2 \\ 0 & 1 \end{pmatrix} \quad (74)$$

Straight forward multiplication of the matrices gives for the elements of this unit-cell matrix as follows:

$$A = 1 - a/f - \frac{b}{f} - \frac{ba}{2f^2} \quad (75)$$

$$B = b + a - \frac{ba}{f} - \frac{b^2}{2f} + \frac{b^2 a}{4f^2} \quad (76)$$

$$C = -2/f + a/f^2 \quad (77)$$

$$D = A = 1 - a/f - b/f - \frac{ba}{2f^2} \quad (78)$$

Using the standard stability requirement in the form

$$0 \leq \frac{A+D+2}{4} \leq 1 \quad , \tag{79}$$

this gives, after some algebraic simplification, the equation

$$0 \leq (1 - \frac{a}{2f})(1 - \frac{b}{2f}) \leq 1 \quad , \tag{80}$$

which is the stability requirement for the assumed cavity. This requirement can be displayed in a fashion similar to a conventional 2-curved-mirror linear cavity.

The stability diagram is sketched in Figure 51 and the operating range for the case where a >> f is noted on the Figure. Also shown sketched are the ray pattern and accompanying gaussian beam (not to scale) for the two extremes of the range of b for which the cavity is stable.

The values of b at the extreme points F and F' of the stable range of b are easily found from equation (80). Point F lies at the point b=2f which makes $(1-\frac{a}{2f})(1-\frac{b}{2f}) = 0$, regardless of the value of a.

$$\text{Point F:} \quad b = 2f \tag{81}$$

The point F' lies at $(1-\frac{a}{2f})(1-\frac{b}{2f}) = 1$ which gives

$$\text{Point F':} \quad b = \frac{2fa}{a-2f}$$

$$= 2f + \frac{4f^2}{a-2f} \quad . \tag{82}$$

Obviously the range of b over which the cavity is stable is, from equations (81) and (82),

$$\Delta b = \frac{4f^2}{a-2f} \quad . \tag{83}$$

The fact that this range can be much larger than that of a conventional 2-mirror cavity, and still have a small spot size at the focal point, is the primary reason for use of the type cavity being studied (Reference 1). As is usual when going from a ray analysis to an actual gaussian beam solution, the perfect focus predicted by the ray analysis at F and F' will lead to an infinite spot size at the lenses and will be physically impossible.

The spot size at the focal point is of fundamental interest since it will affect the gain as shown in Section IV. The waist radius (at the point half way between the lenses) is given by the standard equation, using the elements of the ray matrix given in equations (75-78),

$$\frac{\pi W_o^2}{\lambda} = \frac{-B}{\left[1 - \left(\frac{A+D}{2}\right)^2\right]^{\frac{1}{2}}} \quad . \tag{84}$$

Substituting the values for A, B, and D, equation (94) gives

$$\frac{\pi W_o^2}{\lambda} = \frac{b + a - \frac{ba}{f} - \frac{b^2}{2f} + \frac{b^2 a}{4f^2}}{\sqrt{1 - (1 - \frac{a}{f} - \frac{b}{f} + \frac{ba}{2f^2})^2}} \quad . \tag{85}$$

Using equation (85), Figure 52 shows a plot of waist radius versus b for a cavity having f = 5 cm and a = 90 cm (these values give a total cavity length of 1 meter, giving the required c/2L nominal frequency of 150 MHz). The range of b in Figure 52 is from b = 2f (0.1 meter) to b = $2f + \frac{4f^2}{a-2f}$ (0.1125 m). Thus the stability range of adjustment of b is 1.25 cm. At the center of the stability range, i.e. at

$$b\Big|_{\substack{\text{center of} \\ \text{stability} \\ \text{range}}} = 2f + \frac{2f^2}{a-2f} \quad , \tag{86}$$

the calculated radius of the waist when b is at this point one-half way between F and F' is 28.2 μm.

An equation can be obtained for the waist size when b is adjusted to the center of the stability range. Taking equation (85) and letting b equal the value above in equation (86), the result is

$$\frac{\pi W_o^2}{\lambda}\Bigg|_{\substack{\text{b adjusted} \\ \text{to center} \\ \text{of stability} \\ \text{range}}} = \frac{f^2}{a-2f} \tag{87}$$

Equation (87) shows the desirability of having a >> f to obtain small spot size at the focal point.

The size of the spot at the lens (simulating a mirror) can be found by the standard gaussian beam equation,

$$W^2(z) = W_o^2\left[1 + \left(\frac{\lambda z}{\pi W_o^2}\right)^2\right] \quad . \qquad (88)$$

Substitution of the value of waist radius from equation (85) into equation (88) and evaluating at z = b/2 gives the curve plotted in Figure 53. The curve shows that the spot radius at the lens stays less than 0.6 mm over much of the stability range of b, a very practical result.

An analytical expression can be obtained for the spot size at the lens when b is adjusted to the center of the stability range. The combination of equations (86), (87), and (88) yields

$$\left.W\right|_{\substack{\text{at lens}\\ \text{when b at}\\ \text{center of}\\ \text{stability}\\ \text{range}}} = W_o\sqrt{1 + \left(\frac{a-f}{f}\right)^2}$$

$$= \sqrt{\frac{\lambda}{\pi}\left(\frac{f^2}{a-2f}\right)\left[1+\left(\frac{a-f}{f}\right)^2\right]} \qquad (89)$$

$$\approx \sqrt{\frac{\lambda}{\pi}\, a}$$

The approximation in equation (89) agrees quite well with the exact plot in Figure 53.

B. The Folded Cavity

Now, the two lenses are replaced by concave mirrors at oblique incidence to give the folded cavity of Figure 50(c). Both the laser rod, asumed at Brewster angle to the beam, and the mirrors cause astignatism. The balancing of this astignatism, similar to that of Reference 10 for the one-fold cavity, is the subject of this section.

As shown in reference 10 (describing a dye laser) the effective distances through a cell when at Brewster angle are different for the xz and yz planes sketched

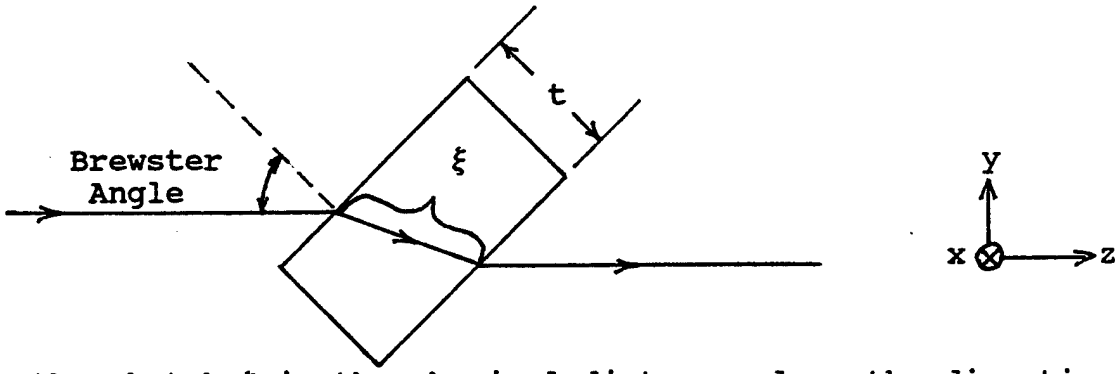

In the sketch ξ is the physical distance along the direction traveled by the beam. It is given by the expression

$$\xi = \frac{t\sqrt{n^2 + 1}}{n} \quad . \tag{90}$$

In the case of a laser rod with Brewster ends, ξ is the length of the rod. Then the effective distances the rays have to traverse are (References 10 and 11)

$$\text{xz plane:} \quad b_x = \xi/n \tag{91}$$

$$\text{yz plane:} \quad b_y = \xi/n^3 \quad . \tag{92}$$

Alternately, with straight-forward algebra, these effective distances are written as with corrections to the physical length ξ of the rod, as follows,

$$b_x = \xi - \left(\frac{n-1}{n}\right) \xi \tag{93}$$

$$b_y = \xi - \left(\frac{n^3-1}{n^3}\right) \xi \quad . \tag{94}$$

Similarly a curved mirror at oblique incidence has different effective focal lengths (Reference 12)

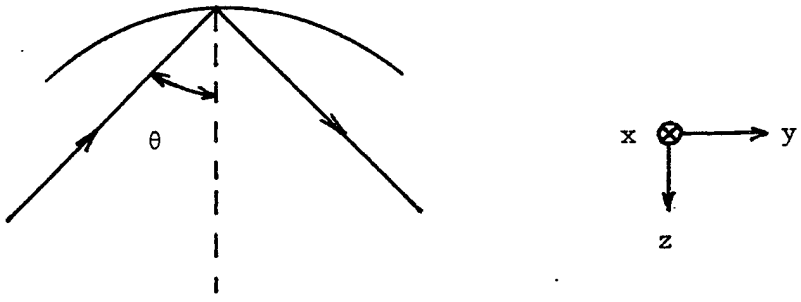

$$\text{xz plane:} \quad f_x = \frac{f}{\cos\,\theta} \tag{95}$$

$$\text{yz plane:} \quad f_y = f \cos\,\theta \tag{96}$$

Again, these can be written as corrections to the focal length,

$$f_x = f + f\,\frac{(1 - \cos\theta)}{\cos\theta} \tag{97}$$

$$f_y = f - f(1 - \cos\theta) \tag{98}$$

Now the stability equation will be different for the xz and yz planes

$$\text{xz plane:}\quad 0 \le (1 - \frac{a}{f_x})(1 - \frac{b_{sx}}{f_x}) \le 1 \tag{99}$$

$$\text{yz plane:}\quad 0 \le (1 - \frac{a}{f_y})(1 - \frac{b_{sy}}{f_y}) \le 1 \tag{100}$$

where f_x and f_y are as given above and

$$b_{sx} = b_{air} + b_x \tag{101}$$

$$b_{sy} = b_{air} + b_y \tag{102}$$

These can be written as, using equations (93) and (94),

$$\begin{aligned} b_{sx} &= b_{air} + \xi - \frac{(n-1)}{n}\,\xi \\ &= b_{phys} - \frac{(n-1)}{n}\,\xi \end{aligned} \tag{103}$$

$$\begin{aligned} b_{sy} &= b_{air} + \xi - \frac{(n^3-1)}{n^3}\,\xi \\ &= b_{phys} - \frac{(n^3-1)}{n^3}\,\xi \end{aligned} \tag{104}$$

In equations (103) and (104) b_{phys} is the actual physical distance between the folding mirrors along the direction of the beam travel.

The result of equations (97), (98), (103), and (104) is that the stability diagrams for the xz and yz plans undergo an origin shift and scale change when plotted versus b_{phys}.

Figures 54, 55, 56, and 57 show plots of the waist radius in the xy and yz planes versus the physical spacing of the folding mirrors, b_{phys}, for folding angles of 14°, 15°, 16°, and 17° respectively. This uses equations (95), (96), (103), (104) and (85) in which b_{sx} or b_{sy} and f_x or f_y are used as appropriate. The stability ranges have different widths for the xz and yz planes and their degree of overlap depends on the value of folding angle θ . Kogelnik, et.al., of Reference 10 had similar results for a single-fold cavity but, with their approximations (necessary for their type cavity), the stability ranges were of equal width and the waist radii in the 2 planes were equal. Here in the symmetric 2-fold cavity it is possible to obtain an exact solution, as shown in the figures, and at no angle are the stability ranges the same.

C. Astignatism Balance Equation

A closed-form theoretical equation for astignatism blanace was obtained by Kogelnik, et.al., (Reference 10) for the single-fold cavity. A similar equation can be obtained for the double-fold cavity by choosing a value of θ that makes the b_{phys} of the xy plane and the b_{phys} of the yz

plane equal at point F on their respective stability diagrams. That is, the lower edges of the stability ranges shown in the respective Figures 54-57 are made to coincide by choosing the proper value of θ. As seen in Figure 56 it obviously occurs at a value close to $\theta = 16°$, with the assumed cavity values of f and a.

In the respective planes, the equations for b_{phys} at the point F, occurs at

$$\text{xz plane:} \quad 1 - \frac{b_{sx}}{f_x} = 0 \tag{105}$$

$$\text{yz plane:} \quad 1 - \frac{b_{sy}}{f_y} = 0 \tag{106}$$

Using equations (97), (98), (103) and (104), the respective equations become (at point F)

$$\text{xz plane:} \quad b_{phys} = 2f+2f\left(\frac{1-\cos\theta}{\cos\theta}\right)+\left(\frac{n-1}{n}\right)\xi \tag{107}$$

$$\text{yz plane:} \quad b_{phys} = 2f-2f(1-\cos\theta)+\left(\frac{n^3-1}{n^3}\right)\xi \tag{108}$$

Equating the b_{phys} of the 2 planes, equations (107) and (108) give

$$2f \sin\theta \tan\theta = \left(\frac{n^3-1}{n^3}\right)\xi \tag{109}$$

This equation (109) is a basic astigmatism compensation equation for the 2-fold symmetric cavity. Equation (109) is in terms of the laser rod length. If equation (90) is used, a compensation equation in terms of thickness, as for a dye cell, is obtained

$$2f \sin h \tan h = \frac{t\sqrt{n^2+1}(n^2-1)}{n^4} \qquad (110)$$

Except for the factor of 2, this is exactly the same as the one-fold equation of Kogelnik, et.al. (reference 10). It should be noted that Wagstaff and Dunn (reference 13) obtained a result like equation (110) by a direct extrapolation of the Kogelnik, et.al., work to a case where the f's of the folding mirrors as well as the folding angles were unequal. This gives (reference 13, modified to conform to present notation)

$$f_1 \sin h_1 \tan h_1 + f_2 \sin h_2 \tan h_2 = \frac{t\sqrt{n^2+1}(n^2-1)}{n^4} \qquad (111)$$

Another fact that should be noted is that the stability range here is considerably larger than that obtained by Kogelnik, et.al. for the one-fold thin dye cell laser in their design. Here, the range over which b_{phys} can be

varied and the cavity remain stable is seen from Figure 57 to be about 1 1/4 cm.

Figures 54-58 show that matching the lower edge of the stability range (points F on the xz and yz stability charts) may not be the best choice. Matching the upper edge (points F' on the xz and yz stability charts) as in Figure 55 with the folding angle equal to 14° (for the cavity being studied) might be preferable. The angle of 15° in Figure 56 causes the center of the stability ranges to coincide. The angles of 13° (Figure 54) and 17° (Figure 58) give a possible point where the waist size is equal in the x and y directions.

In summary, the folding angle given by equation (109), which causes the lower edges of the stability ranges to coincide, may not be the optimum angle. Instead, the optimum angle will be one to two degrees smaller than that predicted by equation (109).

D. Cavity Length

After the folding angle is determined from stability considerations, the overall cavity physical length must be determined so that the optical length will be 1 meter, giving the c/2L frequency equal to the required nominal 150 MHz.

From equation (107) or (108) the physical distance between the two folding mirrors along the beam path is (for operation at point F)

$$b_{phys} = 2f - 2f(1-\cos\theta) + \left(\frac{n^3-1}{n^3}\right)\xi \qquad (112)$$

where f is the focal length of the folding mirrors and ξ is the physical length of the laser rod. As shown in Figures 54-58, however, the best operation will not be exactly at point F and the best folding angle may not be exactly the value given by equation (109).

The best operation from a stability point of view will be when the <u>center</u> of the xz and yz stability curves coincide and when operating at this center. From Figure 56 with the parameters assumed, this would be at a folding angle of 15° and with the physical distance between the folding mirrors along the beam path equal to 0.1185 meters.

Thus, with

$$b_{phys} = b_{air} + \xi = 0.1185 \text{ m} \qquad (113)$$

and with $\xi = 0.02$ m, we have $b_{air} = 0.0985$ m. The optical length between the folding mirrors will be

$$\begin{aligned} b_{opt} &= b_{air} + n\xi \\ &= 0.0985 + (1.7)(.02) \\ &= 0.1325 \text{ m} \quad . \end{aligned} \qquad (114)$$

This means

$$a_{opt} = 1.0 - b_{opt}$$
$$= 0.8675 \text{ m} \quad . \tag{115}$$

One arm of the laser will be air and will thus have a length

$$a_{air}^{\#1} = \frac{a_{opt}}{2} = 0.43375 \text{ m} \quad . \tag{116}$$

The other arm will have the mode locker present which will have an optical length longer than its physical length. When the mode locker has Brewster angle end faces, some astigmatism will be introduced in this arm of the laser. As seen from equation (81), the lower edge of the stability range (point F on stability diagram) is unaffected by the value of a. As seen by equation (82), however, the upper edge (point F' on the stability diagram) is affected by the value of a and hence would be slightly different in the xz and yz planes.

The sensitivity of the upper edge of the stability range to the length a is seen from equation (82) to be

$$\frac{d(b)}{da} = \frac{-4f^2}{(a-2f)^2} \quad . \tag{117}$$

With the numbers being studied, f = 0.05 m and a = 0.9 m, this gives

$$\frac{d(b)}{da} = 0.015625 \tag{118}$$

This means that the necessary change in b to compensate for a change in a is of the order of 1.5 percent of the change in a. Therefore, the slight difference in a in the xz and yz planes due to astigmatism in the mode locker is assumed to be of no consequence and therefore is neglected. The mode locker purchased for use in the laser has a length of 0.065 m giving it an optical length of approximately 0.0975 m. Thus the arm of the laser having the mode locker will have an air length (nominal) of

$$a_{air}^{\#2} = \frac{a_{opt}}{2} - 0.0974$$

$$= 0.43375 - 0.0975$$

$$= 0.33625 \text{ m}$$

Experimental adjustments in a are made possible by mounting the output coupler mirror on a translation stage.

Figure 59 shows the cavity layout.

E. The Grating Tuner

A diffraction grating was provided by USAFSAM for use in Littrow mount for wavelength tuning. Data was not available regarding characteristics of the grating. However, by measuring the angular direction of the various

diffraction orders using a HeNe laser, it was deduced that the grating had 600 grooves per mm.

From any standard reference, the various orders are at angles as shown

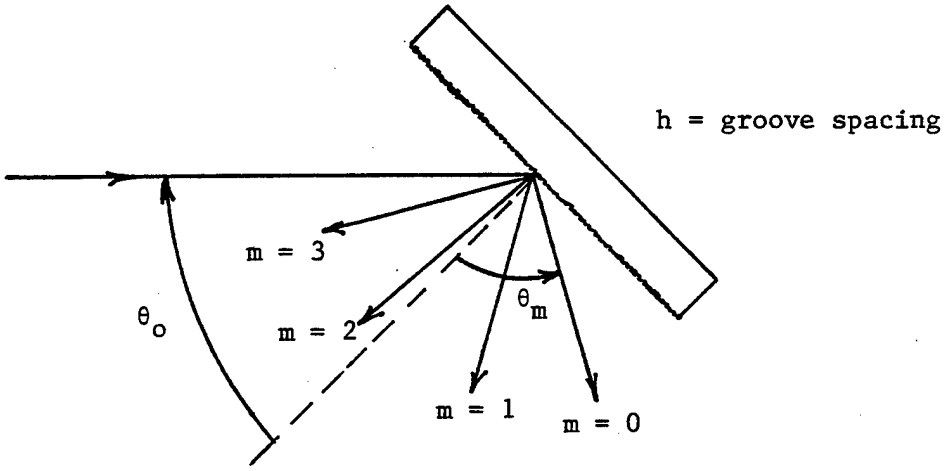

For a given incident angle θ_o, the angle θ_m of the m^{th} order is given by

$$\sin \theta_m - \sin \theta_o = m \lambda/h \quad . \tag{119}$$

The spectral width of a given order is given by

$$\Delta\lambda = \frac{\lambda^2}{Nh(\sin \theta_m + \sin \theta_o)} \tag{120}$$

where N is the number of grooves illiminated by the beam. In the Littrow use, an order m and angle θ_o must be chosen so that the m^{th} order is retro-reflected back along the

direction of incidence. In this case, $\theta_m = -\theta_o$ and therefore, the desired incidence angle is

$$\sin \theta_o = \frac{m}{2} \left(\frac{\lambda}{h}\right) \tag{121}$$

for retro-reflection of the m^{th} mode. At this condition, the linewidth of the grating tuner becomes

$$\Delta\lambda = \frac{\lambda^2}{Nh\ 2\sin \theta_o} \tag{122}$$

or, using equation (121), for Littrow operation

$$\Delta\lambda = \frac{\lambda}{mN} \tag{123}$$

which then depends on the order m used and the number of grooves N illiminated.

In using the Littrow mount operation, a diffraction order must be chosen that will permit the desired wavelength tuning range (unless orders are switched during the tuning process). Also, for low loss the order must be one with reasonably high reflectivity (will depend on the blazing of the grating). From tests with a HeNe laser, it was determined that the grating reflection loss was lowest at angles of incidence in a range near 45°. For tuning over the range desired in this work, that corresponds to the use of the m=3 diffraction order. Using equation (121) and

(122), table I shows the range of θ_o needed and the linewidths $\Delta\lambda$ of the tuner. Nh is the illuminated width on the grating surface.

Table I
Calculated Grating Performance in m=3 order

		Without Telescope Nh ≃ 1 mm		With Telescope Nh ≃ 10 mm	
λ(nm)	θ_o	$\Delta\lambda$(nm)	$\Delta\nu$(GHz)	$\Delta\lambda$(nm)	$\Delta\nu$(GHz)
700	39.0	0.389	238	0.0389	23.8
750	42.4	0.417	222	0.0417	22.2
800	46.0	0.448	208	0.0448	20.8
850	50.0	0.472	196	0.0472	19.6
900	54.0	0.501	185	0.0501	18.5

Without a telescope beam expander (Nh ≃ 1 mm), the $\Delta\lambda$ are quite wide for mode locking and tend to create stability problems. With a telescope beam expander (Nh ≃ 10 mm) the $\Delta\lambda$ is somewhat small to give short mode-locked pulse widths.

The grating as delivered was mounted so that linear motion produced by a drive screw was converted directly to an incremental wavelength as sketched below

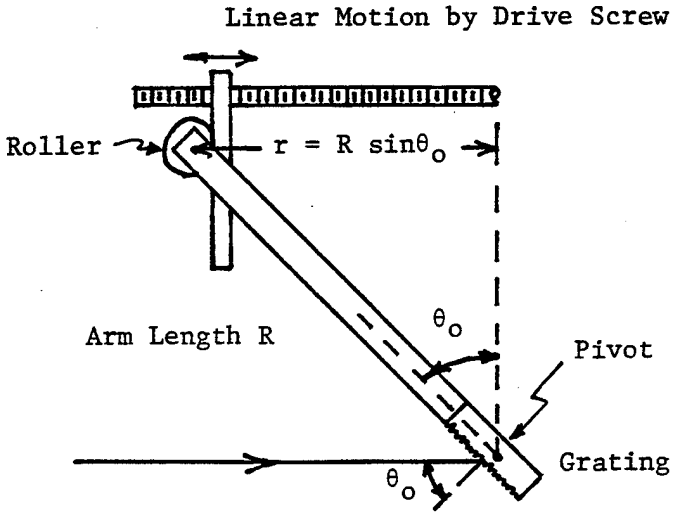

The effective arm length R was 20 cm. Thus

$$r = R \sin \theta_o \tag{124}$$

or, using equation (121),

$$r = R \frac{m}{2} \frac{\lambda}{h} \tag{125}$$

or

$$\lambda = \frac{2d}{Rm} r \quad . \tag{126}$$

For the grating used $h = \frac{1}{600}$ mm, and with R = 0.2 m and using the m=3 order, the λ to which the tuner is tuned is dependent upon the value r as

$$\lambda = 5.56 \times 10^{-6} r \quad , \tag{127}$$

or as in use,

$$\text{Change in } \lambda = 5.55 \times 10^{-6} \Delta r \quad . \tag{128}$$

For a HeNe laser at 632.8 nm, the angle of incidence $\theta_o = 34.7°$, which is not too far from the value at the lower edge of the desired tuning range. Experimentally, then, a HeNe laser can be used to calibrate the value of r and then the relationship (128) used to calibrate the tuner adjustment for other wavelengths. The total change in r

needed to tune from 700 nm (θ_o = 39.0°) to 900 nm (θ_o = 54.0°) is then

$$\Delta r = 0.2[\sin 54.0° - \sin 39.0°]$$
$$= 35.9 \text{ mm} \qquad (129)$$

VII. Design and Performance

Using the techniques of Section IV and Section V the performance of the complete laser can be calculated.

A. Cavity Parameters

From the work included in Sections IV, V, and VI the selected characteristics were as follows:

Ti Sapphire laser rod:
- 0.5 cm x 0.5 cm x 2 cm (square cross section)
- length = 2 cm
- $\alpha_{514} = 1.0 \text{ cm}^{-1}$
- FOM ≥ 200
- Brewster ends, laser grade polish, π polarization
- Ground-surface sides
- Vendor -- Crystal Systems Inc.
  27 Congress St.
  Salem, Massachusetts 01970

Fused Quartz acousto-optic mode locker
- Wavelength -- for use at 750 nm-850nm
- Acoustic center frequency -- 75.041 MHz ± 19 KHz
- Acoustic mode spacing -- 460 KHz
- RF bandwidth -- ± 15% of center frequency
- Active optical aperture -- 3mm x 5 mm
- Diffraction efficiency -- 750%
- Maximum drive power (water cooled) -- 5 watts
- Temperature tuning -- +7 KHz/°C
- Static Optical insertion loss -- < 0.3%
- Windows -- Brewster
- with fittings for water cooling
- Vendor -- Intra Action Corp.
  3719 Warren Avenue
  Bellwood, Illinois 60104

Mirror set
2 each 3/4" diameter x 1/4" thick, 10 cm radius of curvature, H.R. 780-900 nm, pass 614.5 nm
1 each 1" diameter x 1/4" thick, flat, H.R. 780-900 nm
1 each 1" diameter x 1/4" thick, flat, 5% transmission 780-900 nm
Vendor -- Schwartz Electro-Optics, Inc.
3404 North Orange Blossom Trail
Orlando, Florida 32804

Littrow Prism:
600 grooves/mm
Mounted with $\sin\theta$ drive mechanism
Furnished by USAFSAM

Then in equation (38) for the round trip loss coefficient,

$$\text{Loss} = T + L_i + \frac{\alpha_m d}{\text{FOM}/2} \quad , \tag{38}$$

We have

$$T = 0.05 \quad ,$$
$$\alpha_m d = (1)(2) = 2 \quad , \tag{130}$$
$$\text{FOM} = 200 \quad ,$$

and assuming the grating has about 80% reflection,

$$L_i \approx 0.2 \quad , \tag{131}$$

which give the round trip loss coefficient

$$\text{Loss} = 0.29 \quad . \tag{132}$$

Then, under these conditions the pump threshold is calculated from equation (39),

$$P_{th} = \frac{\pi W^2}{2} \frac{\lambda}{\lambda_p} I_s \frac{(T + L_i + \frac{\alpha_m d}{FOM/2}}{1 - e^{-\alpha_m d}} \quad . \tag{39}$$

where it is assumed that

$$\begin{aligned} W &= 50\ \mu m \\ \lambda_{pump} &= 514.5\ nm \\ \lambda &= 800\ nm \end{aligned} \tag{133}$$

and the result is

$$P_{th} = 63.6 \text{ watts} \tag{134}$$

The peak power, averaged over the mode-locked pulses, will have to reach a value exceeding 64 watts during the Q-switched pulse of the pump. From the work in Section III, it is seen that the average pump power will have to exceed approximately 400 mW in order for the effective pump to grow to the threshold value during the Q-switched 100 ns pulse.

B. Performance

In a computer simulation, we assume that the peak pump power is 75 watts. Then from equation (37) the small signal gain coefficient is

$$g_o = 0.341 \tag{135}$$

From Table I the linewidth will be assumed to be 200 GHz. The cw power output is calculated from equation (42) to be

$$(P_{out})_{cw} = 0.55 \text{ watts}$$

This is the free running power calculated for one free-running mode as would be for homogeneous saturation. Figure 60 shows the mode amplitudes, effective unsaturated gain, and loss in arbitrary units versus mode number n for $\alpha_c = 0.50$, the largest value that could reasonably be expected from the mode locker. Figure 61 shows the resultant shape of P_{out}. The pulse peak power is 39.4 W, the average power is 0.54 W, and the intensity pulse FWHM is 55.5 ps. If a larger α_c could be obtained, then the pulse would be more narrow with a larger peak power.

This performance is relatively poor because of the large loss of the grating. If the grating were replaced by a birefringent tuner and a high reflectivity flat mirror, the performance could be improved greatly. Also, a higher peak pump power would improve the performance. From the calculations in Section III for the USAFSAM pumping source (Q-switched Nd:YAG with frequency doubling), the required average pump power to obtain the assumed 75 watt peak pump power would be approximately 480 mW average pump power.

VIII. Conclusions

The design and construction of a longitudinally pumped Titanium Sapphire laser has been completed. It was designed to meet the requirements of the Vision Biophysics Function of the Clinical Sciences Division of the USAF School of Aerospace Medicine. The design techniques are included in detail in this report and can be used to modify the design of the laser if needed. In order to reach optimum performance it will be necessary to replace the diffraction grating furnished by USAFSAM by a plane mirror/birefringent filter combination. A satisfactory plane mirror was purchased as a part of this project, but funds were not available for a birefringent filter. This rather straightforward modification will greatly decrease the necessary pump requirements.

IX. References

1. Anthony J. Alfrey, "Modeling of Longitudinally Pumped CW Ti:Sapphire Laser Oscillators," IEEE J. Quantum Electronics, Vol. 25, pp. 760-766, April 1989.

2. O. P. McDuff, D. T. Scott, and J. Taboada, "A Computer Simulation of a Feedback-Stabilized Actively Mode-Locked Laser," Proceedings of IEEE Southeastcon '86 (IEEE Publishing Services, Piscataway, NJ, 1986), pp. 99-103, 1986.

3. Odis P. McDuff and Dinesh Thati, "A Non-Linear Coupled-Mode Analysis of Gain-Modulated Lasers," Proceedings of International Conference on Lasers '87, Lake Tahoe, Nevada, pp. 620-627, 1987.

4. G. B. Al'tshuler, V. B. Karasev, N. V. Kondratyuk, G. S. Kruglik, A. V. Okishev, G. A. Skripko, V. S. Urbanouich, and A. P. Shkadeerenich, "Generation of Ultrashort Pulses in a Synchronously Pumped Ti^{3+} Laser," Sov. Tech. Phys. Lett., Vol. 13, pp. 324-325, July 1987.

5. O. P. McDuff and S. E. Harris, "Nonlinear Theory of the Internally Loss Modulated Laser," IEEE J. Quant. Electronics, Vol. QE-3, pp. 101-111, march 1967.

6. S. E. Harris and O. P. McDuff, "Theory of FM Laser Oscillation," IEEE J. Quant. Electr., Vol. QE-1, pp. 245-262, September 1965.

7. W. E. Lamb, Jr., "Theory of an Optical Laser," Phys. Rev. 134, A1429-A1450, June 1964.

8. B. D. Fried and S. D.Conte, The Plasma Dispersion Function (Hilbert Transform of the Gaussian), New York, Academic Press, 1961.

9. O. P. McDuff, Final Technical Report on Subcontract 84 RIP 51 from Southeastern Center for Electrical Engineering Education, "Stabilization of Mode-Locked lasers," BER Report No. 362-70, The University of Alabama, December 1985. Work was done for USAF School of Aerospace Medicine.

10. H. Kogelnik, E. P. Ippen, A. Dienes, and C. V. Shank, "Astigmatically Compensated Cavities for CW Dye Lasers," IEEE J. Quant. Electronics, Vol. QE-8, pp. 373-379, March 1972.

11. D. C. Hanna, "Astignatic Gaussian Beams Produced by Axially Asymmetric Laser Cavities," IEEE J. Quant. Electronics, Vol. QE-5, pp. 483-488, October 1969.

12. H. Kogelnik and T. Li, "Laser Beams and Resonators," Appl. Opt., Vol. 5, pp. 1550-1567, October 1966.

13. C. E. Wagstaff and M. H. Dunn, "A Second-Harmonic, Ring Dye Laser for the Generation of Continuous-Wave, Single-Frequency UV Radiation," J. Phys. D: Appl. Phys., Vol. 12, pp. 355-383, 1979.

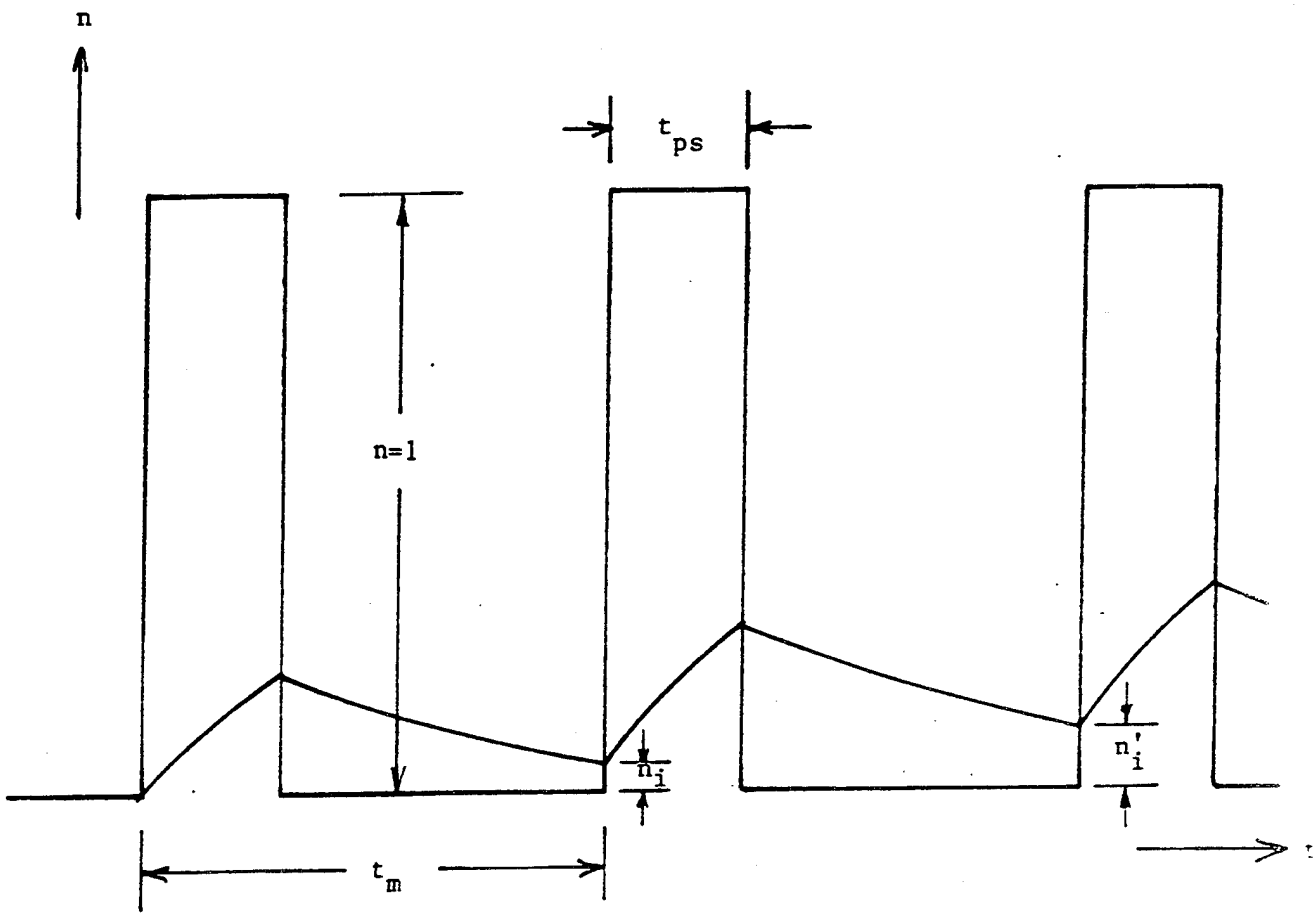

Figure 1. Variation of Normalized Inversion n During the Pump Laser Mode-Locked Pulsing.

t_m = Mode-Locked Period ≈ 6.67 ns

t_{ps} = Mode-Locked Pulse Width ≈ 100 ps

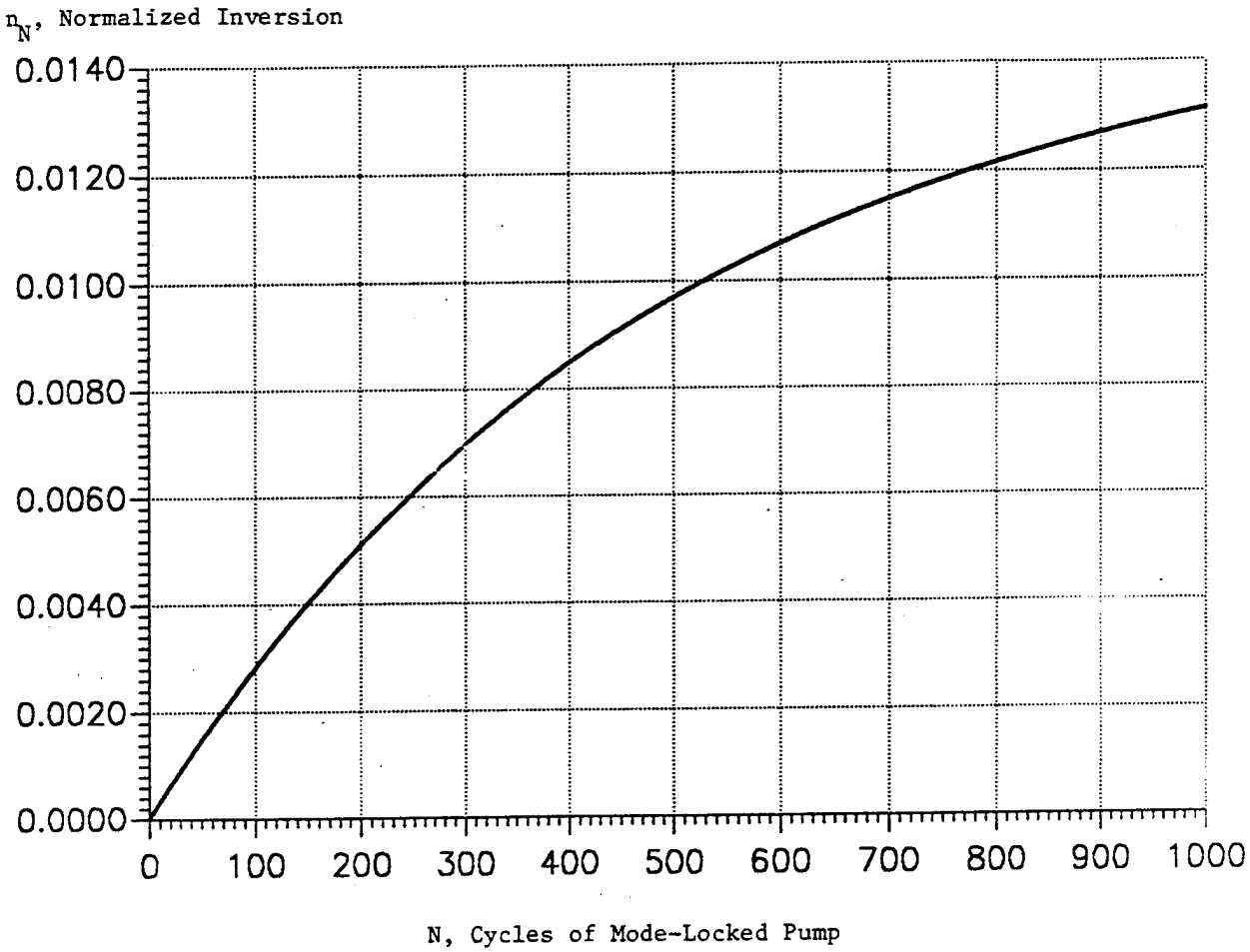

Figure 2. Build Up of the Inversion in the Titanium Sapphire When Pumped with 100 ps Pulses at 6.67 ns Intervals.

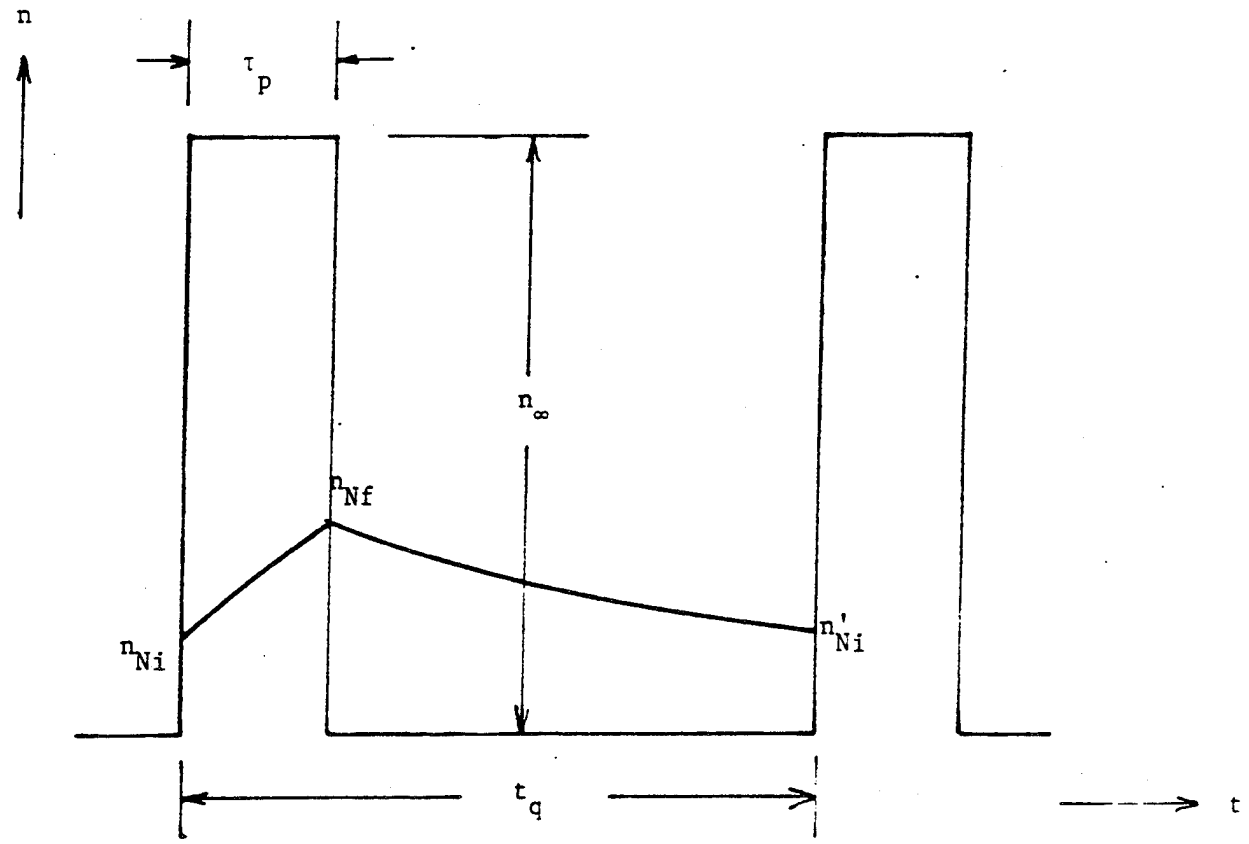

Figure 3. Variation of Normalized Inversion n During the Pump Laser Q-Switched Pulsing.

t_q = (Q-Switch Repetition Rate)$^{-1}$ ≈ 0.5 ms

τ_p = Width of Q-Switched Pulse ≈ 100 ns

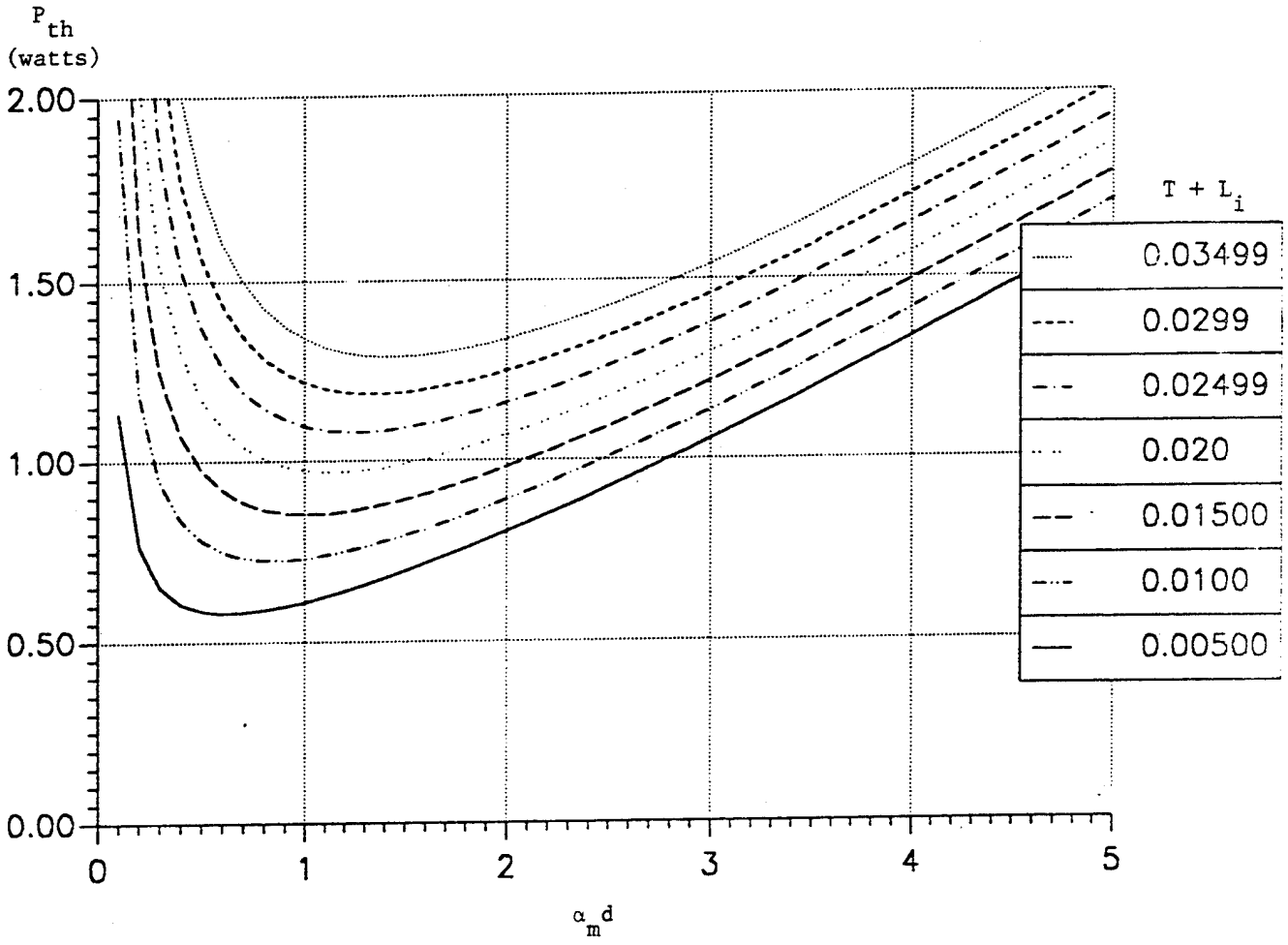

Figure 4. Dependence of Pump Threshold Power upon Laser Rod $\alpha_m d$ and Losses $T + L_i$.
FOM = 100. W = 50 μm.

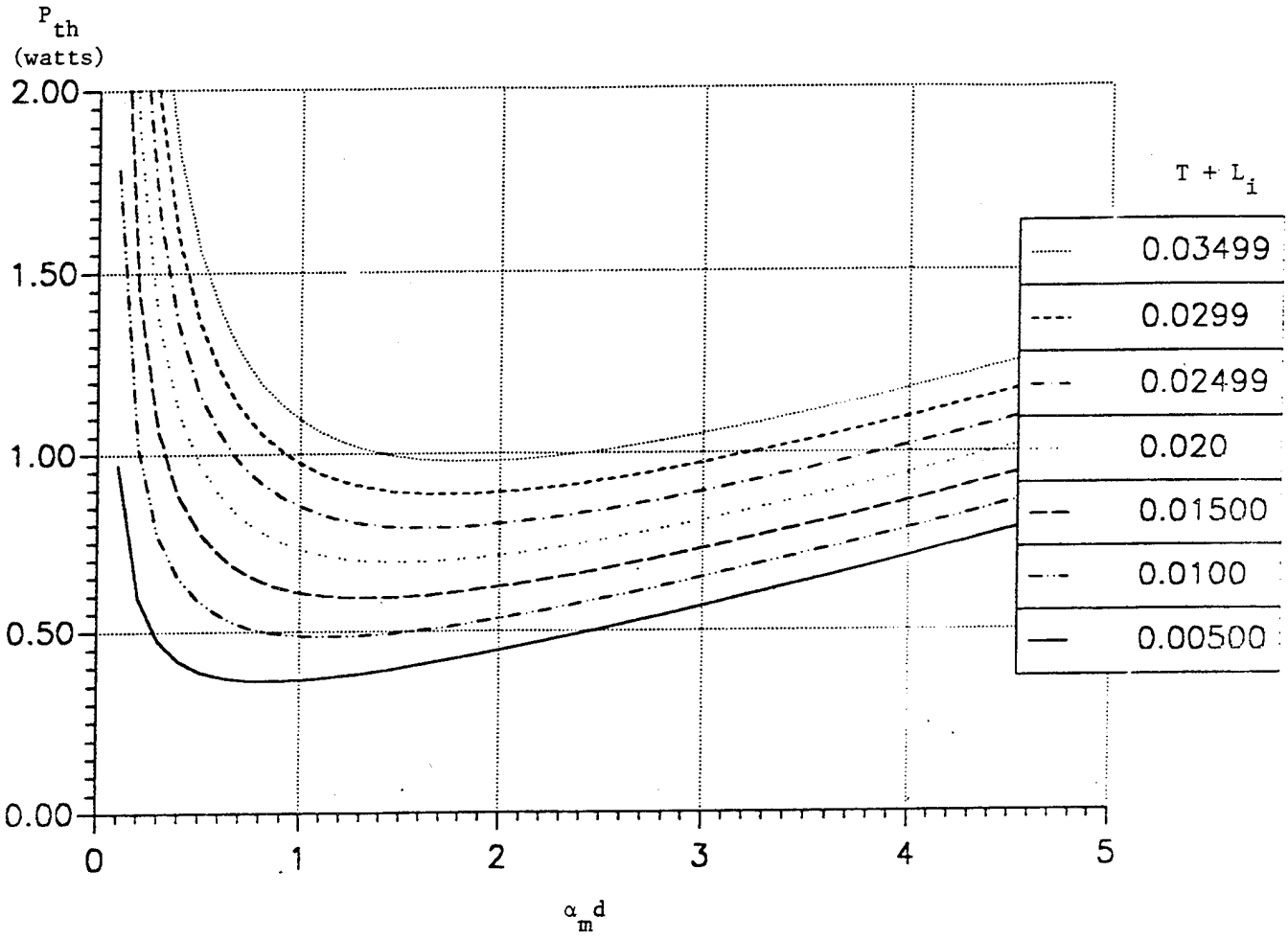

Figure 5. Dependence of Pump Threshold Power upon Laser Rod $\alpha_m d$ and Losses $T + L_i$.
FOM = 200. W = 50 μm.

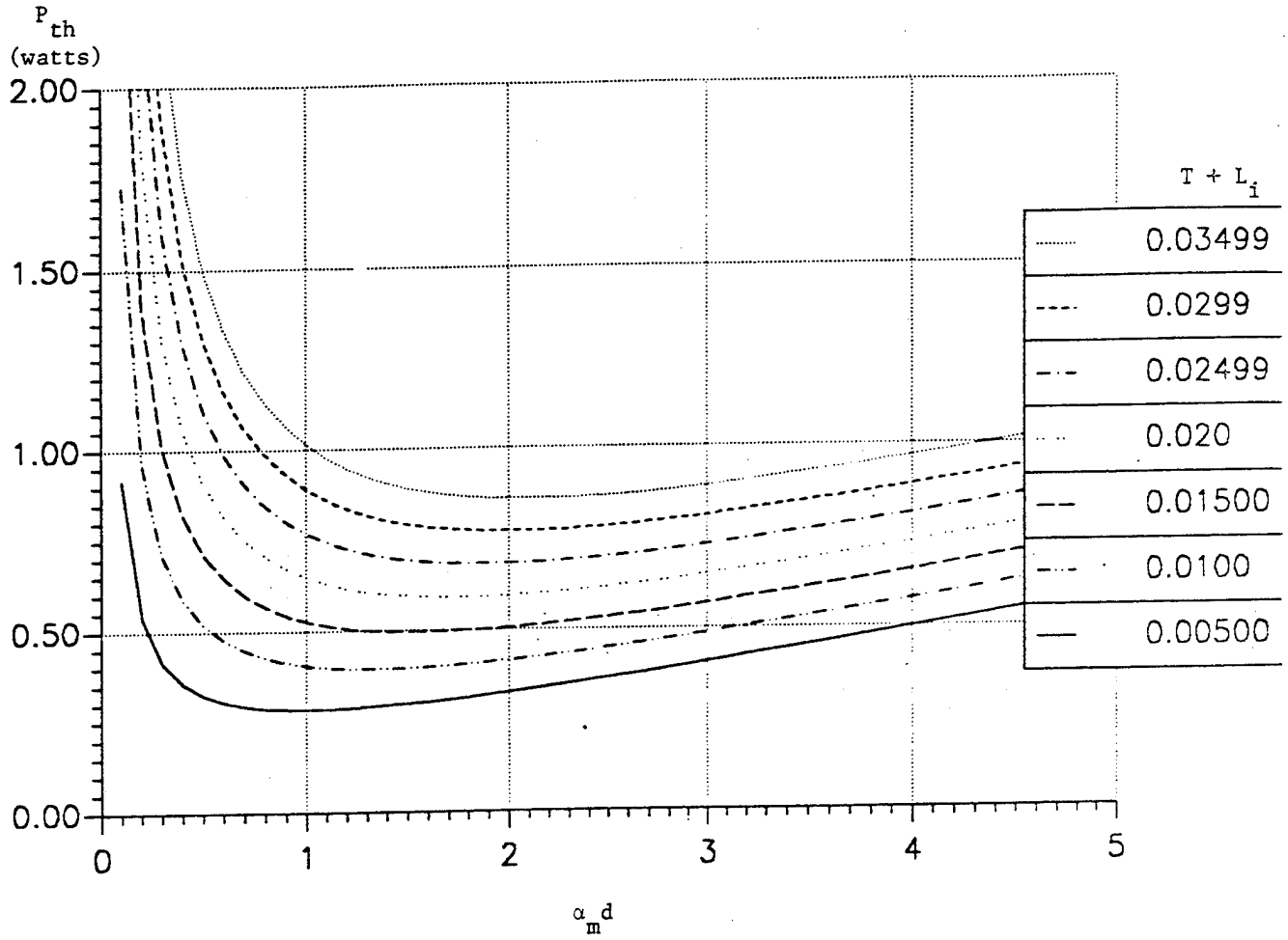

Figure 6. Dependence of Pump Threshold Power upon Laser Rod $\alpha_m d$ and Losses $T + L_i$.
FOM = 300. W = 50 μm.

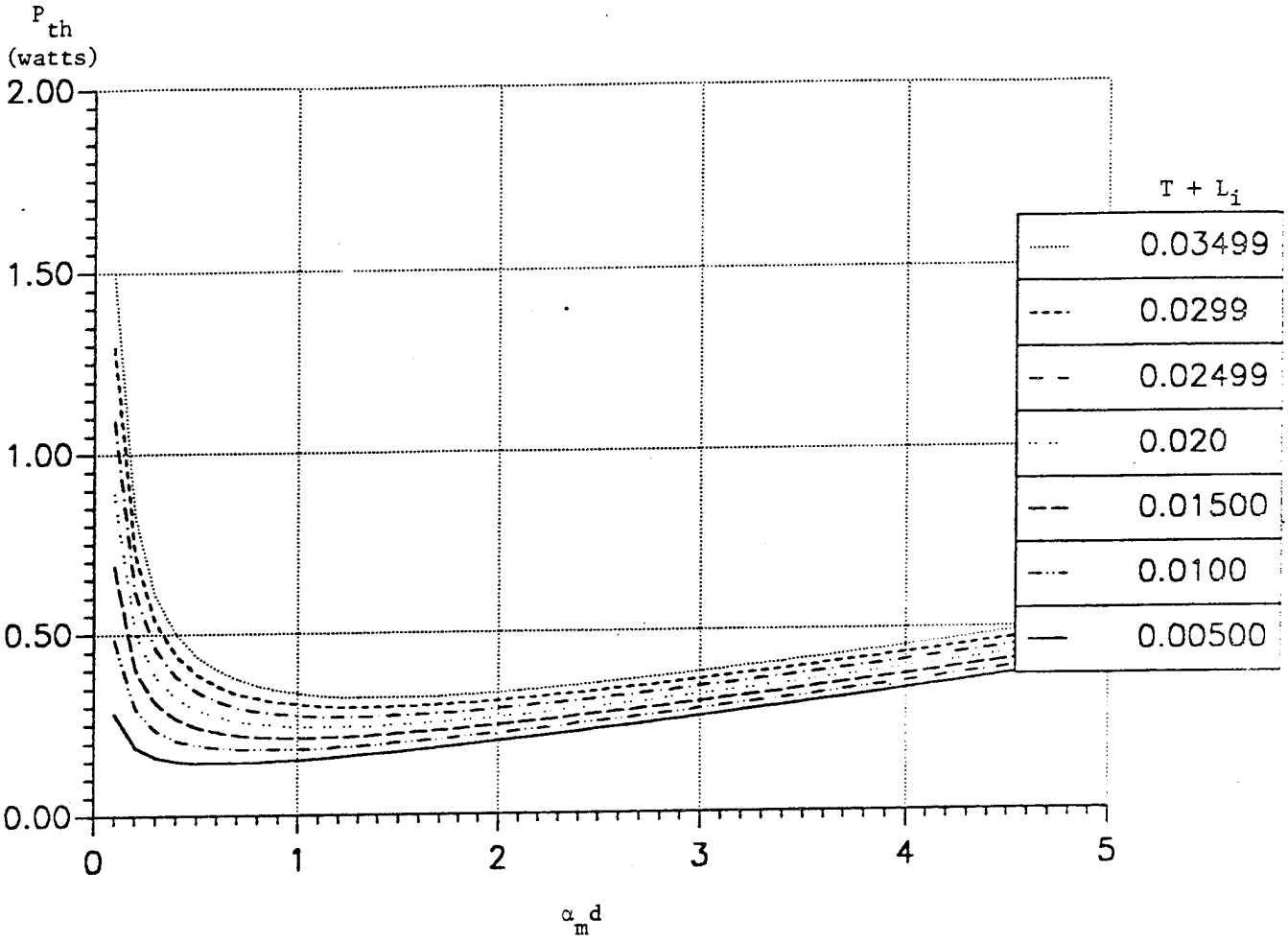

Figure 7. Dependence of Pump Threshold Power upon Laser Rod $\alpha_m d$ and Losses $T + L_i$.
FOM = 100. W = 25 μm.

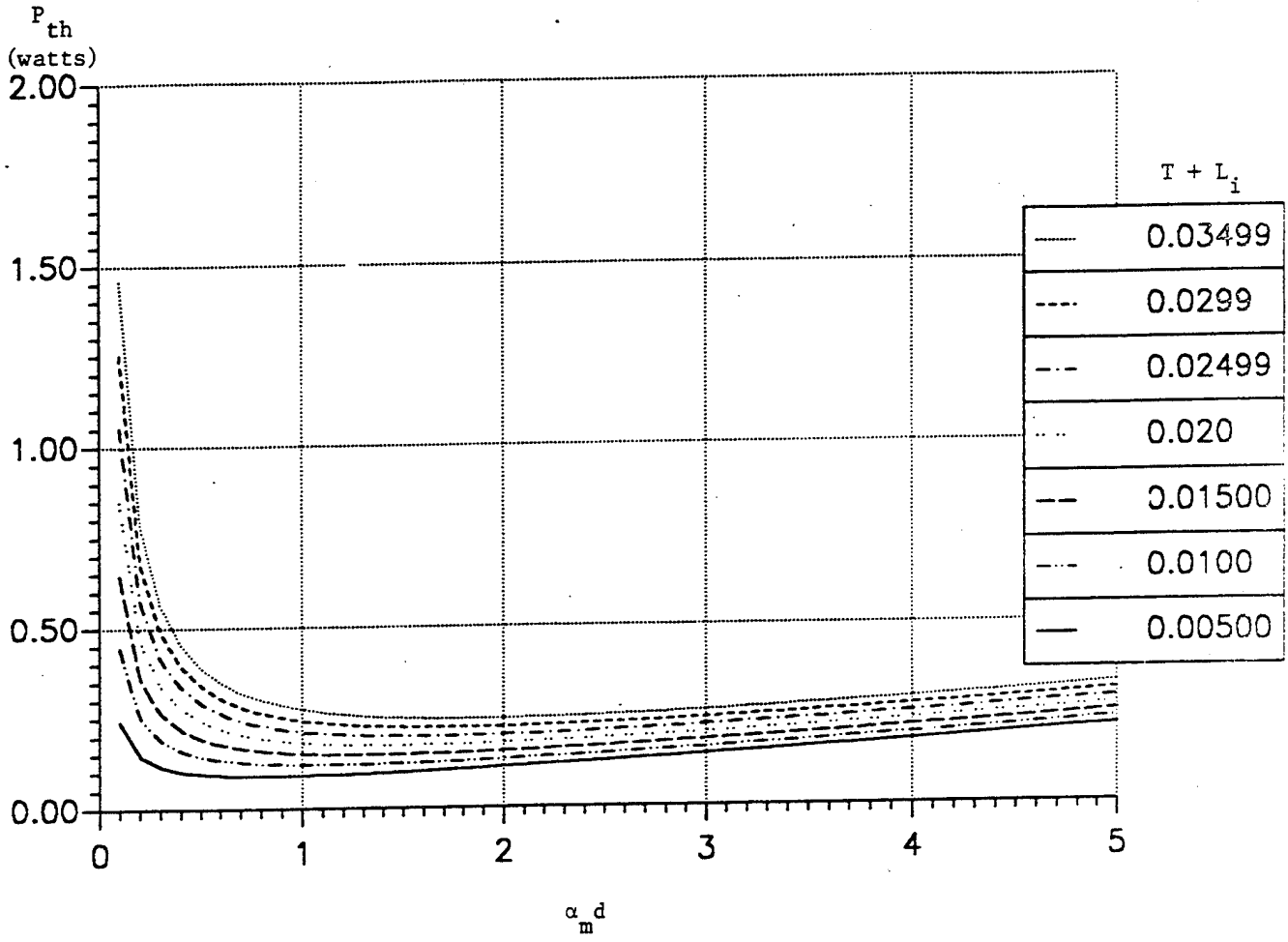

Figure 8. Dependence of Pump Threshold Power upon Laser Rod $\alpha_m d$ and Losses $T + L_i$.
FOM = 200. W = 25 μm.

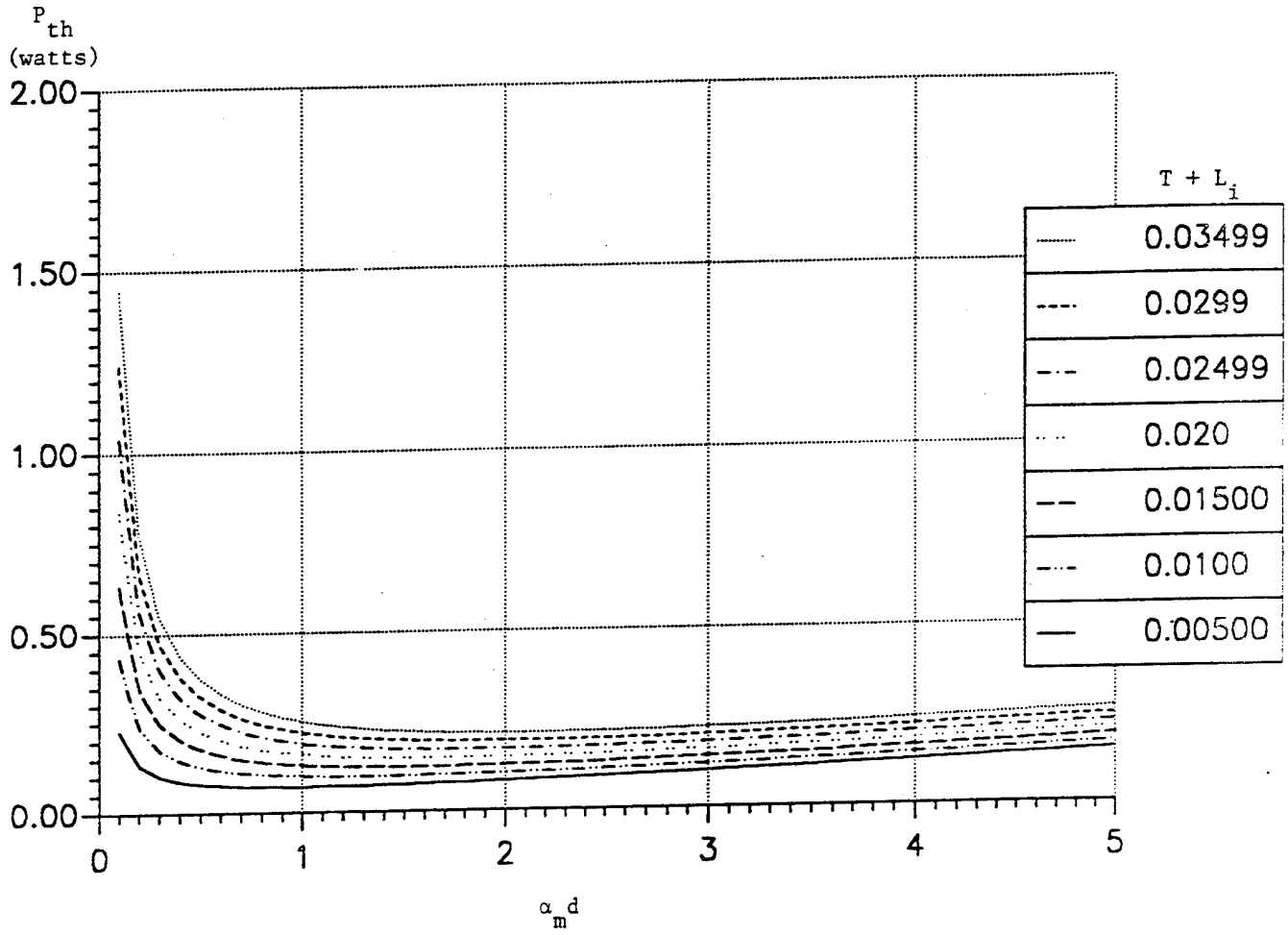

Figure 9. Dependence of Pump Threshold Power upon Laser Rod $\alpha_m d$ and Losses $T + L_i$.
FOM = 300. W = 25 μm.

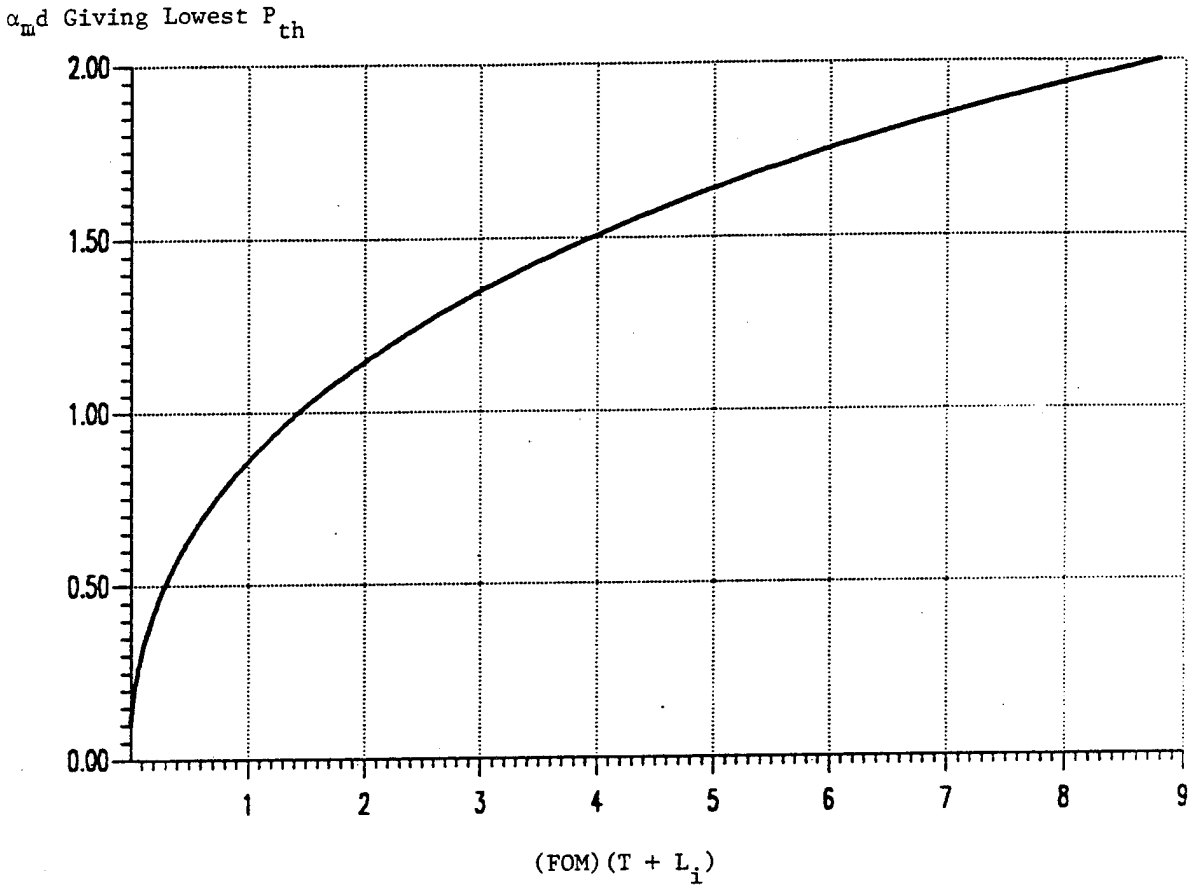

Figure 10. The Value of Laser Rod $\alpha_m d$ That Will Give Lowest Pump Threshold Power, P_{th}. General Curve.

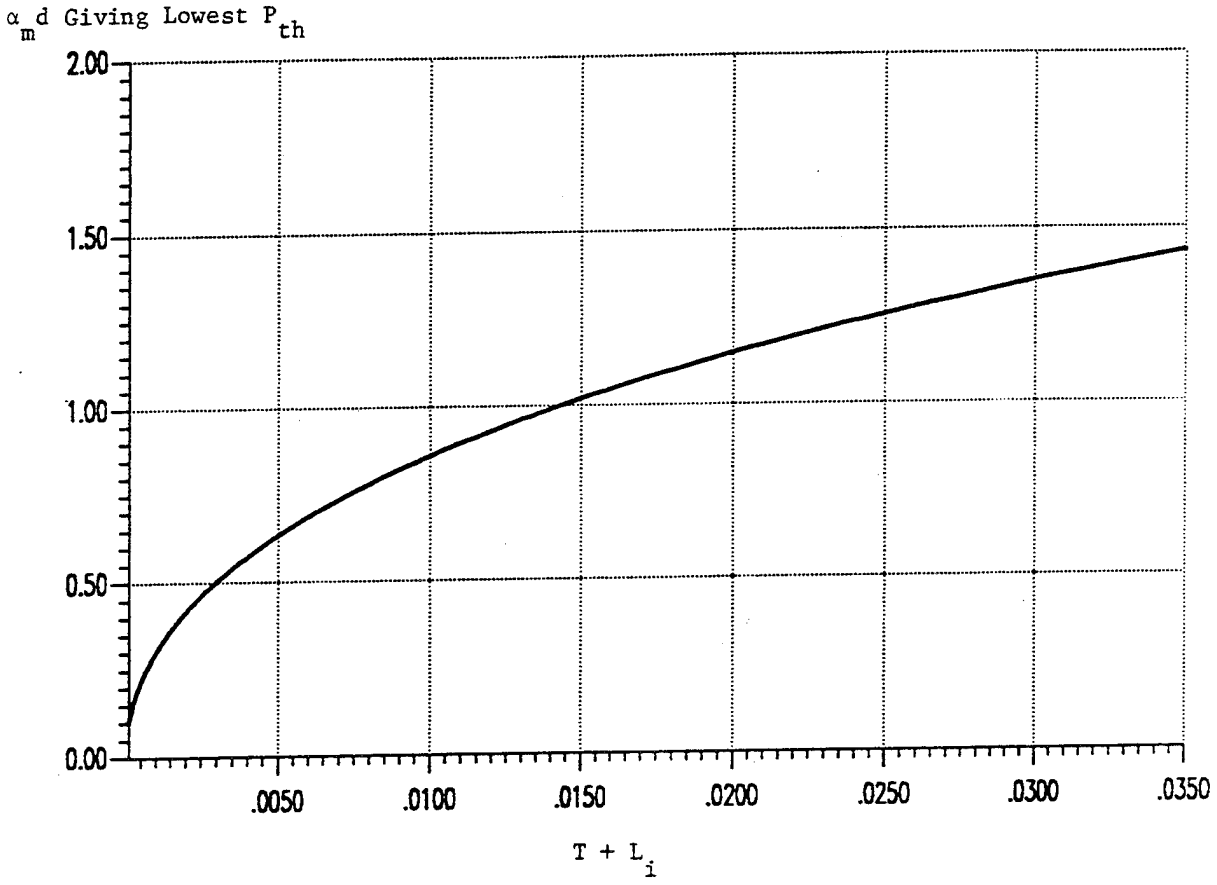

Figure 11. The Value of Laser Rod $\alpha_m d$ That Will Give Lowest Pump Threshold Power, P_{th}.
FOM = 100.

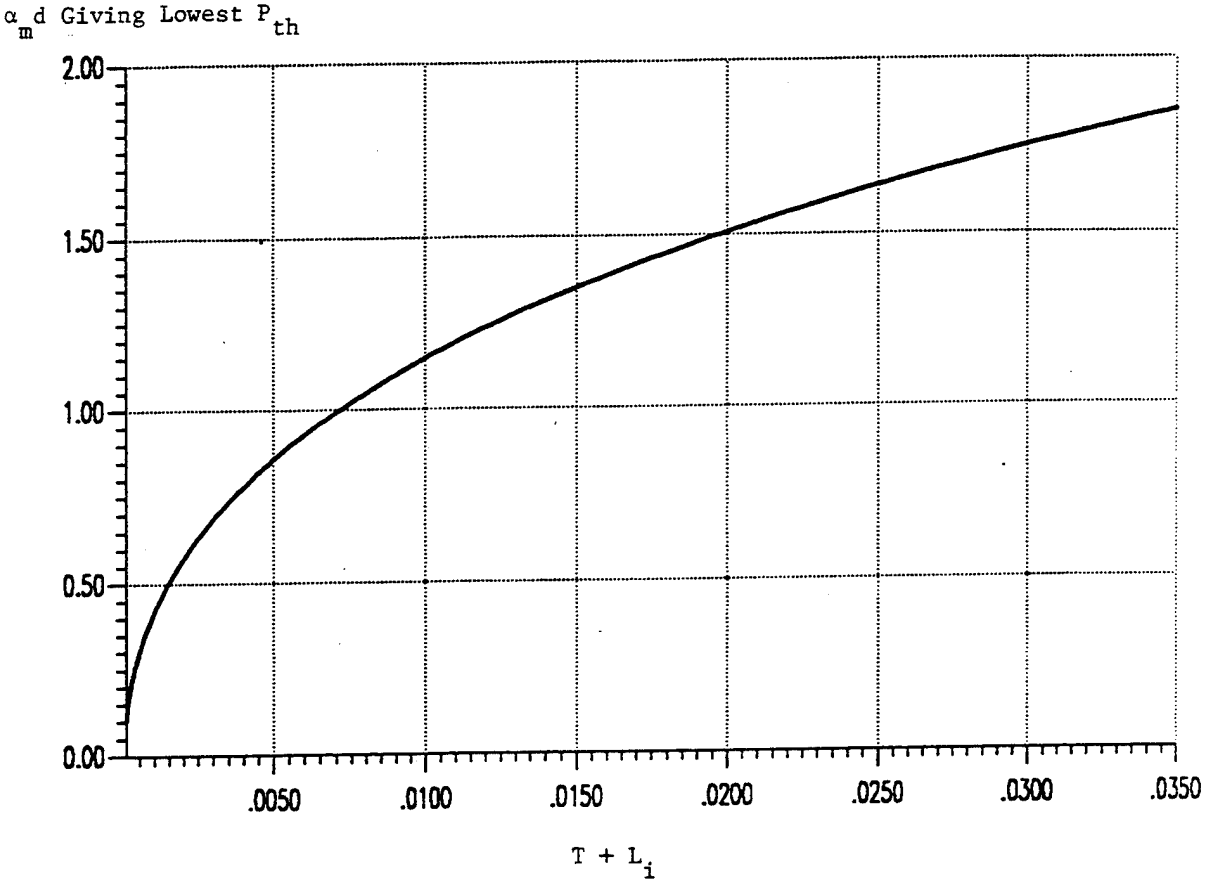

Figure 12. The Value of Laser Rod $\alpha_m d$ That Will Give Lowest Pump Threshold Power, P_{th}.
FOM = 200.

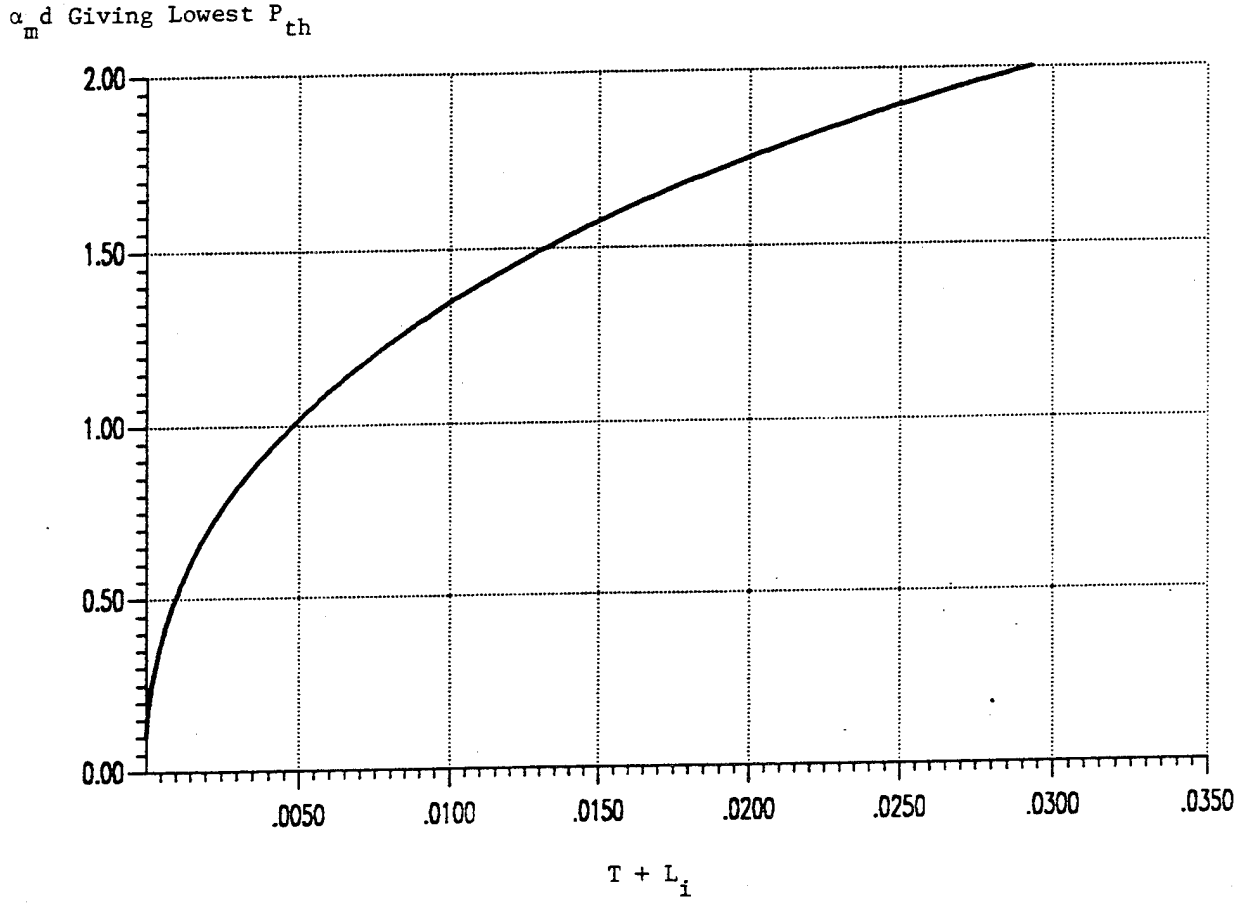

Figure 13. The Value of Laser Rod $\alpha_m d$ That Will Give Lowest Pump Threshold Power, P_{th}.
FOM = 300.

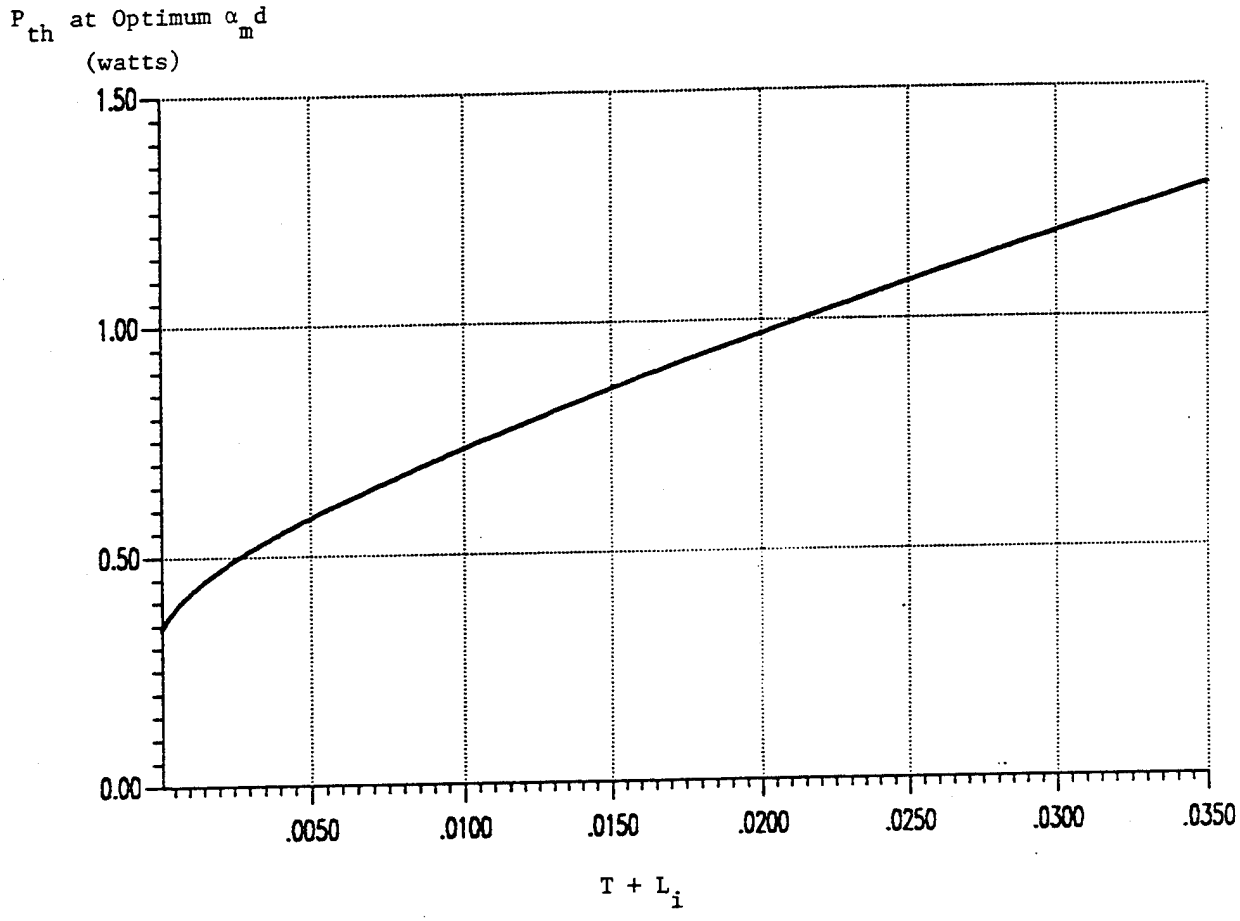

Figure 14. Dependence of Pump Threshold Power at Optimum $\alpha_m d$ upon the Losses $T + L_i$.
FOM = 100. W = 50 μm.

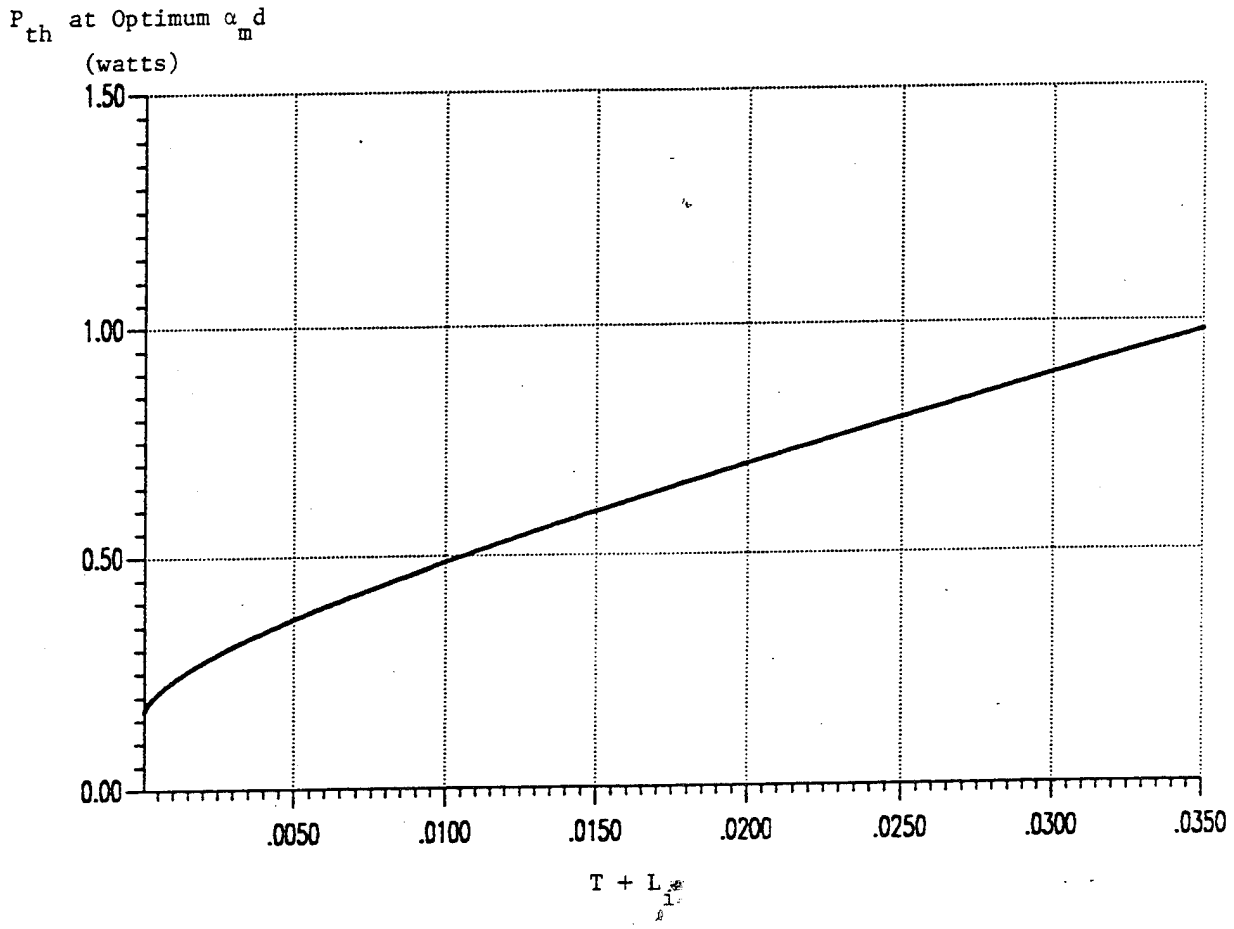

Figure 15. Dependence of Pump Threshold Power at Optimum $\alpha_m d$ upon the Losses $T + L_i$.
FOM = 200. W = 50 μm.

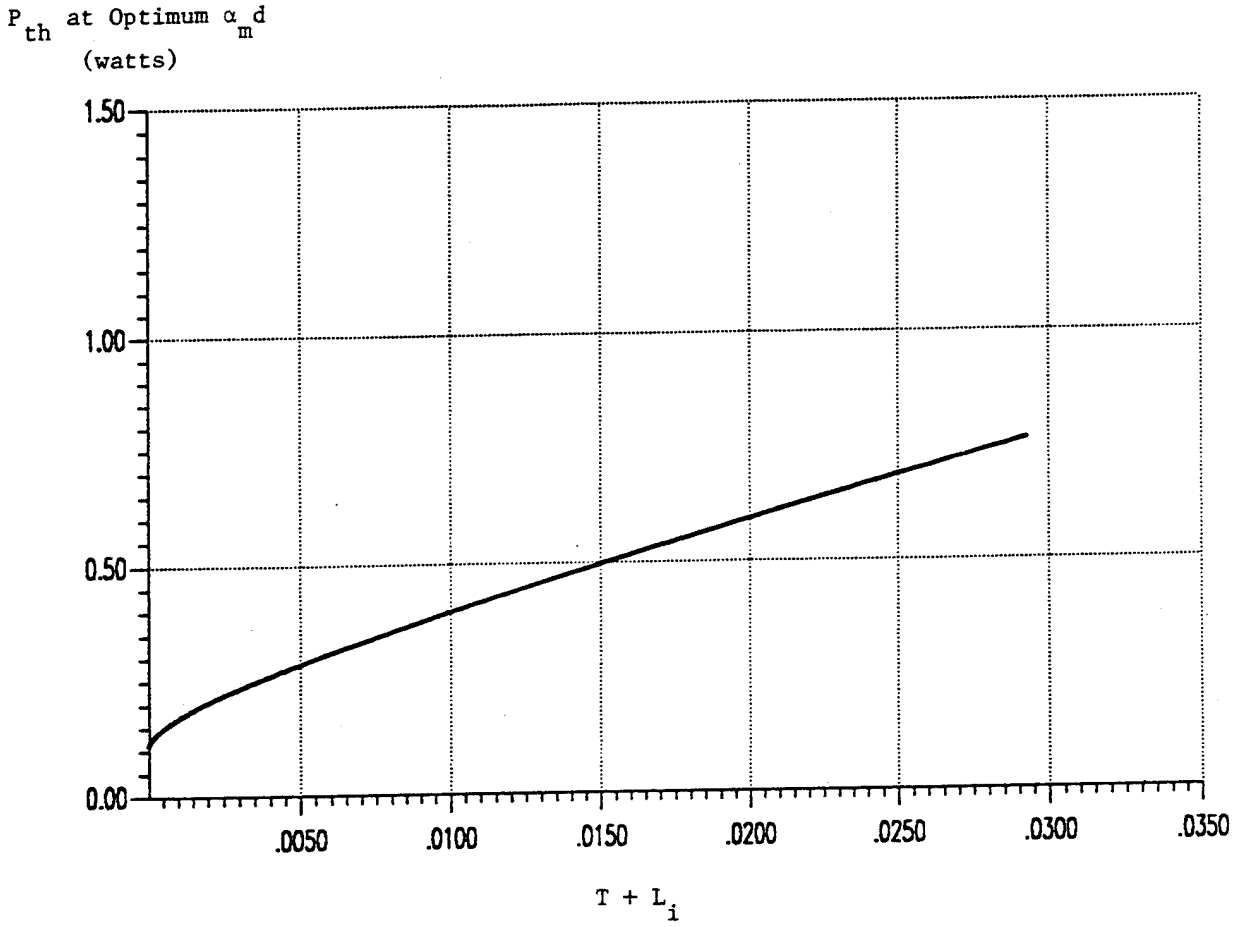

Figure 16. Dependence of Pump Threshold Power at Optimum $\alpha_m d$ upon the Losses $T + L_i$.
FOM = 300. W = 50 μm.

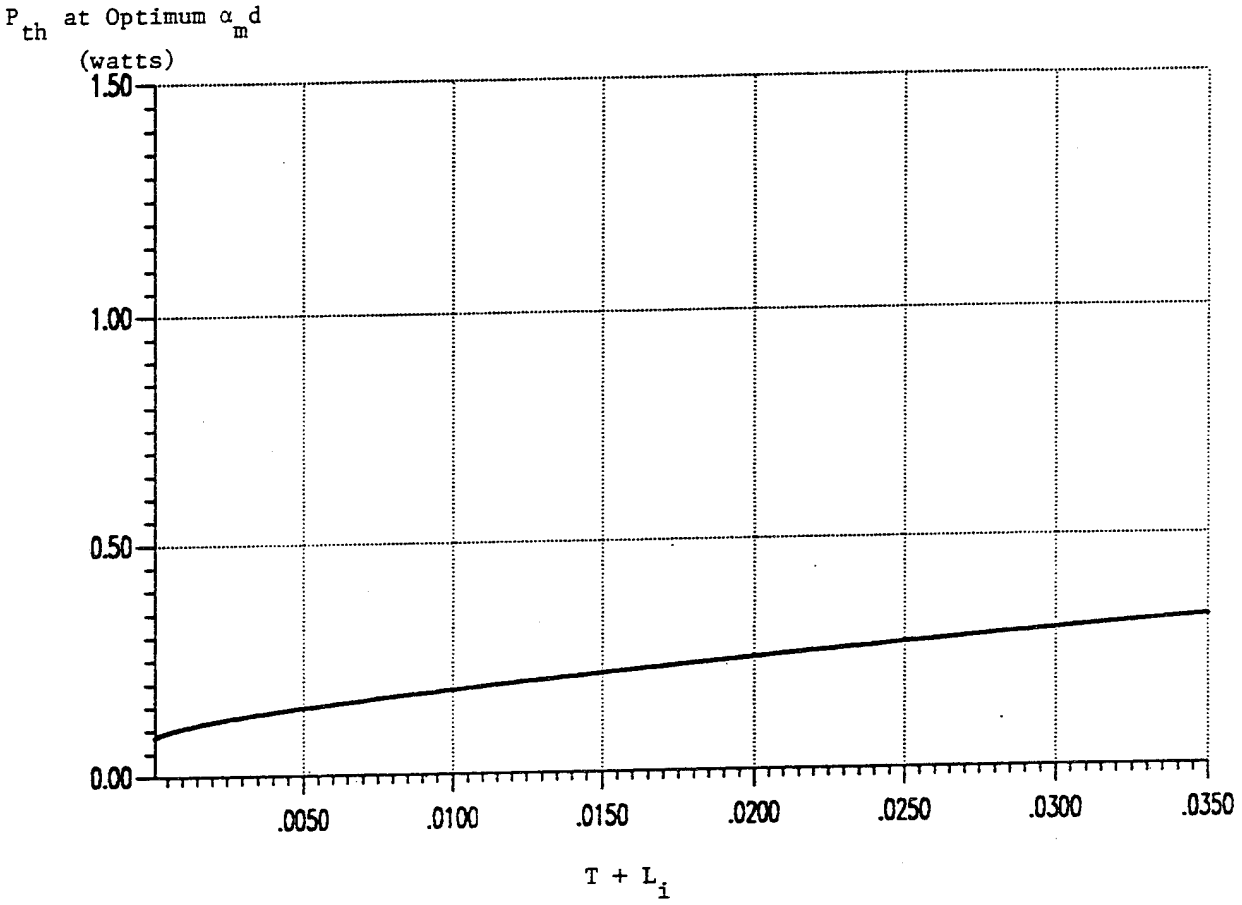

Figure 17. Dependence of Pump Threshold Power at Optimum $\alpha_m d$ upon the Losses $T + L_i$.
FOM = 100. W = 25 μm.

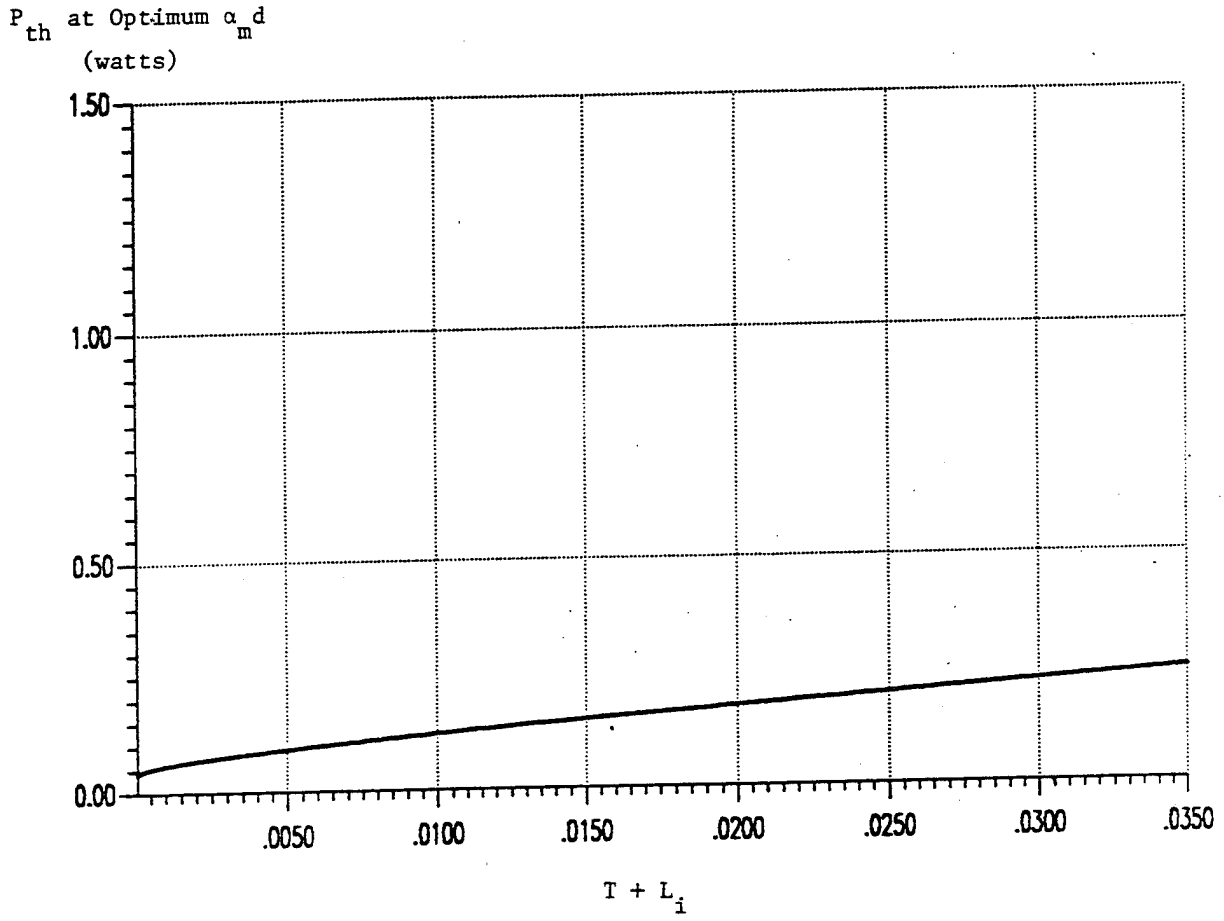

Figure 18. Dependence of Pump Threshold Power at Optimum $\alpha_m d$ upon the Losses $T + L_i$.
FOM = 200. W = 25 μm.

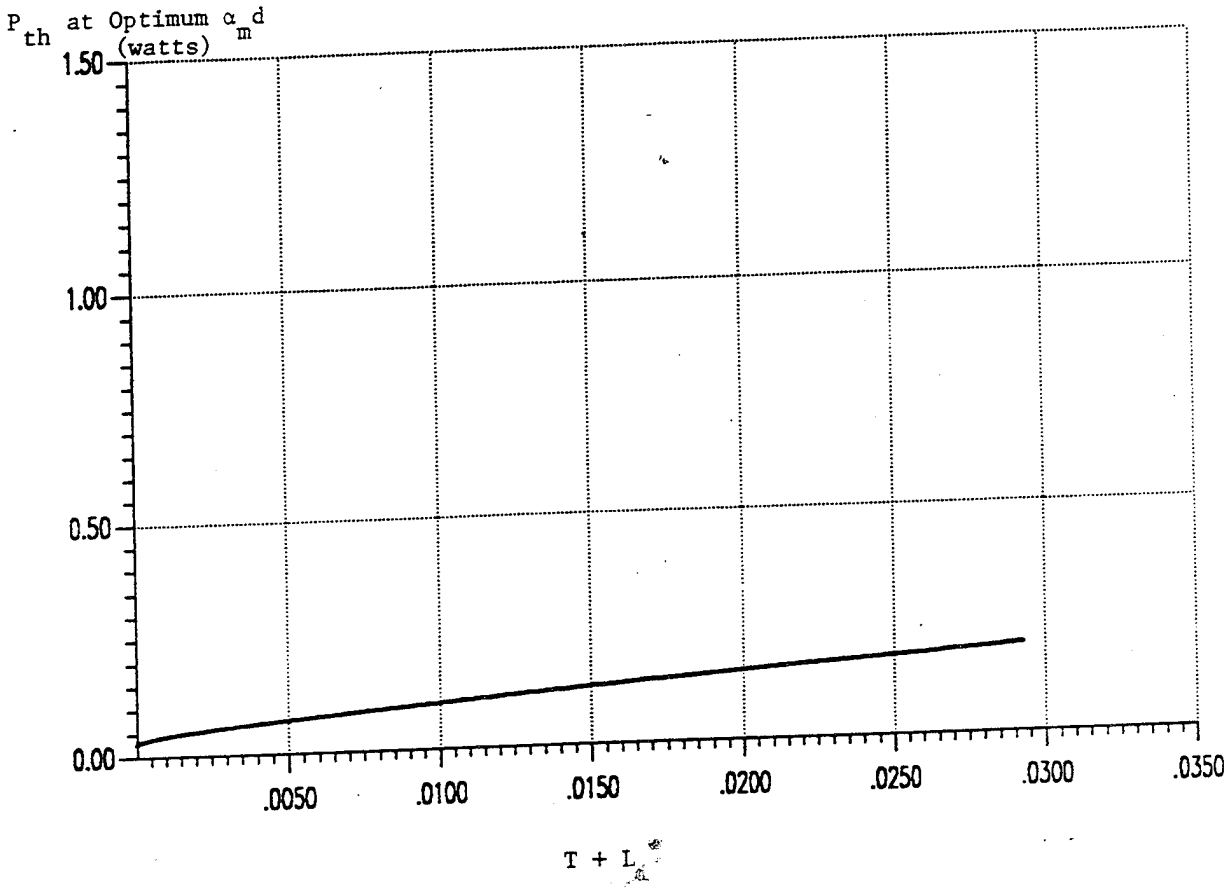

Figure 19. Dependence of Pump Threshold Power at Optimum $\alpha_m d$ upon Losses $T + L_i$.
FOM = 300. W = 25 μm.

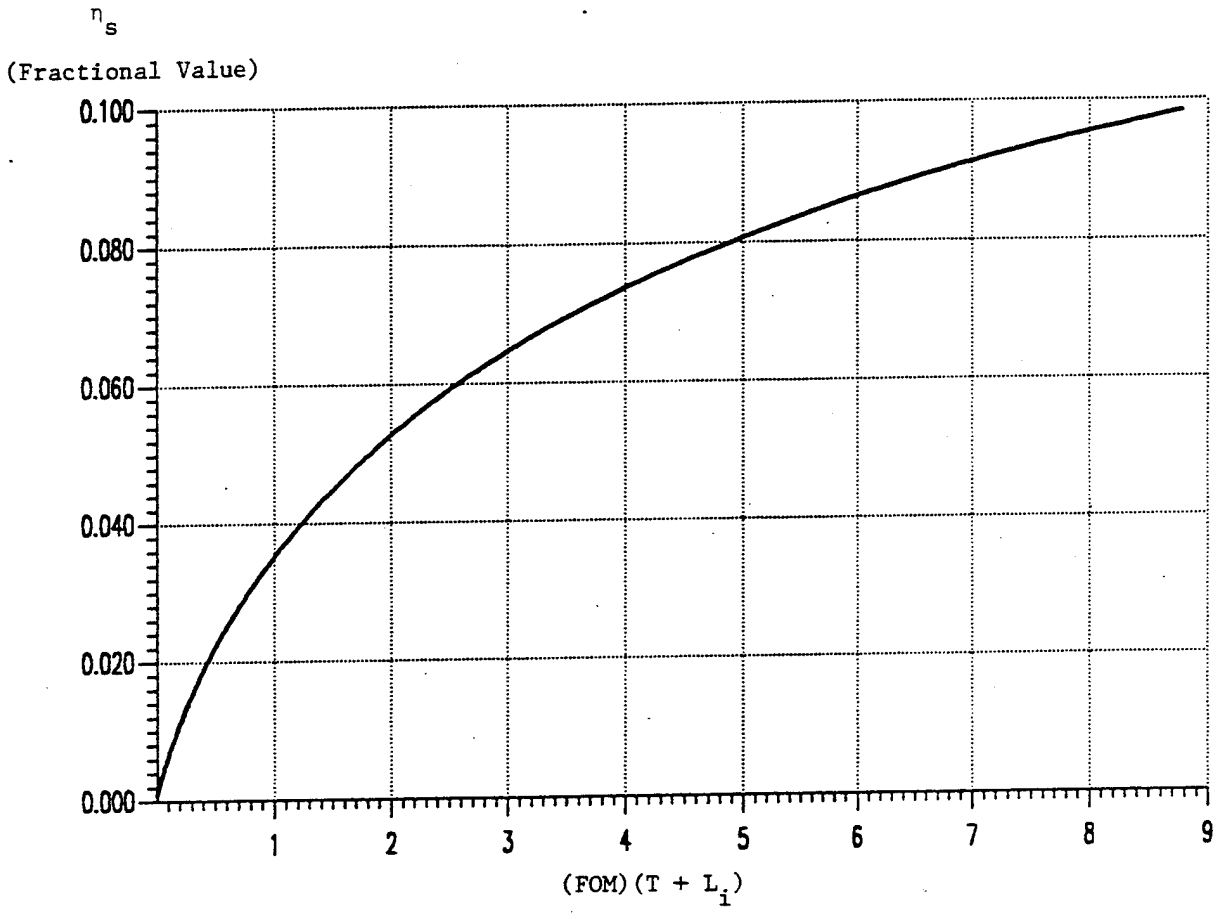

Figure 20. Slope Efficiency Dependence Upon (FOM)(T + L_i), Assuming $\alpha_m d$ is the Value That Minimizes P_{th} at Each T + L_i and That T = L_i. General Curve for all FOM's.

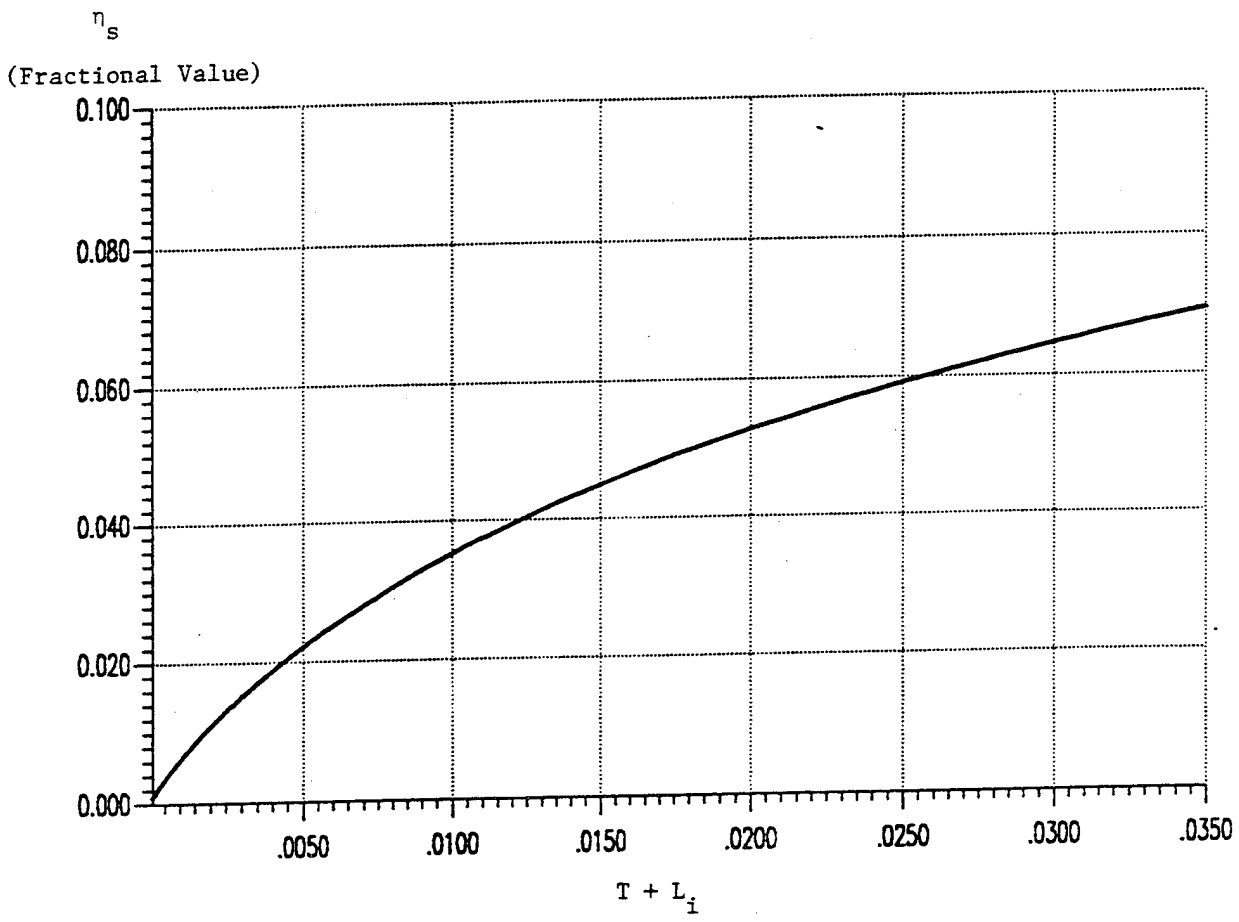

Figure 21. Slope Efficiency Dependence Upon $T + L_i$, Assuming $\alpha_m d$ is the Value That Minimizes P_{th} at Each $T + L_i$ and That $T = L_i$. FOM = 100.

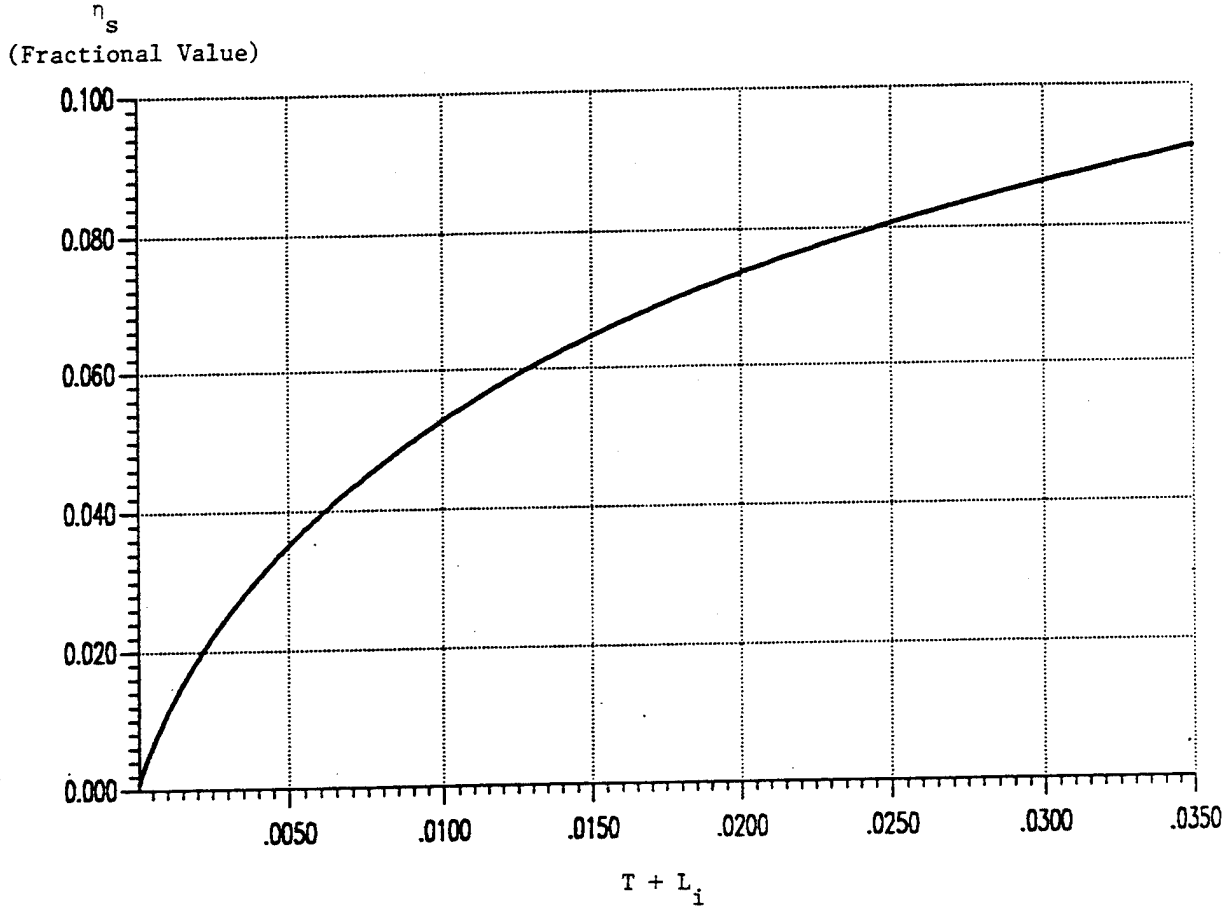

Figure 22. Slope Efficiency Dependence Upon T + L_i, A-suming $\alpha_m d$ is the Value That Minimizes P_{th} at Each T + L_i and That T = L_i. FOM = 200.

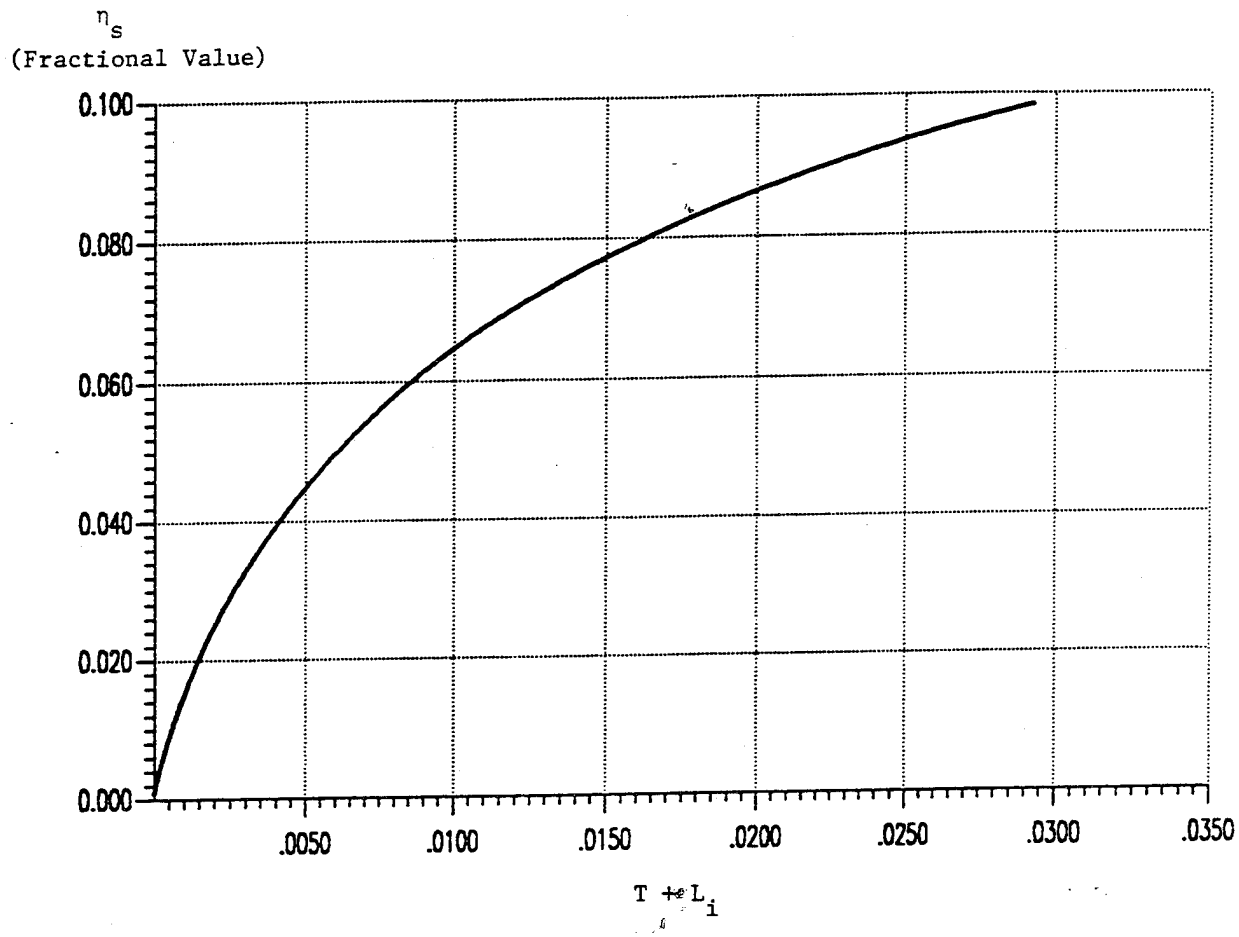

Figure 23. Slope Efficiency Dependence Upon $T + L_i$, Assuming $\alpha_m d$ is the Value That Minimizes P_{th} at Each $T + L_i$ and That $T = L_i$. FOM = 300.

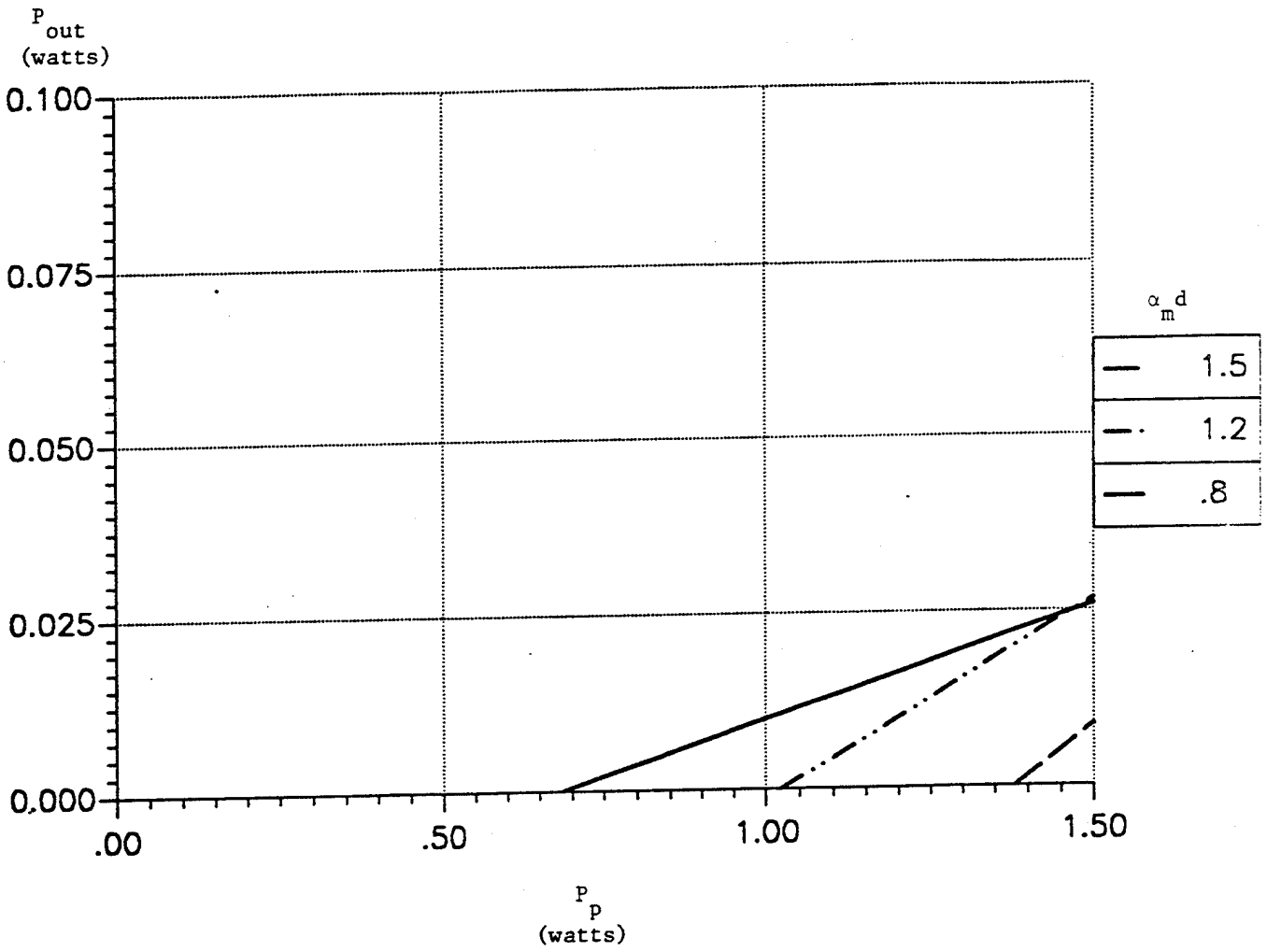

Figure 24. Power Output When the $\alpha_m d$ -- T + L_i Combination is That Which Gives Lowest Pump Threshold Power at the Given $\alpha_m d$, and T = L_i. FOM = 100. W = 50 μm.

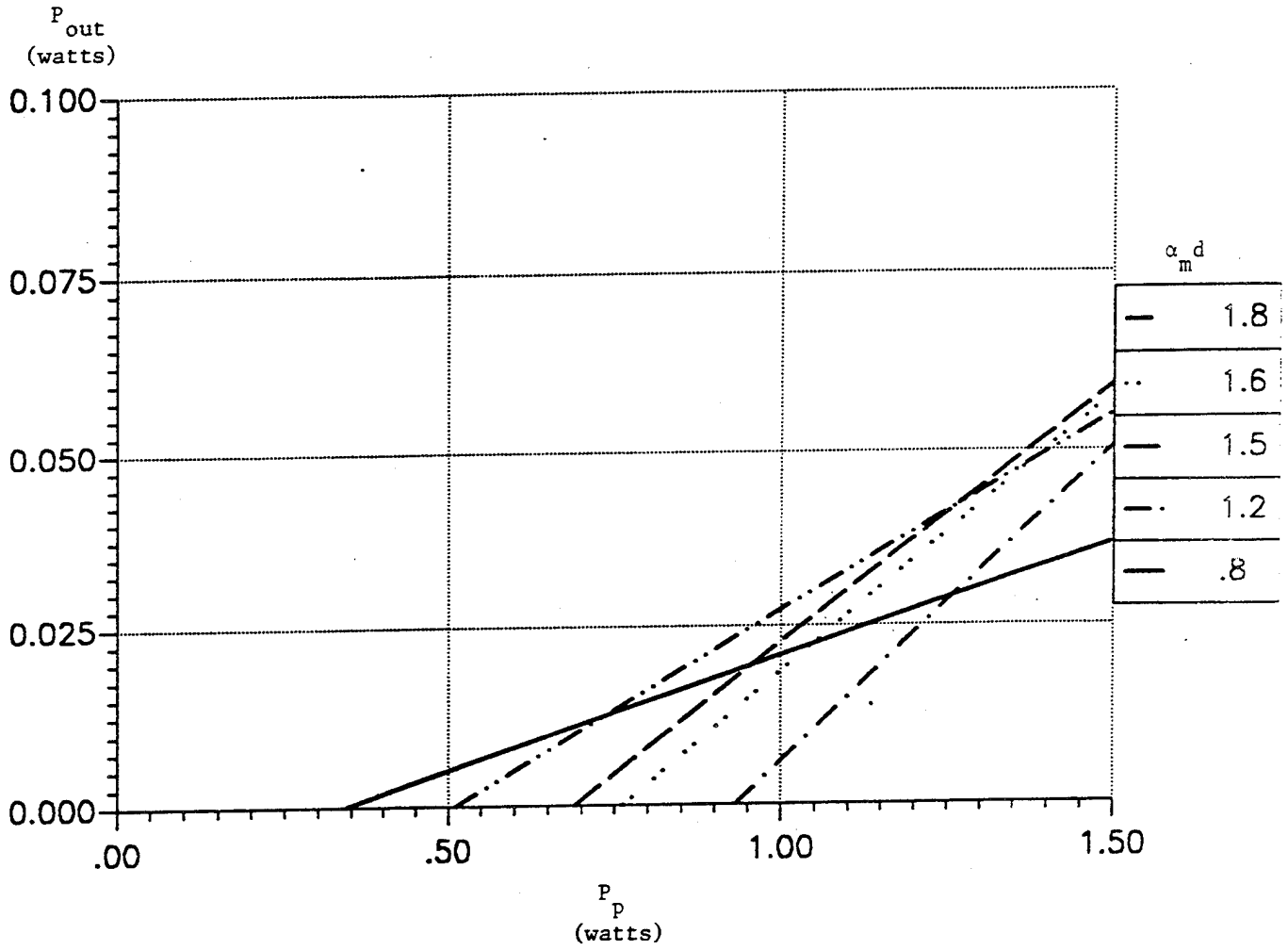

Figure 25. Power Output When the $\alpha_m d$ -- $T + L_i$ Combination is That Which Gives Lowest Pump Threshold Power at the Given $\alpha_m d$, and $T = L_i$. FOM = 200. W = 50 μm.

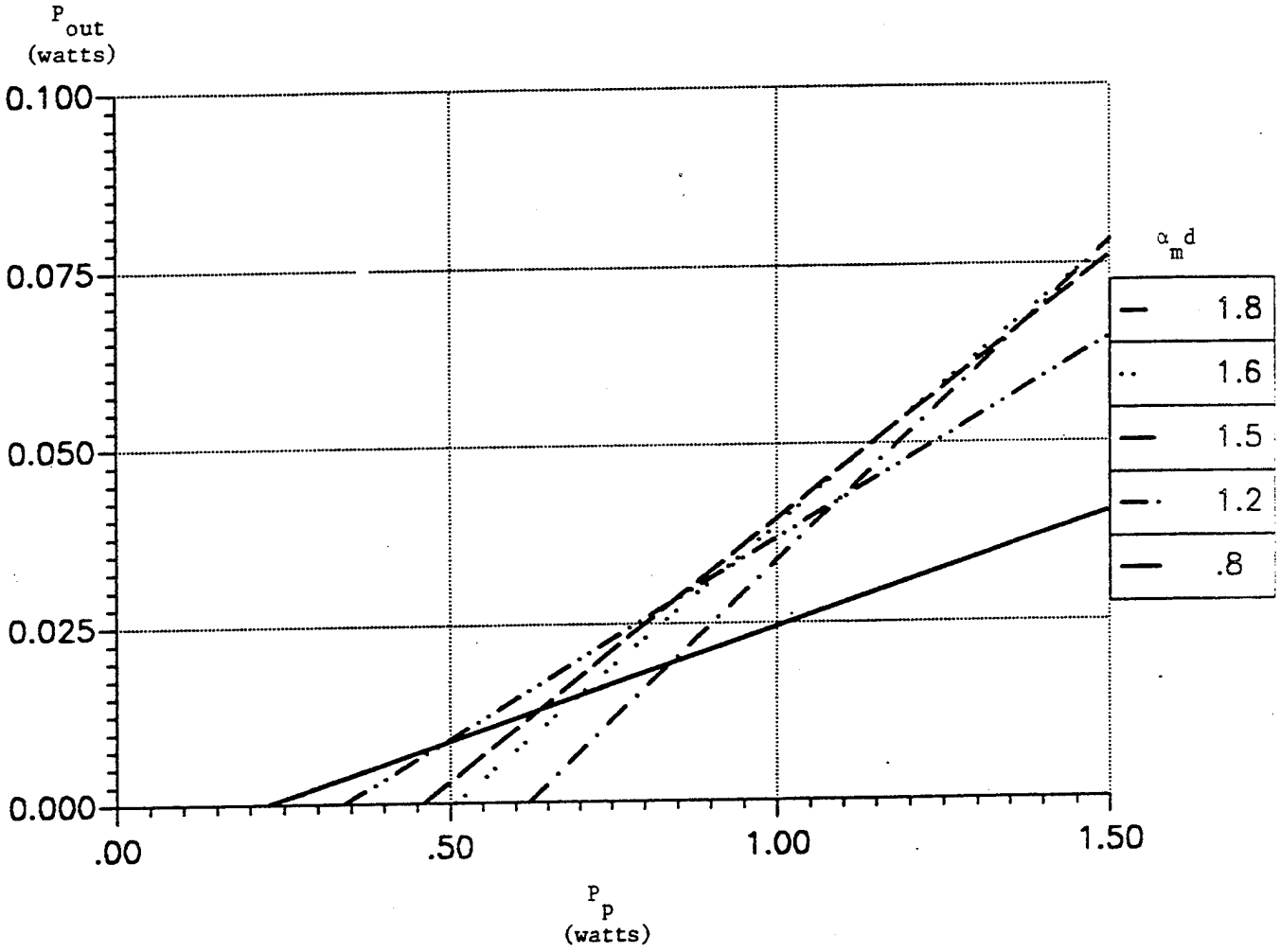

Figure 26. Power Output When the $\alpha_m d$ -- $T + L_i$ Combination is That Which Gives Lowest Pump Threshold Power at the Given $\alpha_m d$, and $T = L_i$. FOM = 300. W = 50 μm.

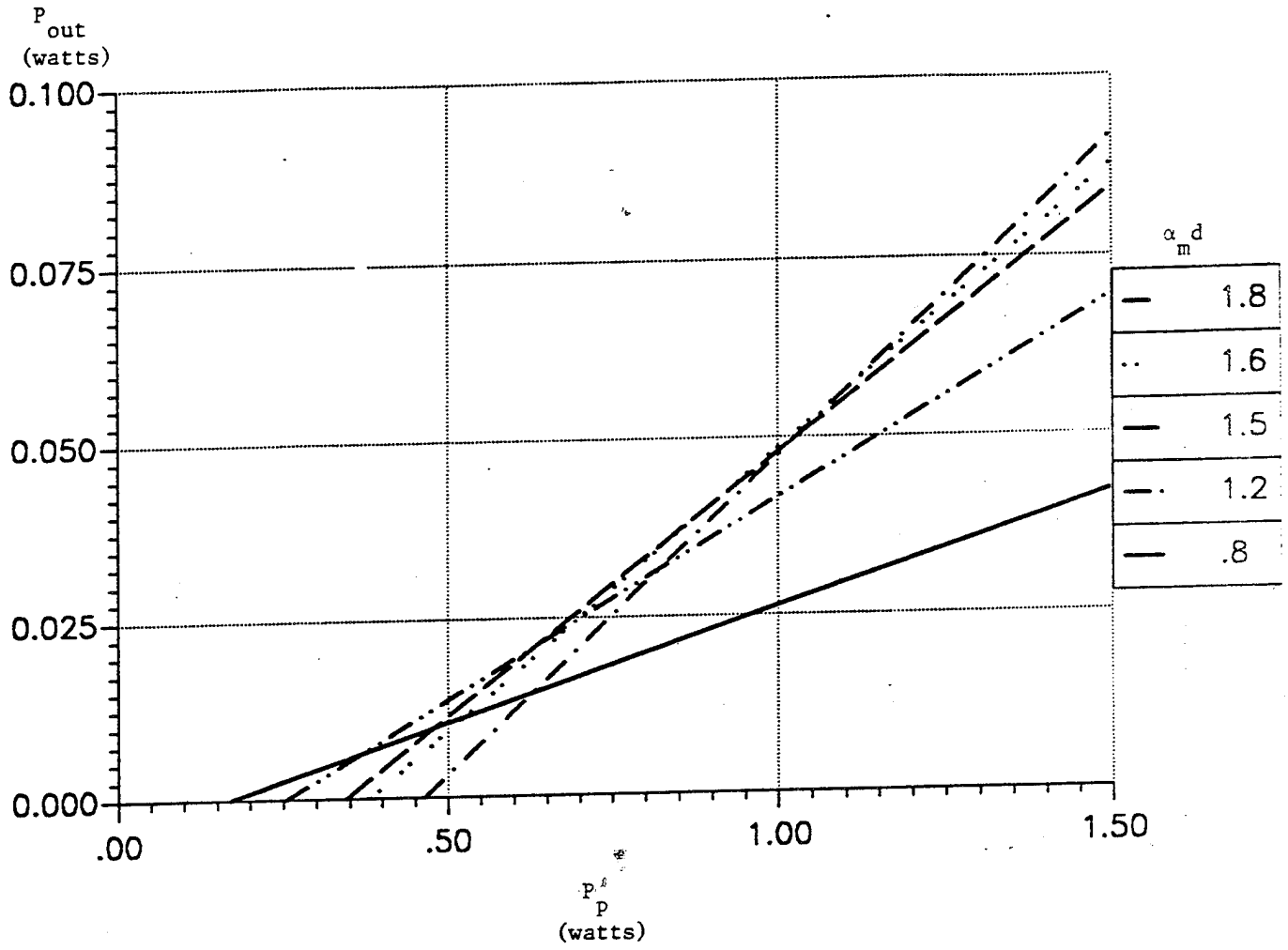

Figure 27. Power Output When the $\alpha_m d$ -- $T + L_i$ Combination is That Which Gives Lowest Pump Threshold Power at the Given $\alpha_m d$, and $T = L_i$. FOM = 100. W = 25 μm.

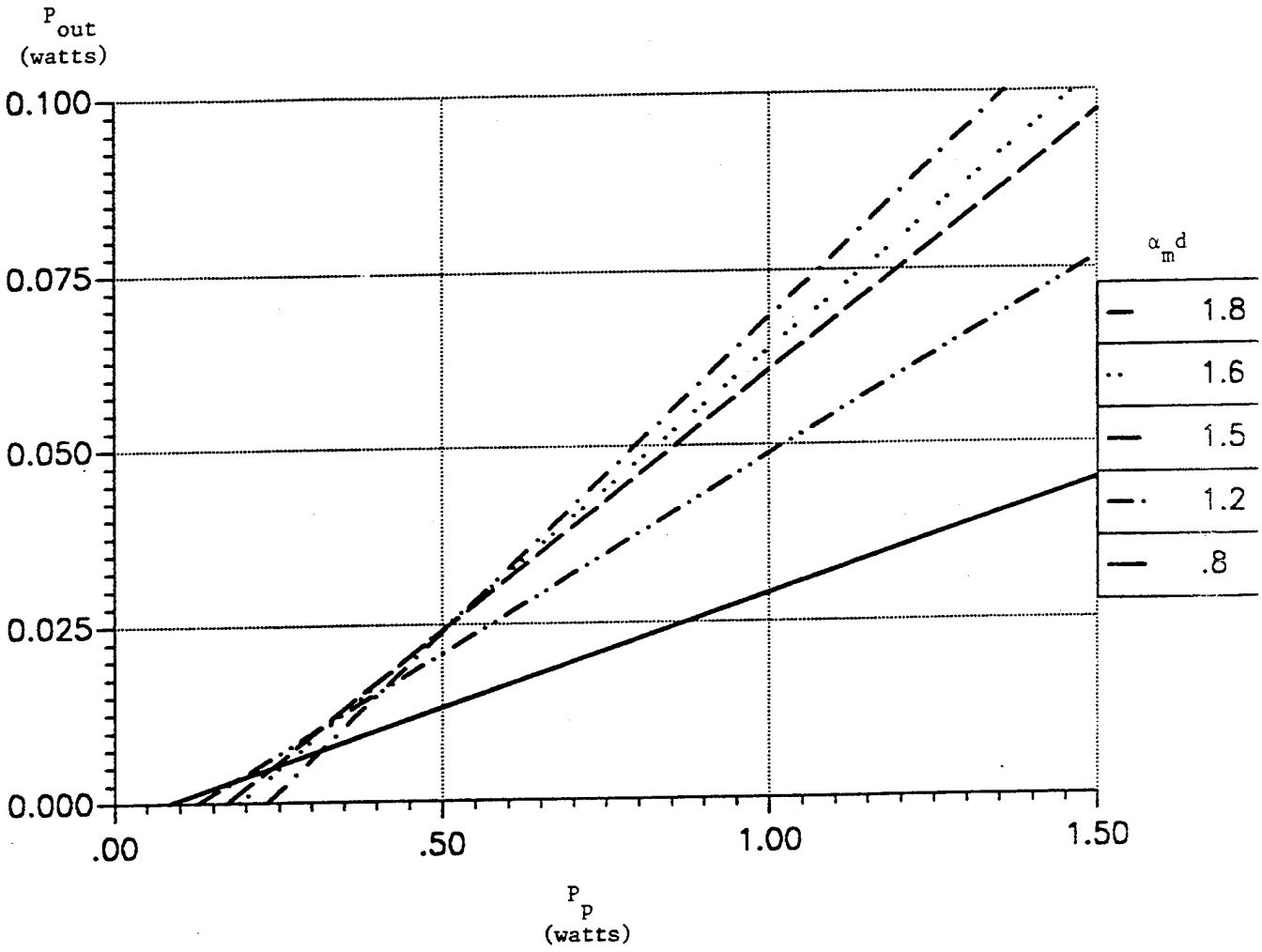

Figure 28. Power Output When the $\alpha_m d$ -- T + L_i Combination is That Which Gives Lowest Pump Threshold Power at the Given $\alpha_m d$, and T = L_i. FOM = 200. W = 25 μm.

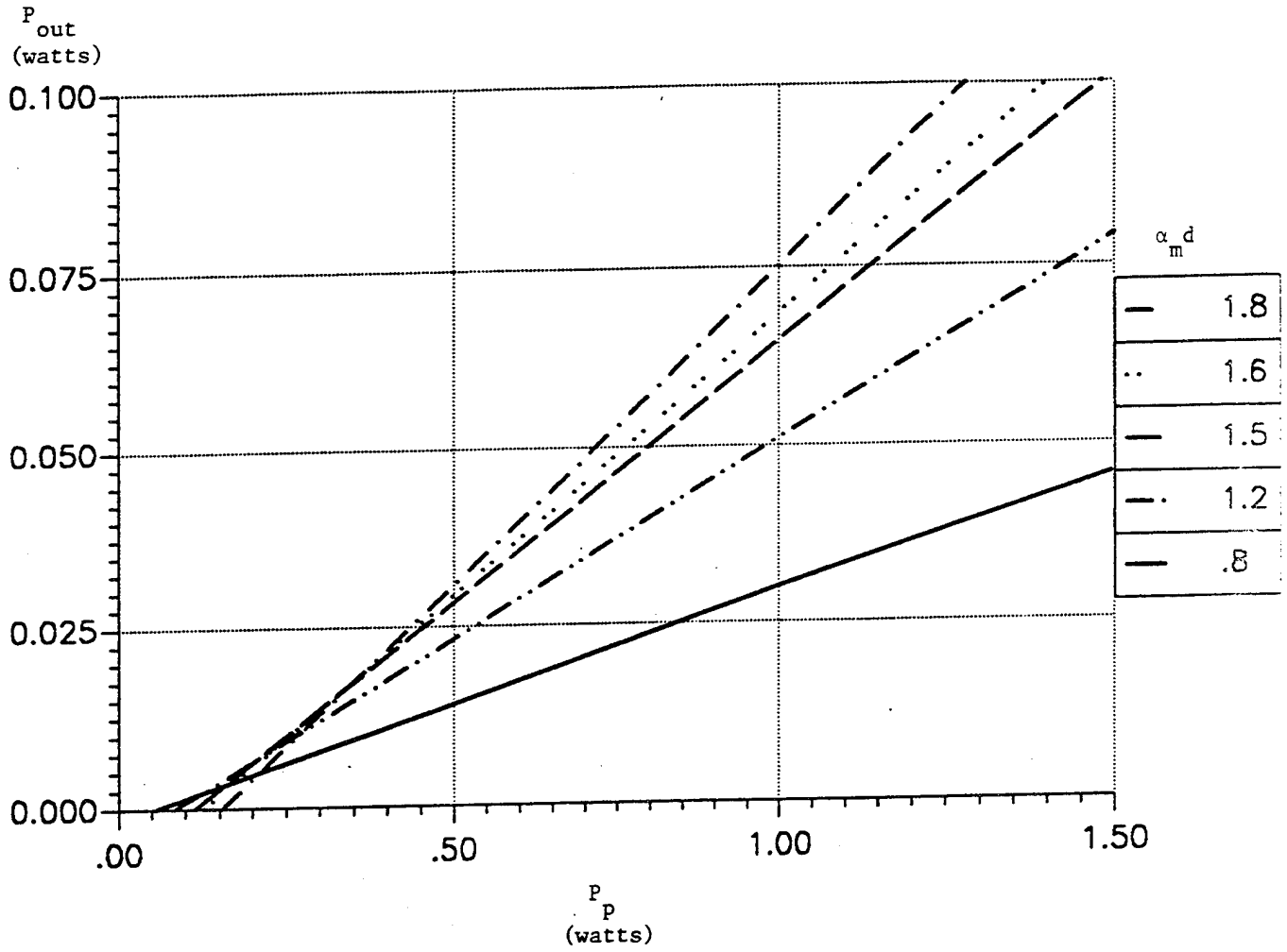

Figure 29. Power Output When the $\alpha_m d$ -- $T + L_i$ Combination is That Which Gives Lowest Pump Threshold Power at the Given $\alpha_m d$, and $T = L_i$. FOM = 300. W = 25 μm.

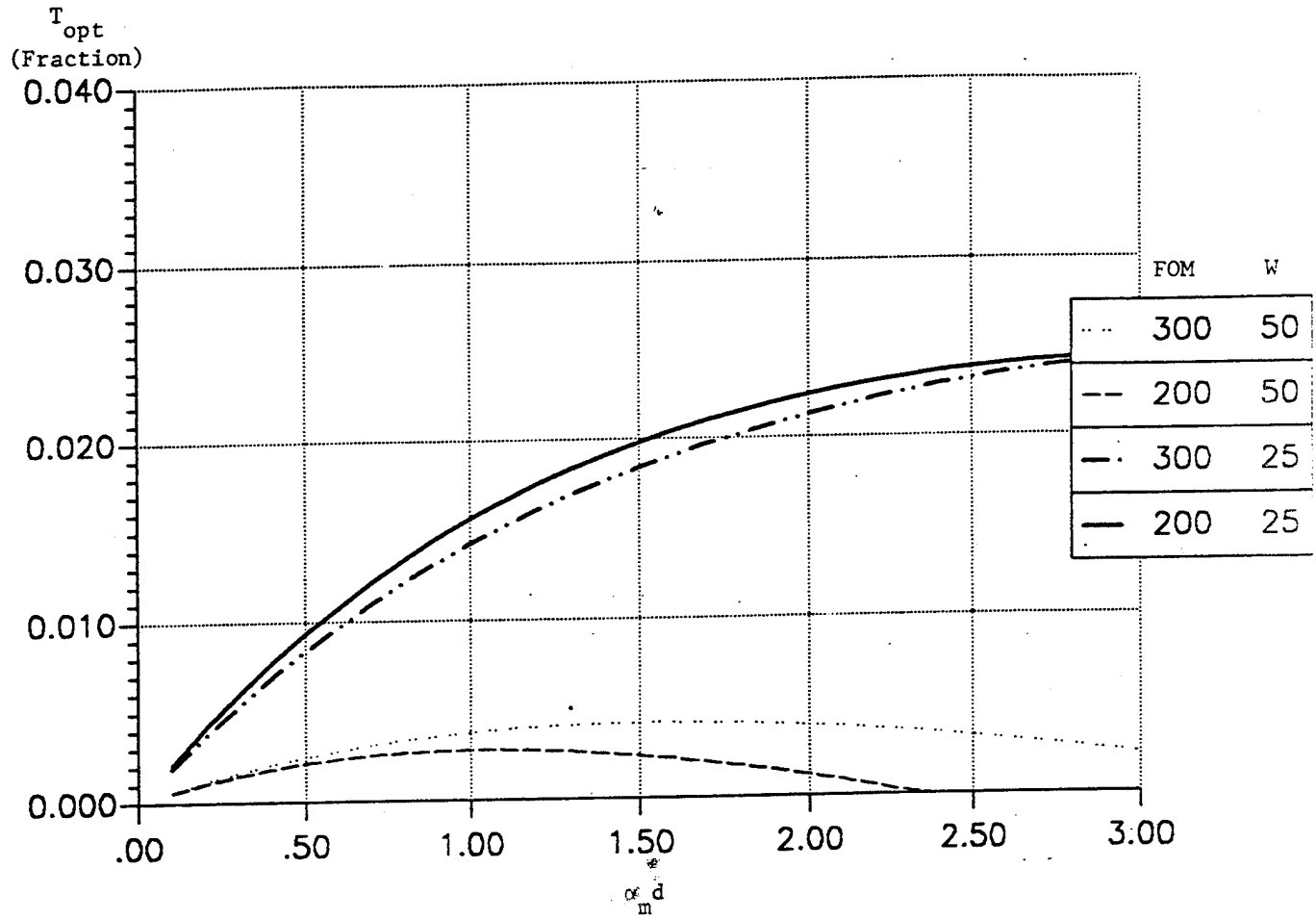

Figure 30. Optimum Coupling Dependence on $\alpha_m d$.
L_i = 0.0, Pump Power = 400 mw.

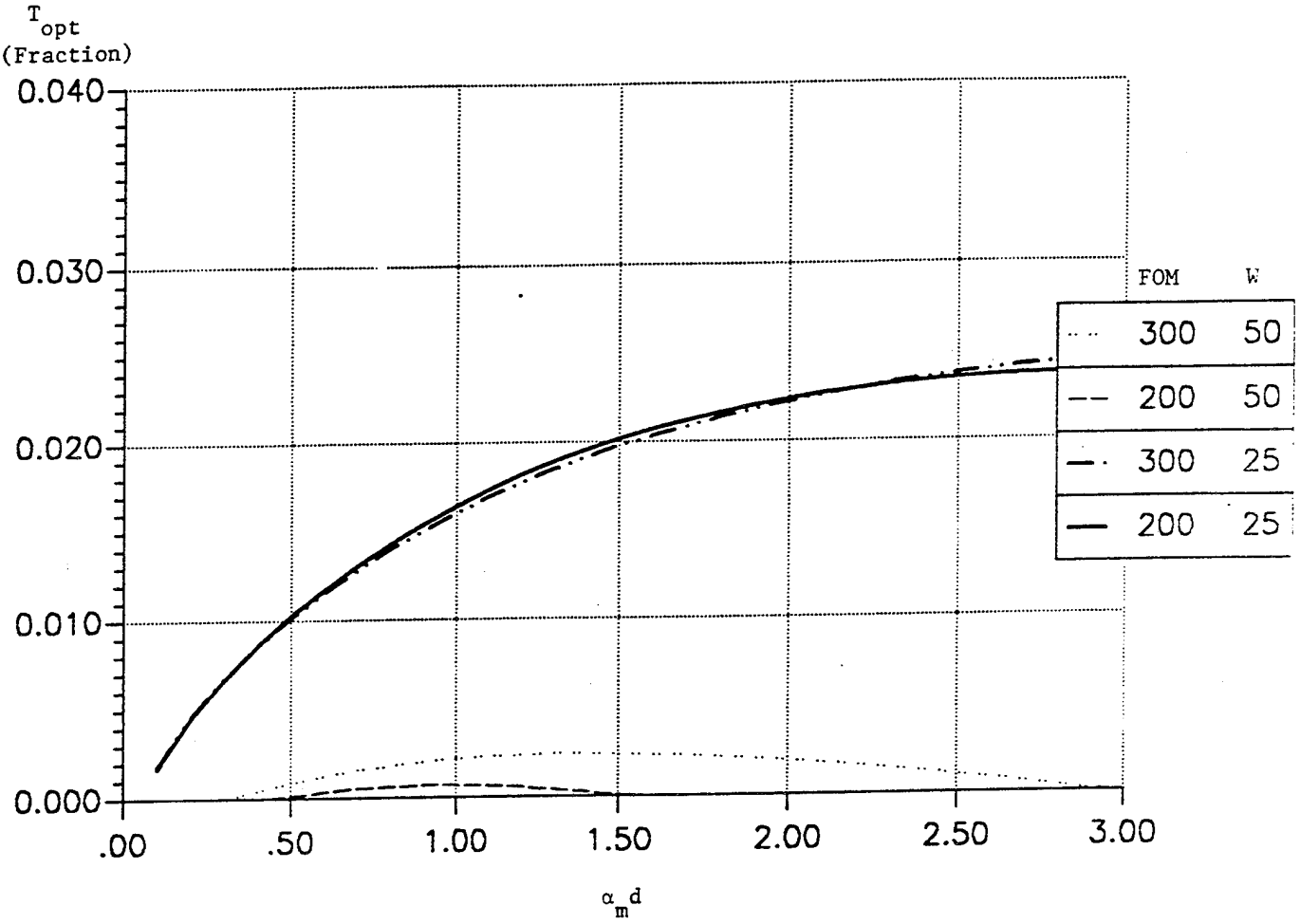

Figure 31. Optimum Coupling Dependence on $\alpha_m d$.
L_i = 0.005, Pump Power = 400 mw.

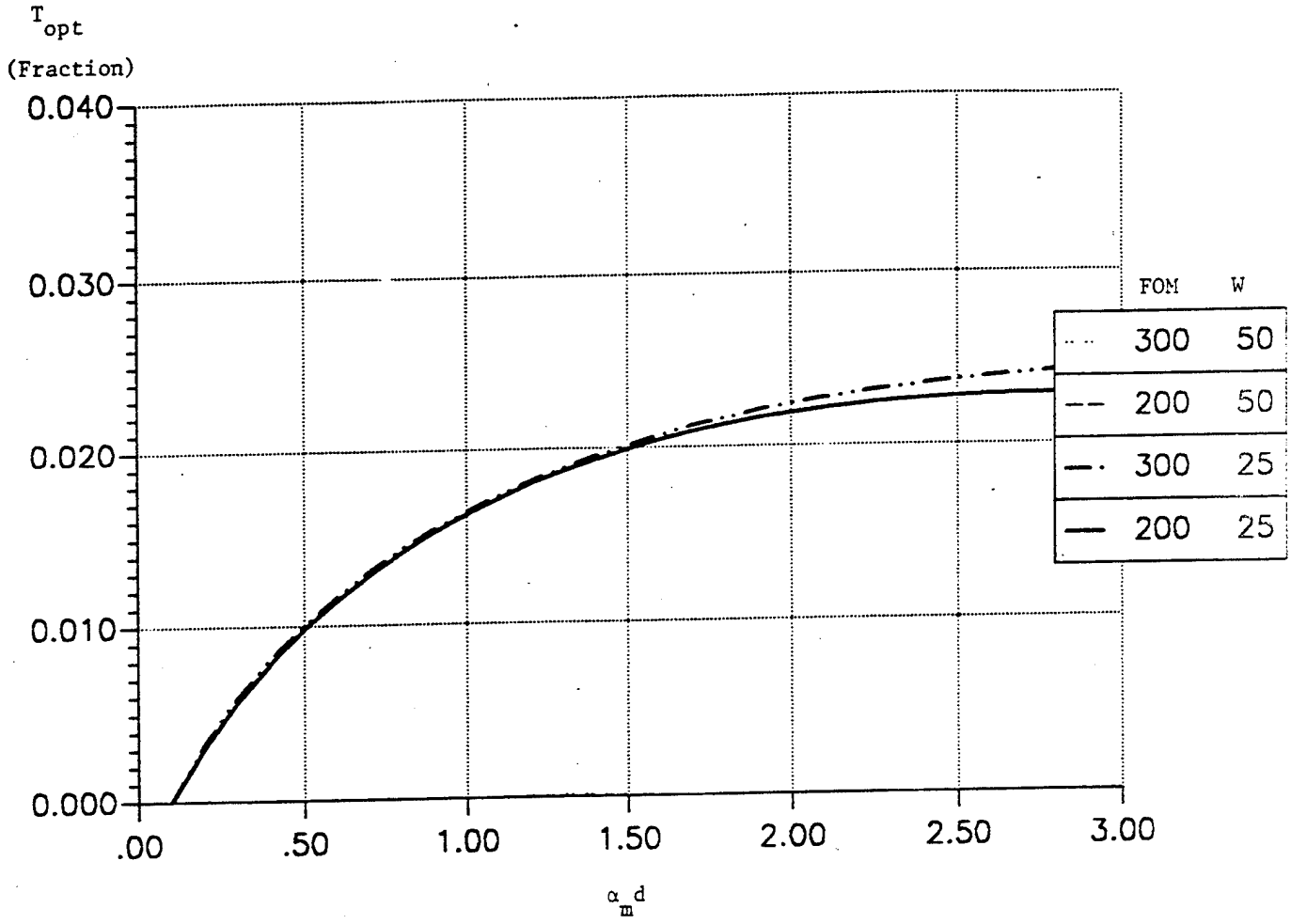

Figure 32. Optimum Coupling Dependence on $\alpha_m d$.
L_i = 0.010, Pump Power = 400 mw.

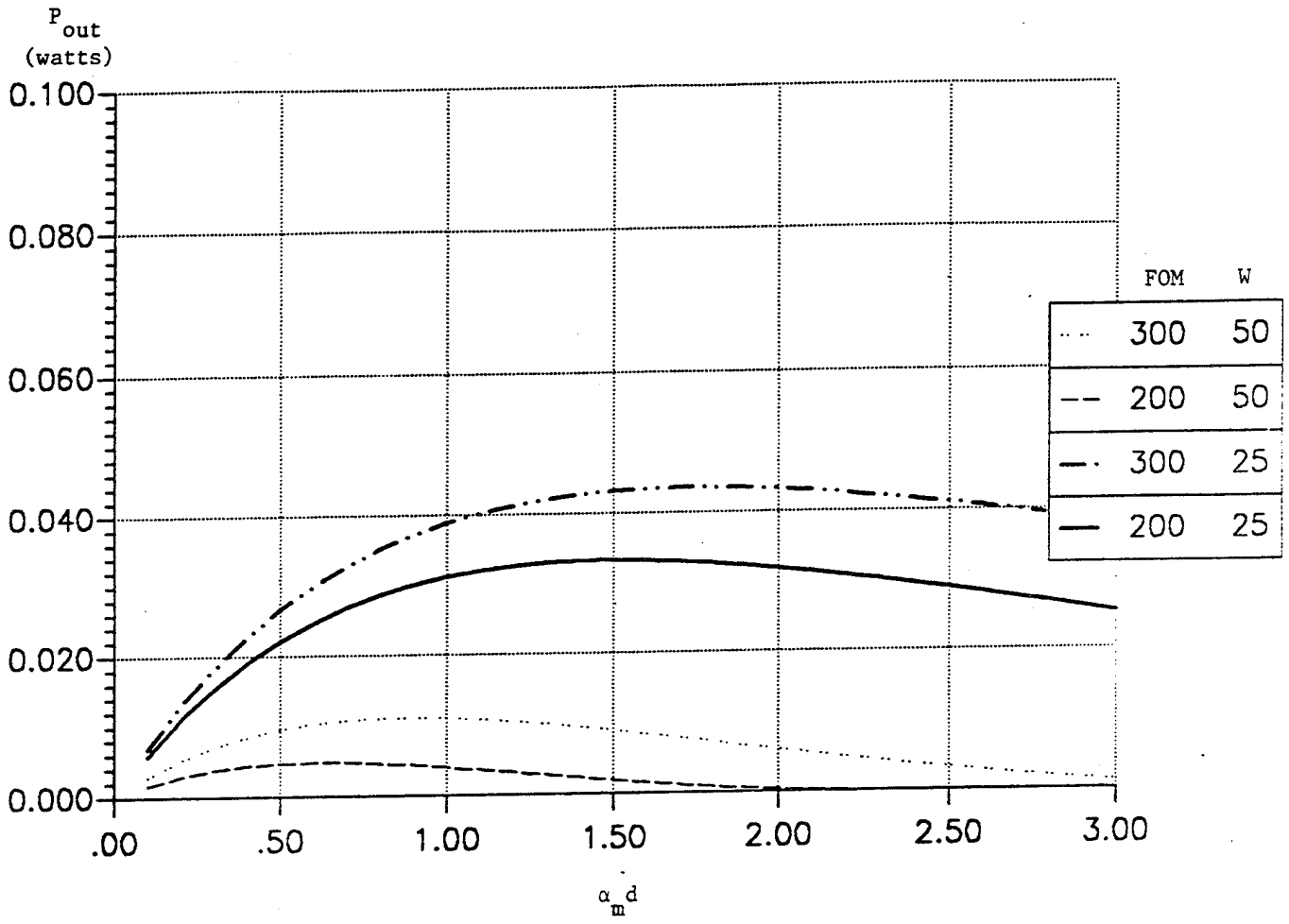

Figure 33. Power Output With T_{opt} Coupling at Each $\alpha_m d$.
L_i = 0.000, Pump Power = 400 mw.

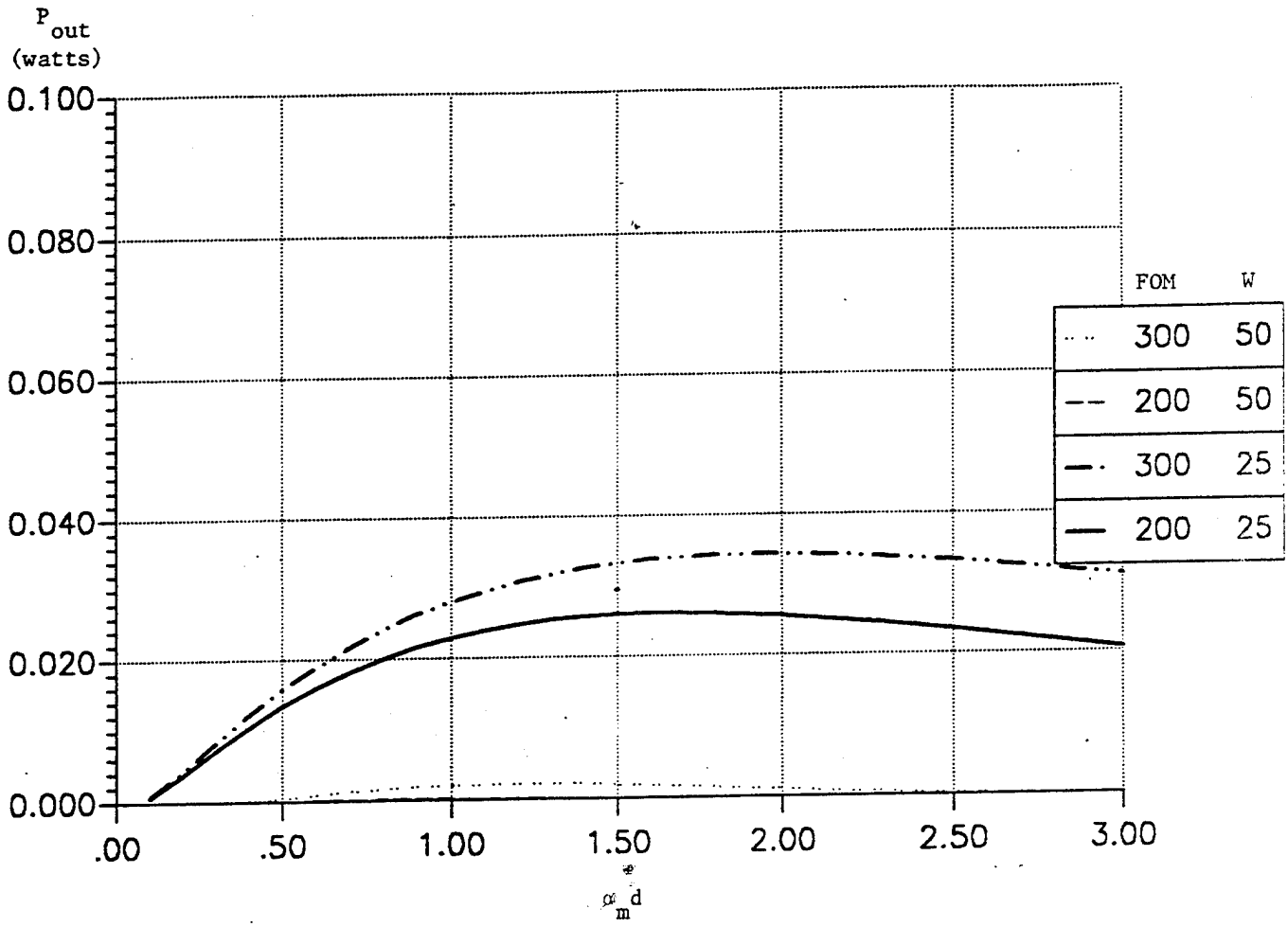

Figure 34. Power Output With T_{opt} Coupling at Each $\alpha_m d$.
L_i = 0.005, Pump Power = 400 mw.

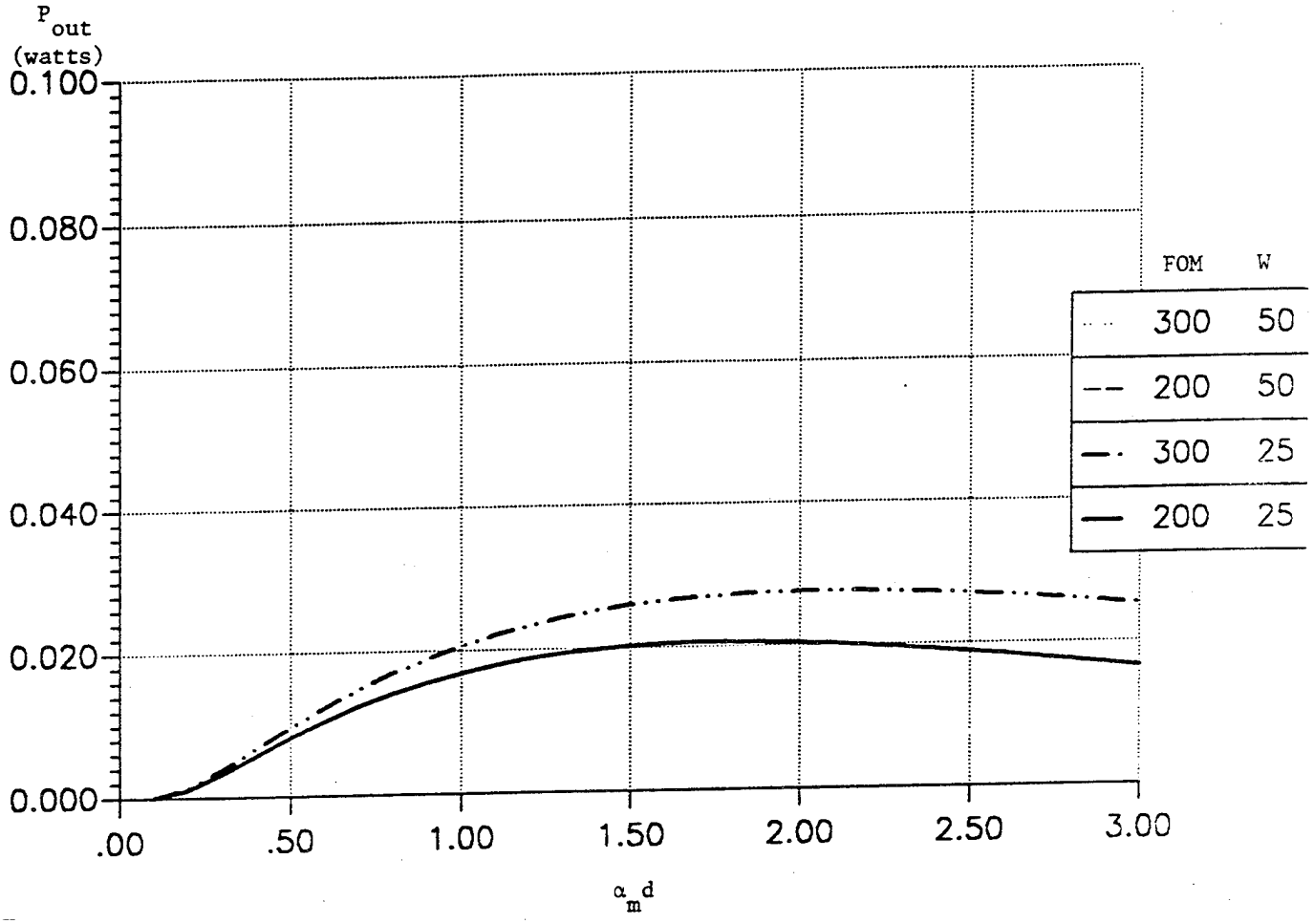

Figure 35. Power Output With T_{opt} Coupling at Each $\alpha_m d$.
L_i = 0.010, Pump Power = 400 mw.

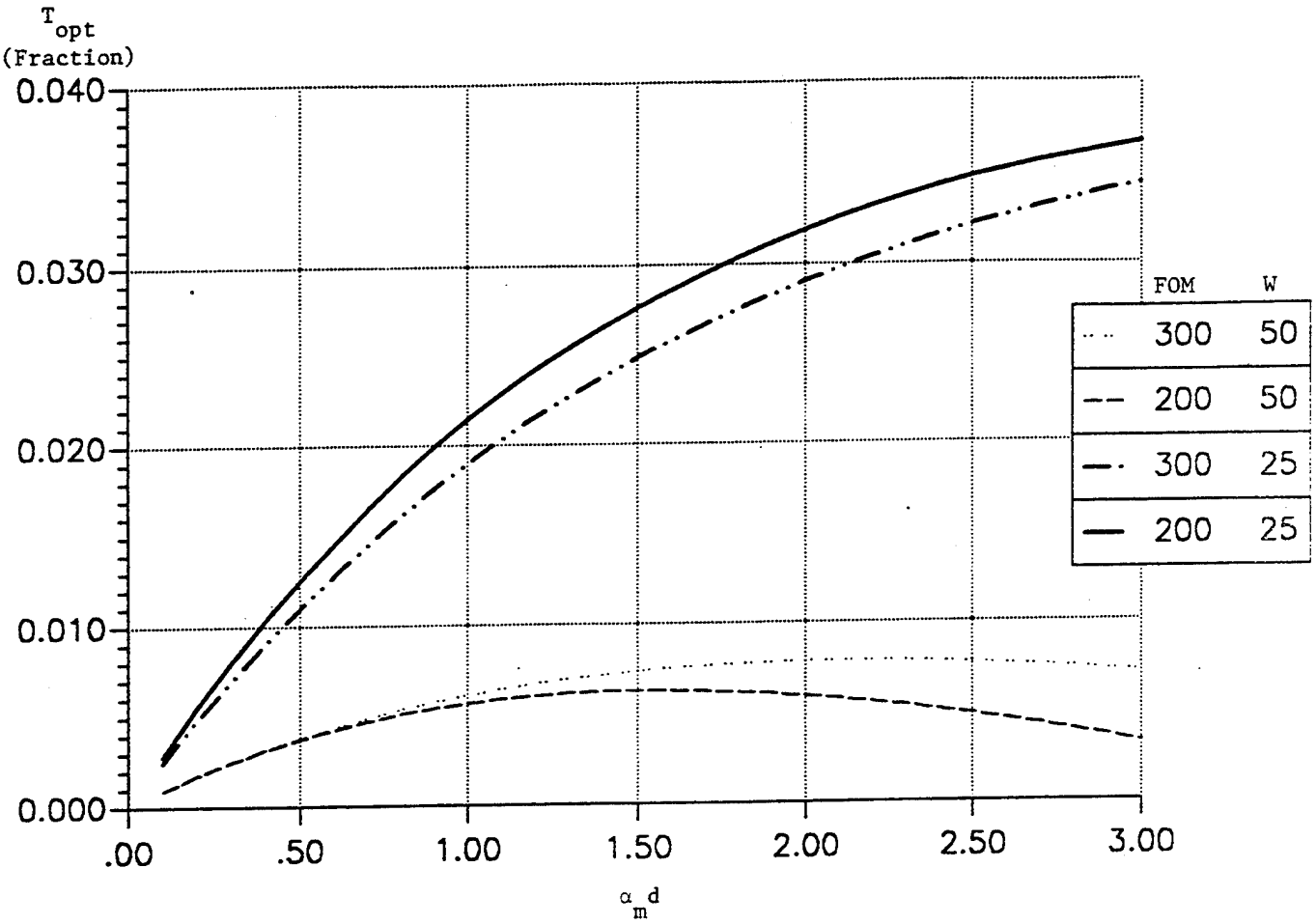

Figure 36. Optimum Coupling Dependence on $\alpha_m d$.
L_i = 0.000, Pump Power = 600 mw.

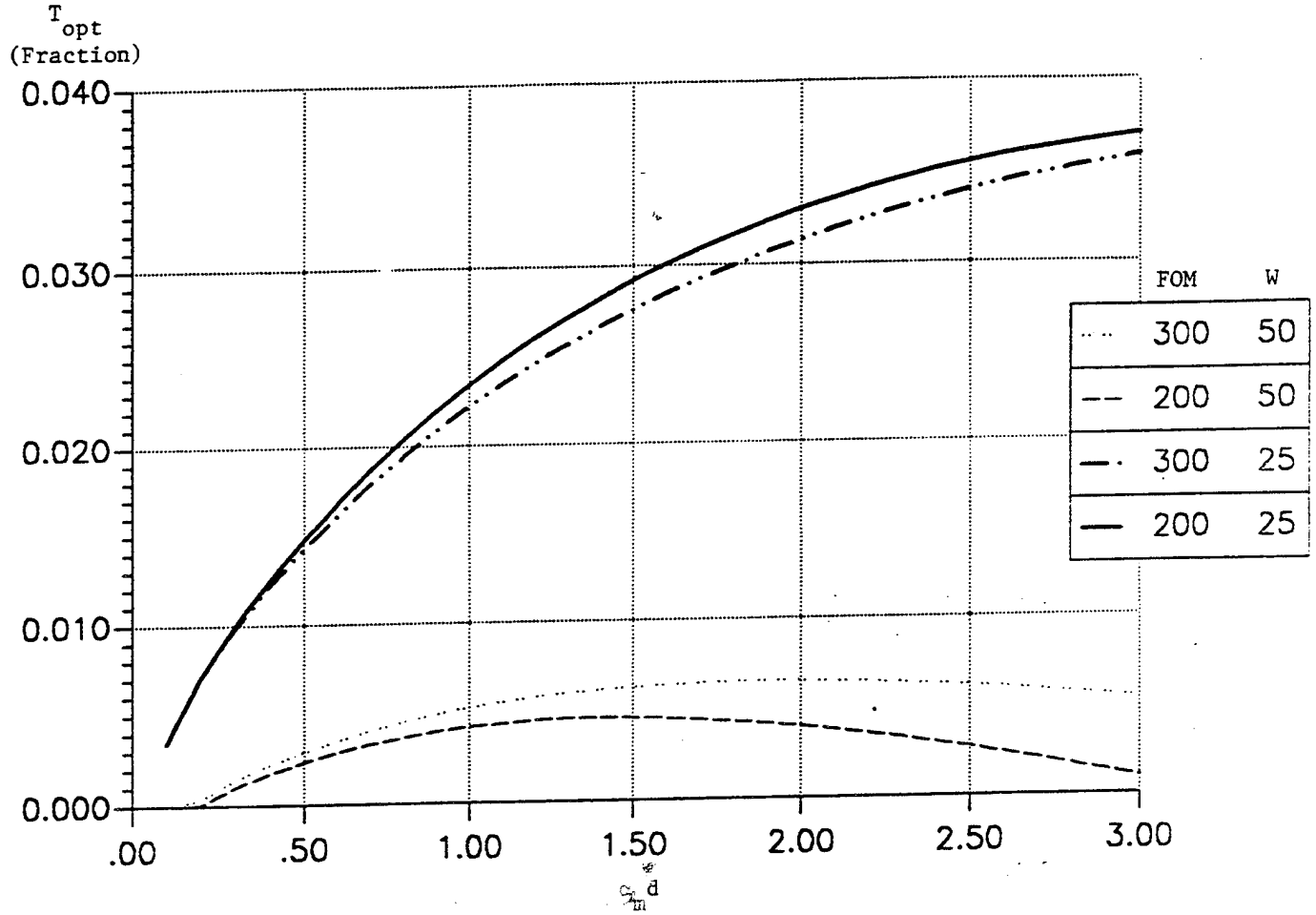

Figure 37. Optimum Coupling Dependence on $\alpha_m d$.
L_i = 0.005, Pump Power = 600 mw.

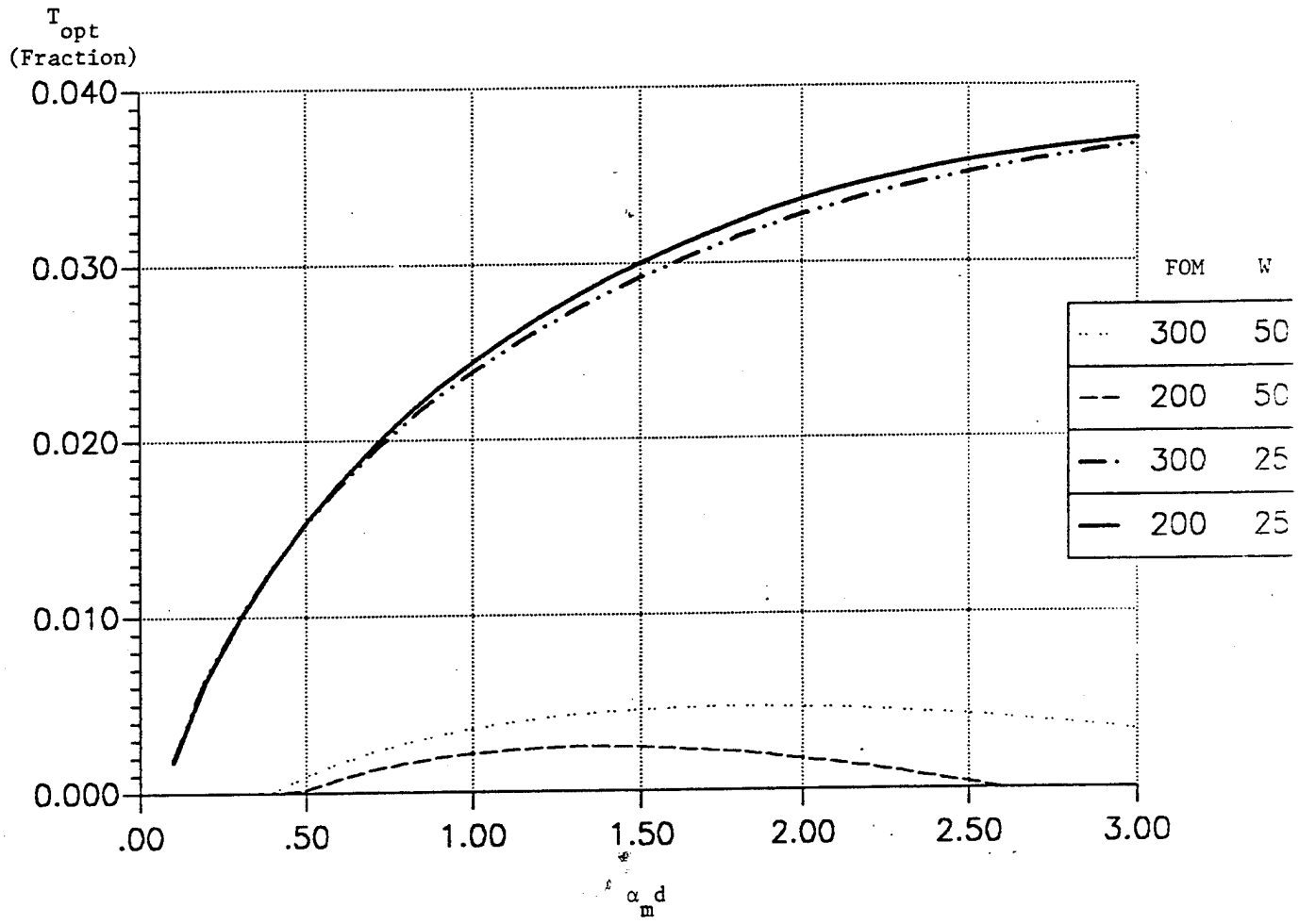

Figure 38. Optimum Coupling Dependence on $\alpha_m d$.
L_i = 0.010, Pump Power = 600 mw.

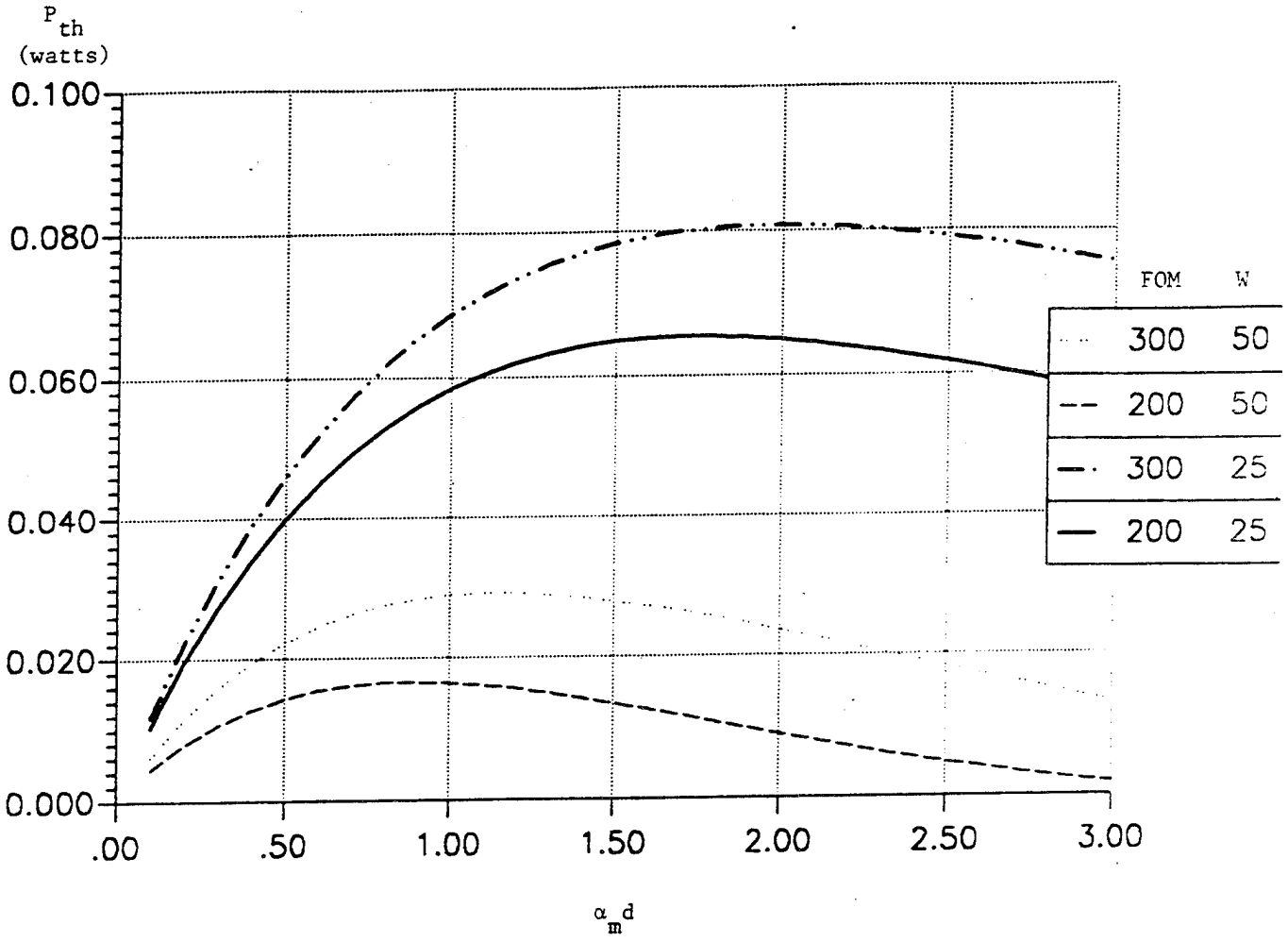

Figure 39. Power Output With T_{opt} Coupling at Each $\alpha_m d$.
L_i = 0.000, Pump Power = 600 mw.

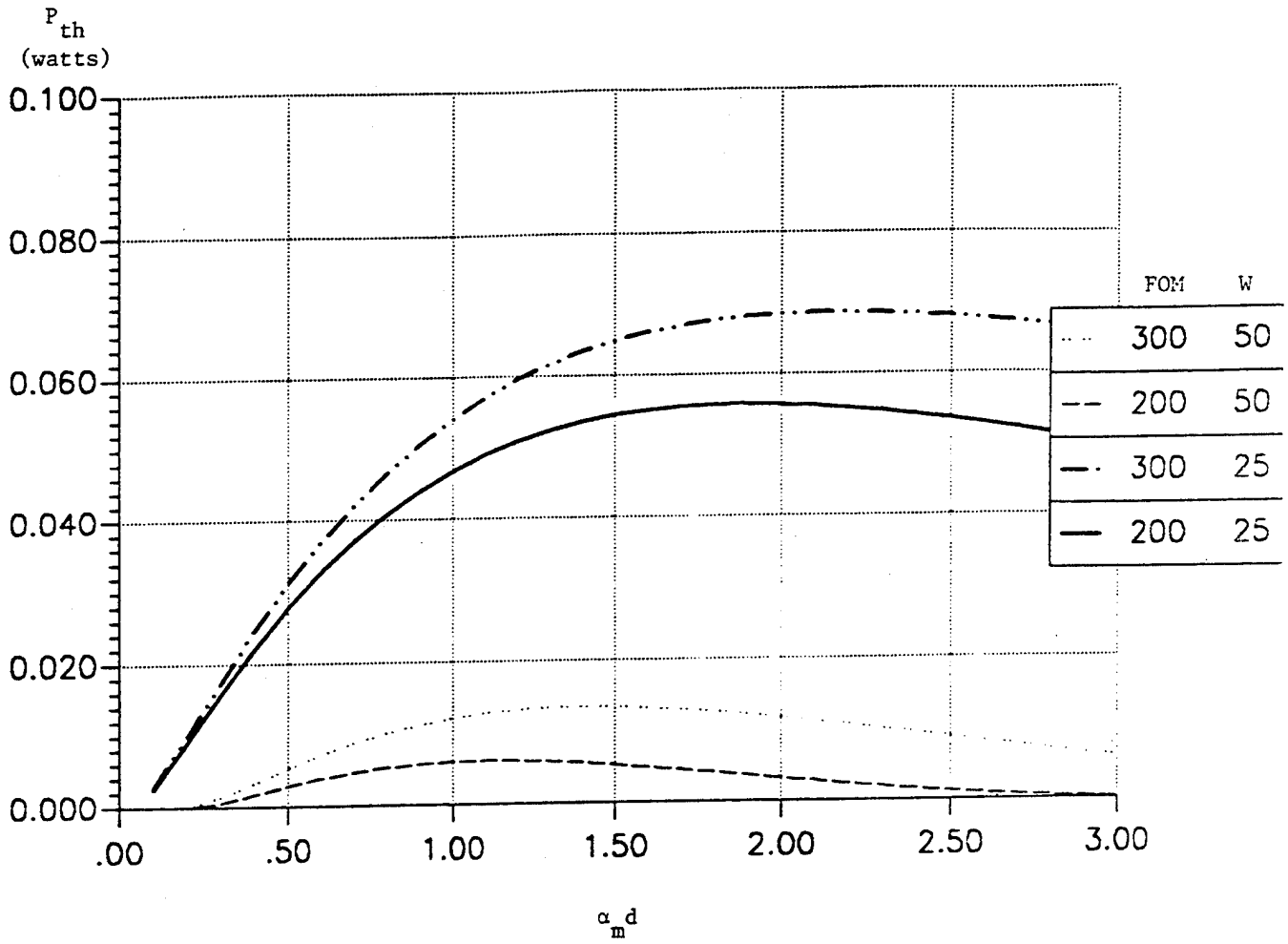

Figure 40. Power Output With T_{opt} Coupling at Each $\alpha_m d$.
L_i = 0.005, Pump Power = 600 mw.

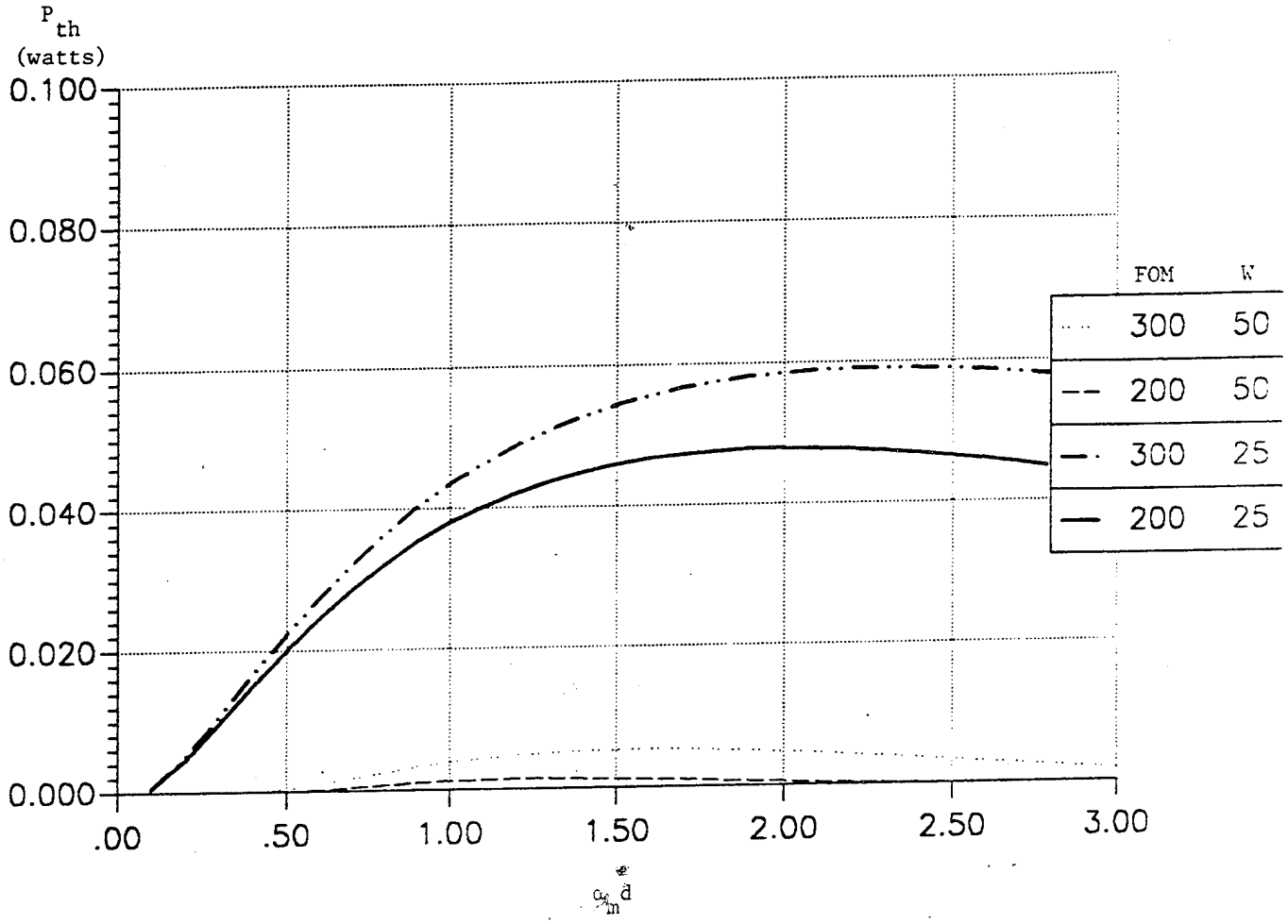

Figure 41. Power Output with T_{opt} Coupling at Each $\alpha_m d$.
L_i = 0.010, Pump Power = 600 mw.

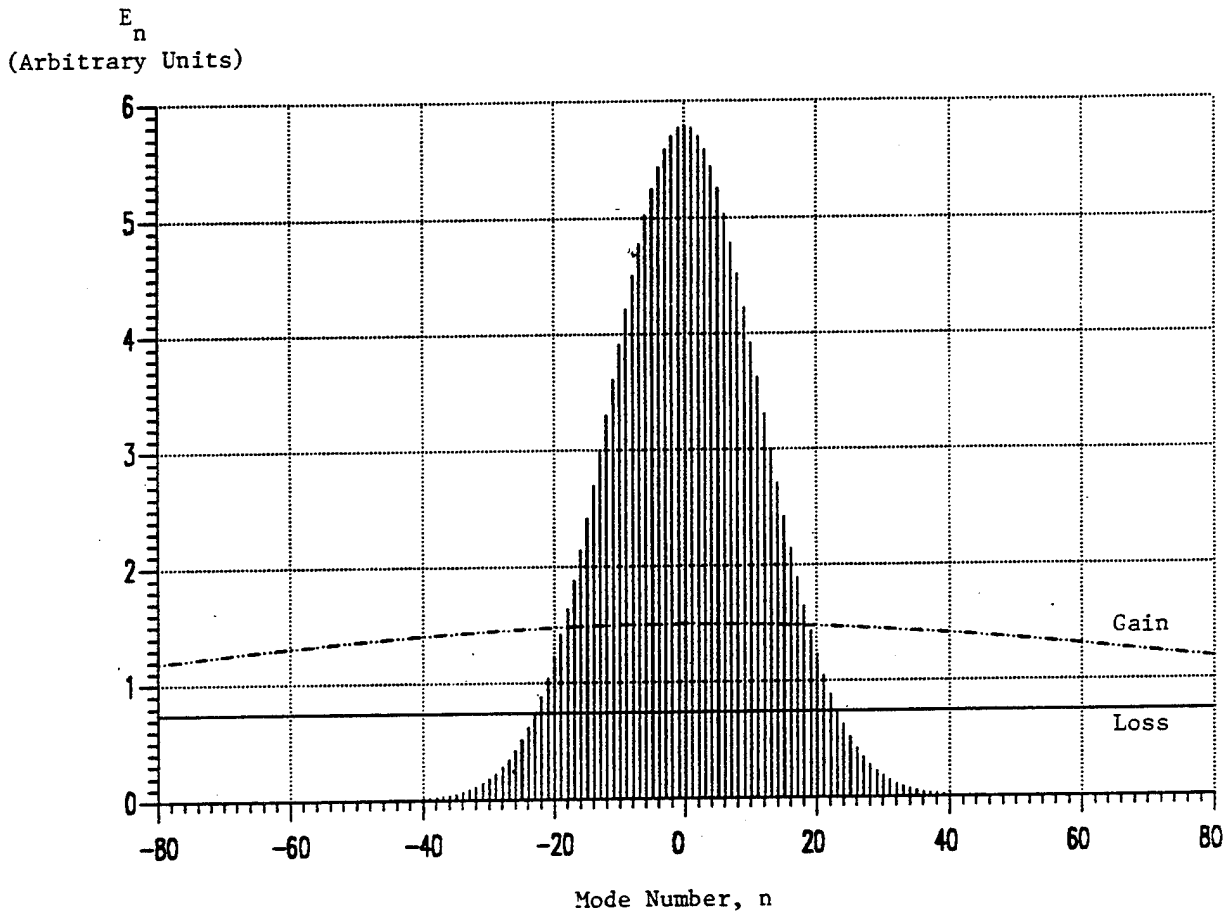

Figure 42. Mode Amplitudes for $\alpha_c = 0.053$.
Pump Power = 400 mw.

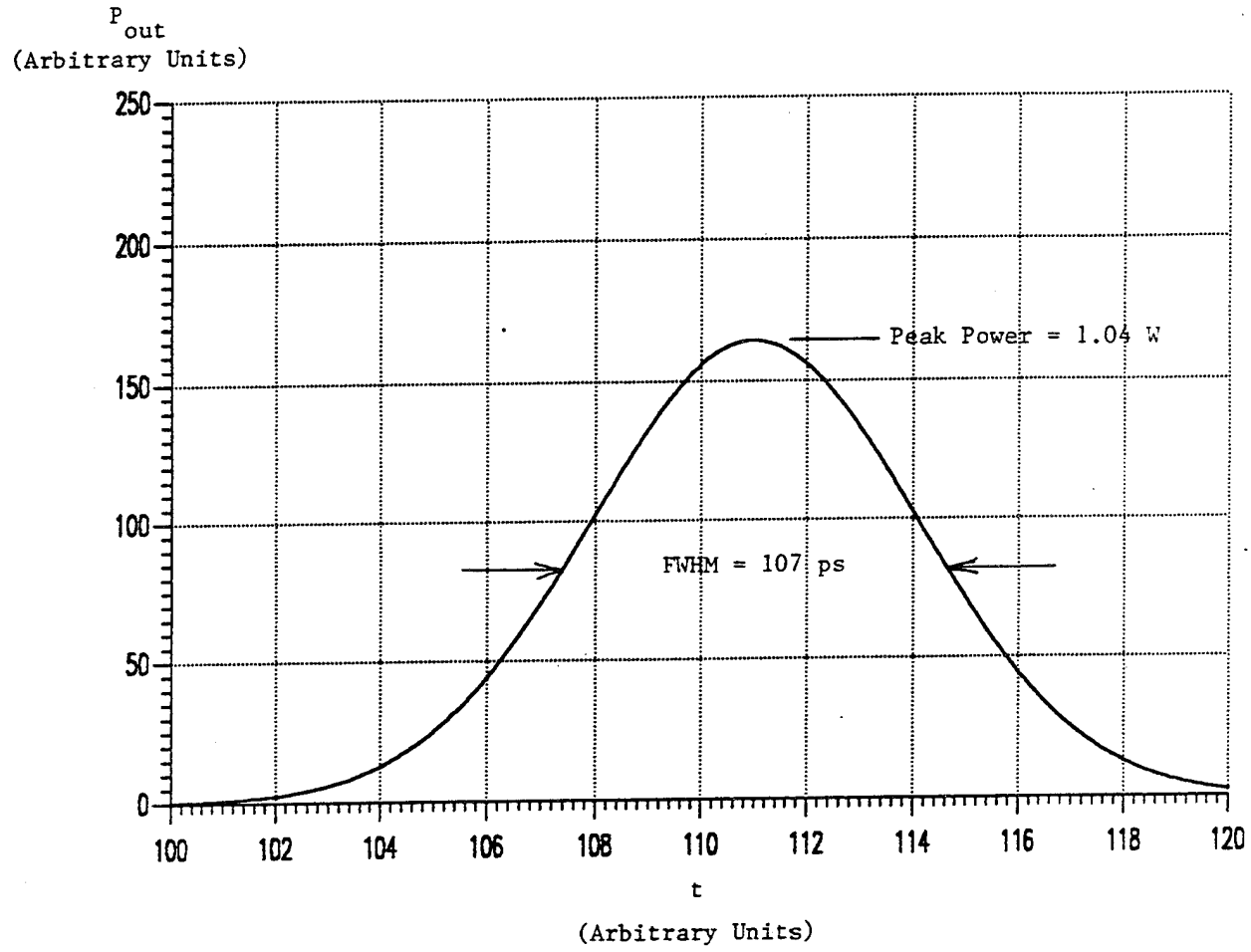

Figure 43. Output Pulse Shape for α_c = 0.053.
Pump Power = 400 mw.

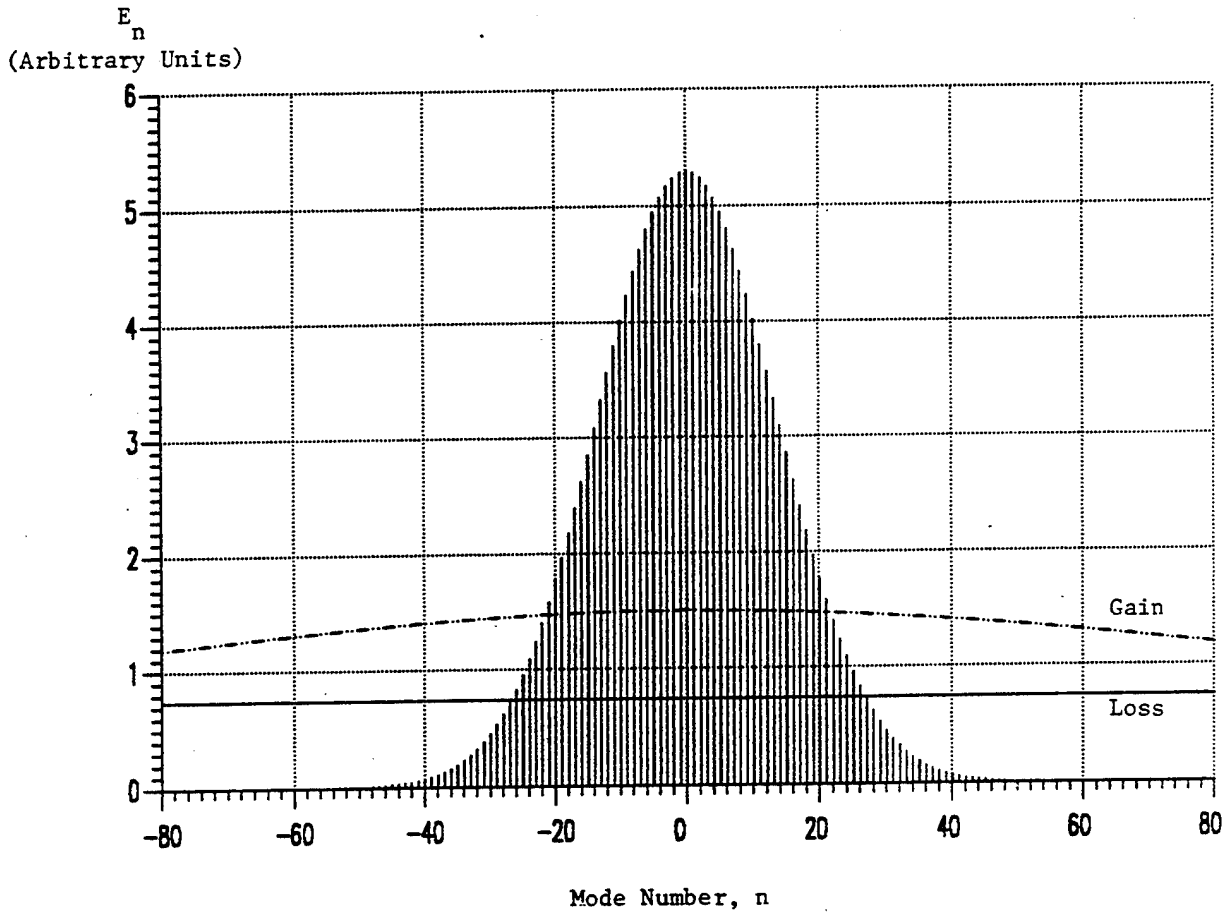

Figure 44. Mode Amplitudes for $\alpha_c = 0.107$.
Pump Power = 400 mw.

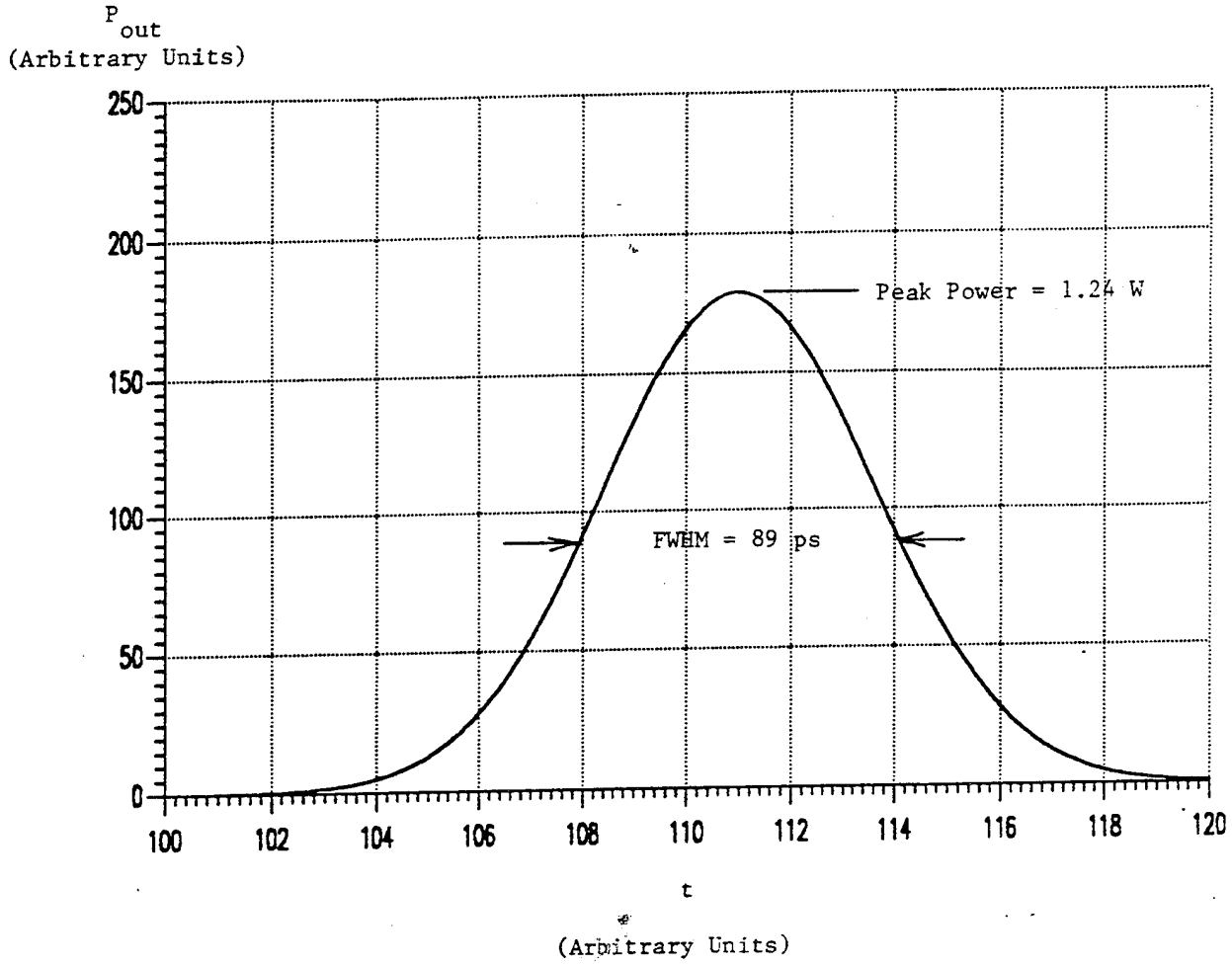

Figure 45. Output Pulse Shape for α_c = 0.107.
Pump Power = 400 mw.

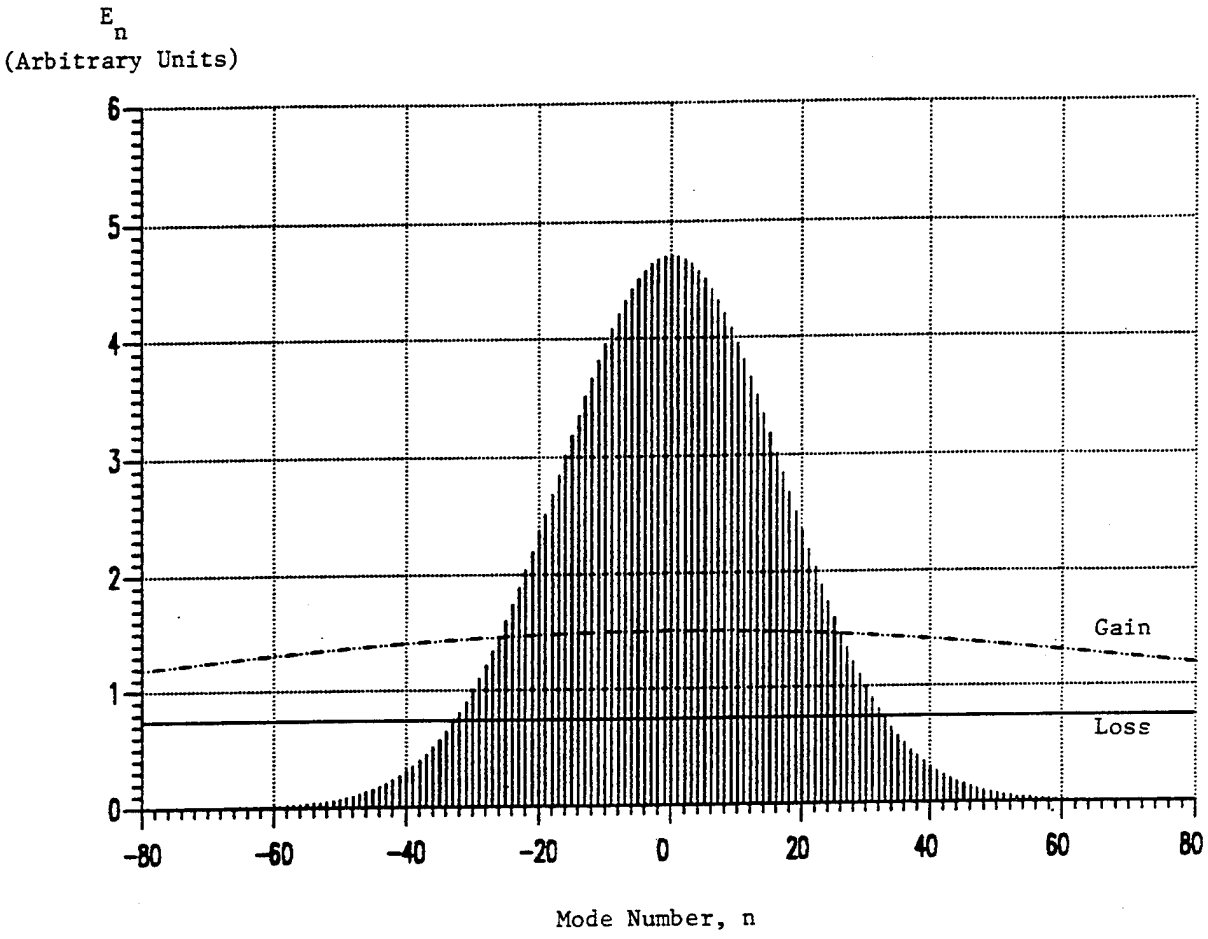

Figure 46. Mode Amplitudes for $\alpha_c = 0.269$
Pump Power = 400 mw.

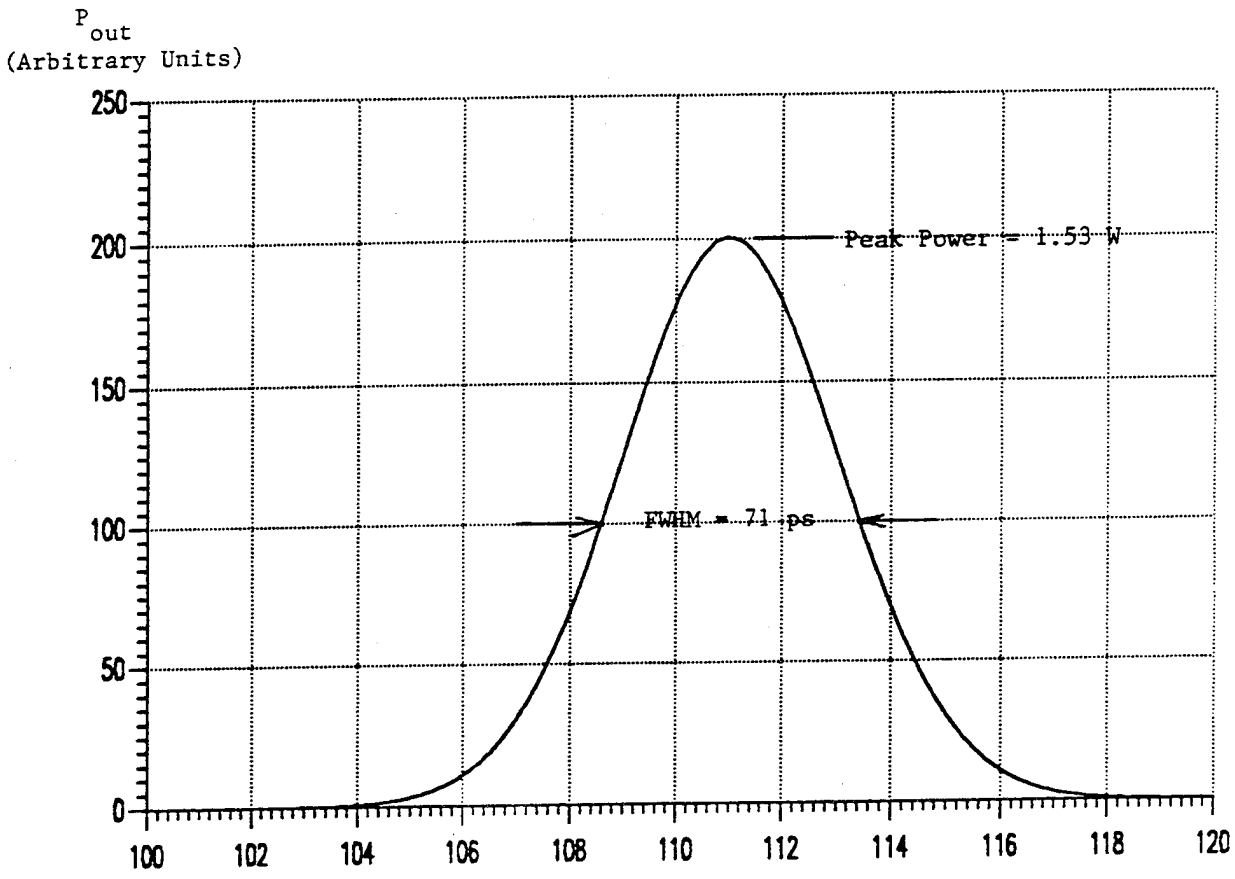

Figure 47. Output Pulse Shape for α_c = 0.269
Pump Power = 400 mw.

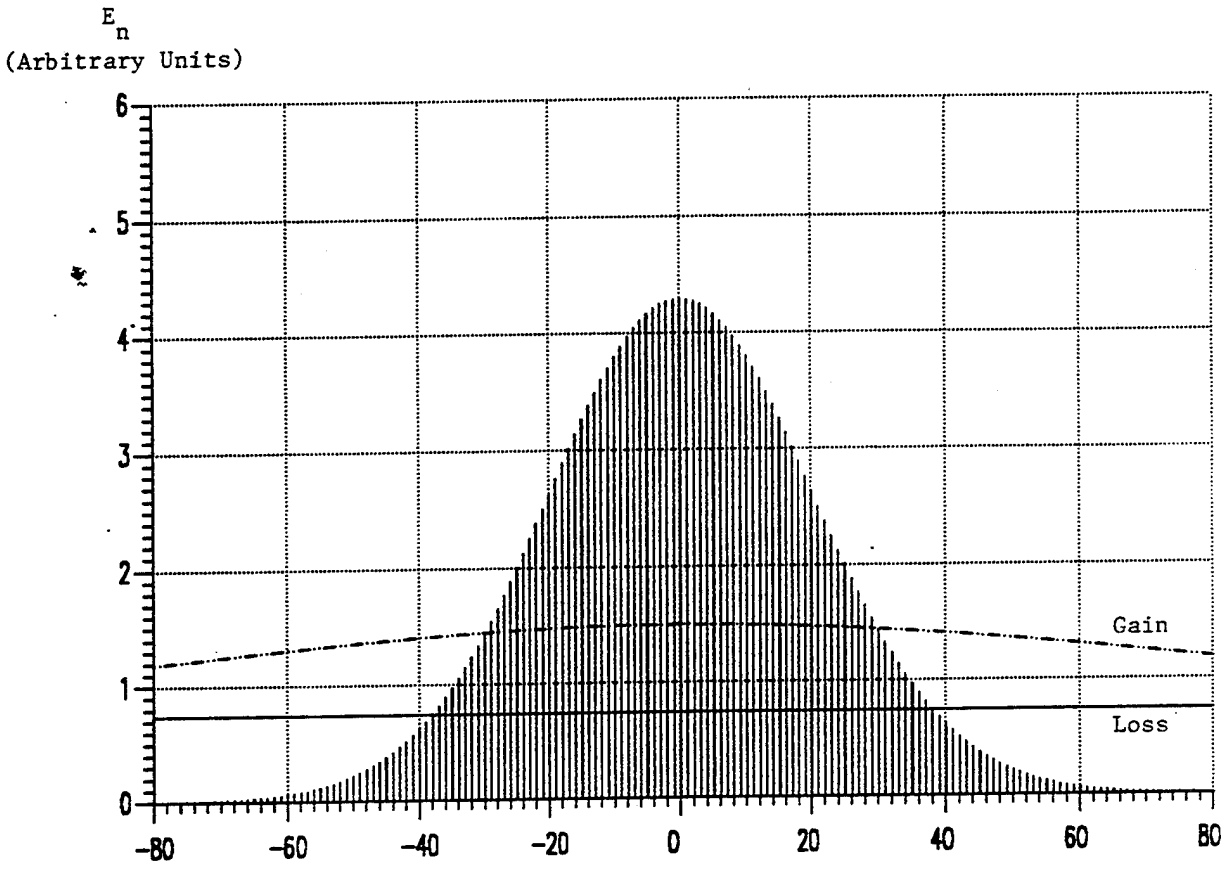

Figure 48. Mode Amplitudes for $\alpha_c = 0.54$.
Pump Power = 400 mw.

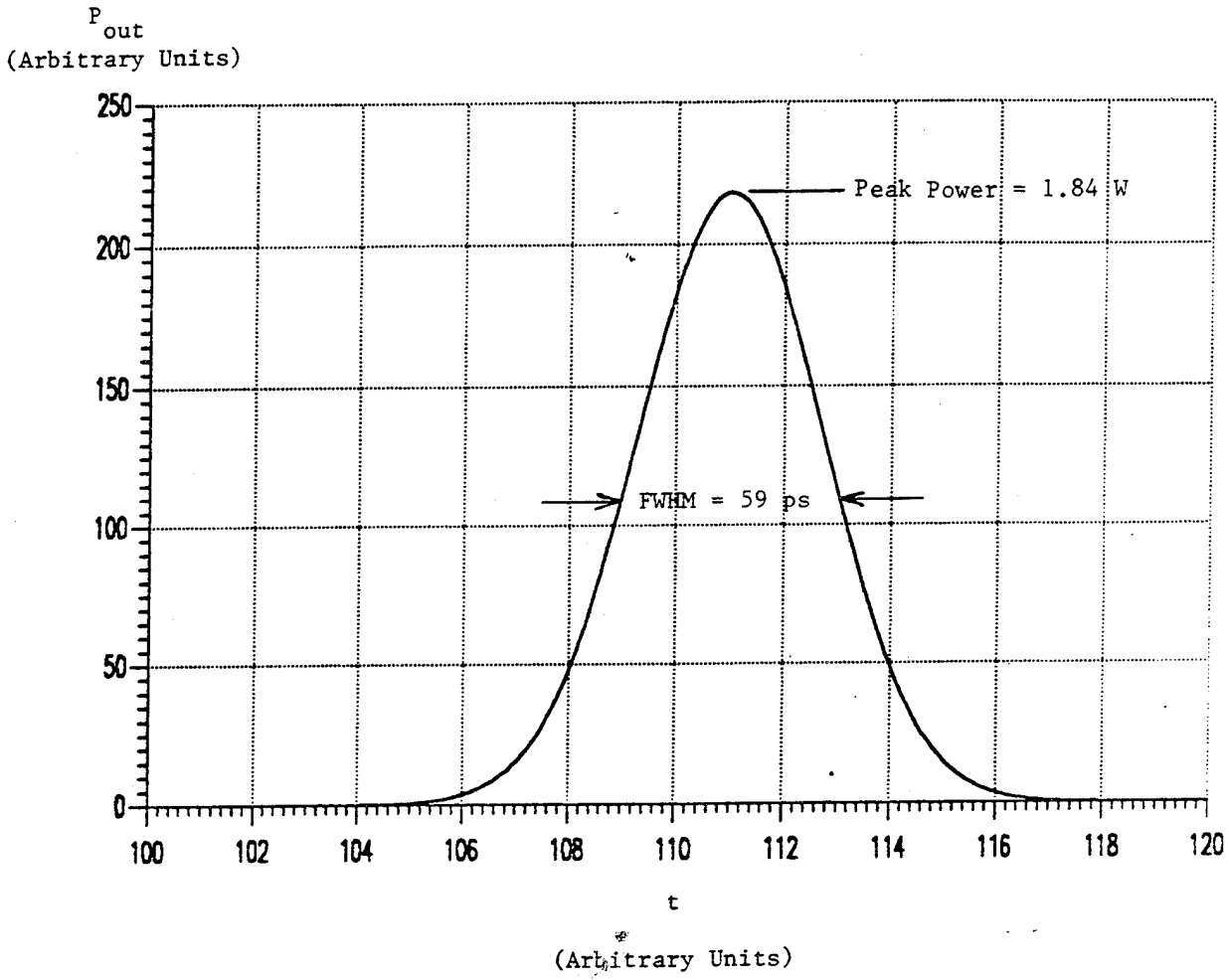

Figure 49. Output Pulse Shape for α_c = 0.54.
Pump Power = 400 mw.

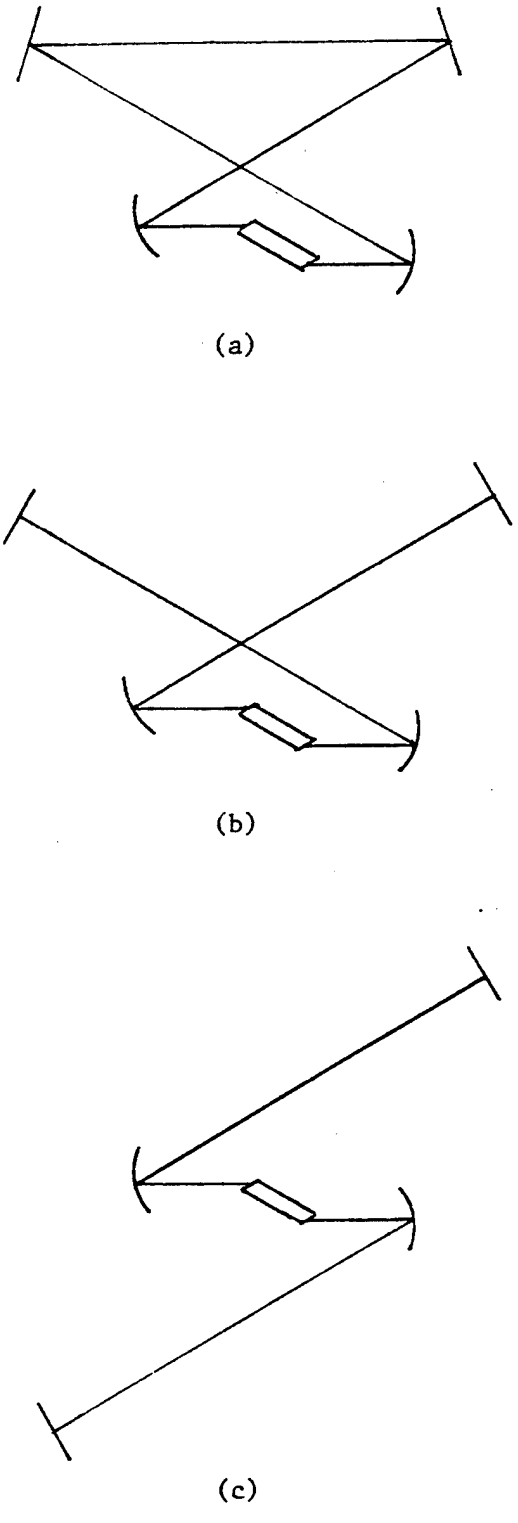

Figure 50. Possible Cavity Configurations

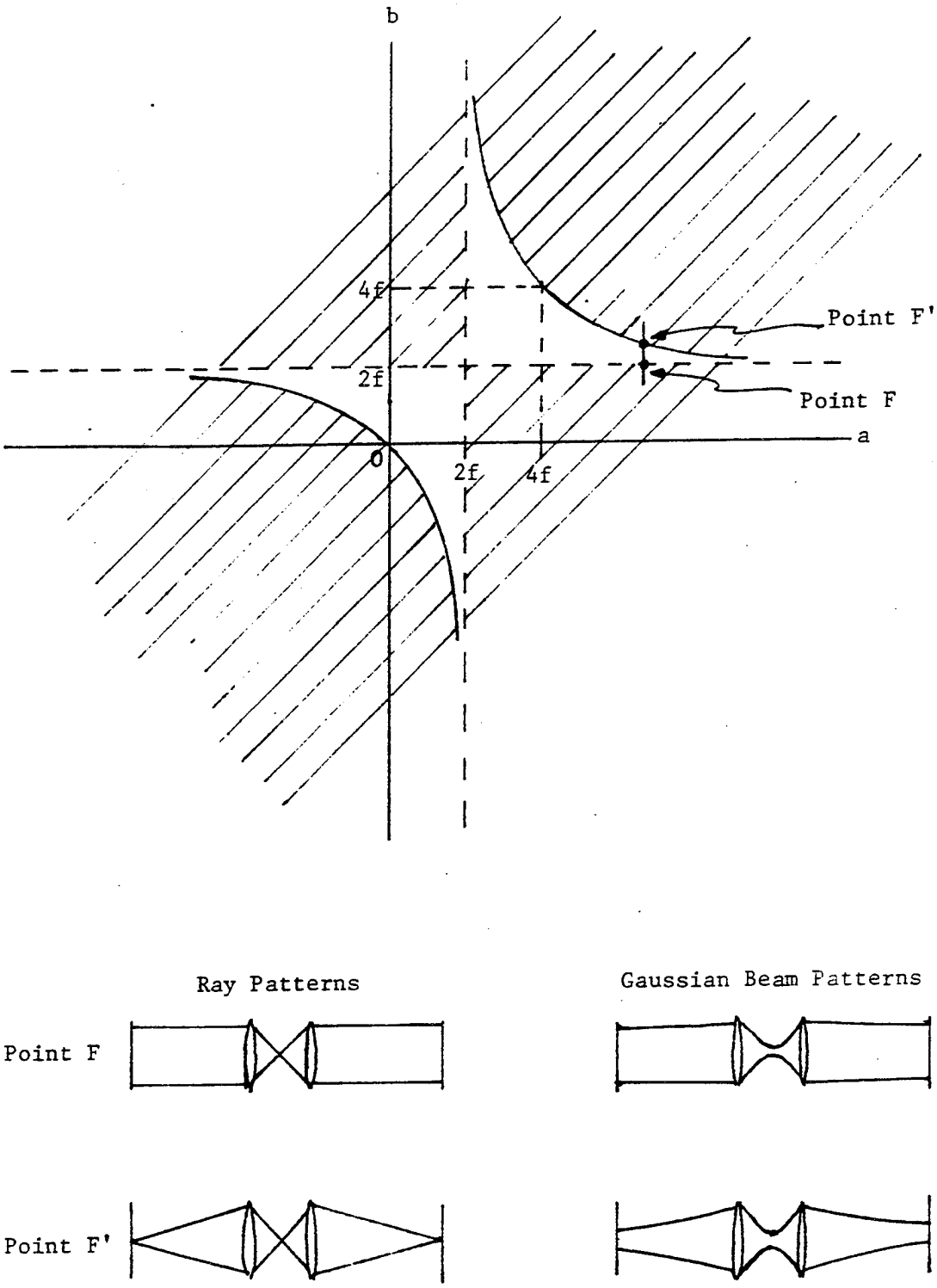

Figure 51. Stability Diagram with Stable Range Shown

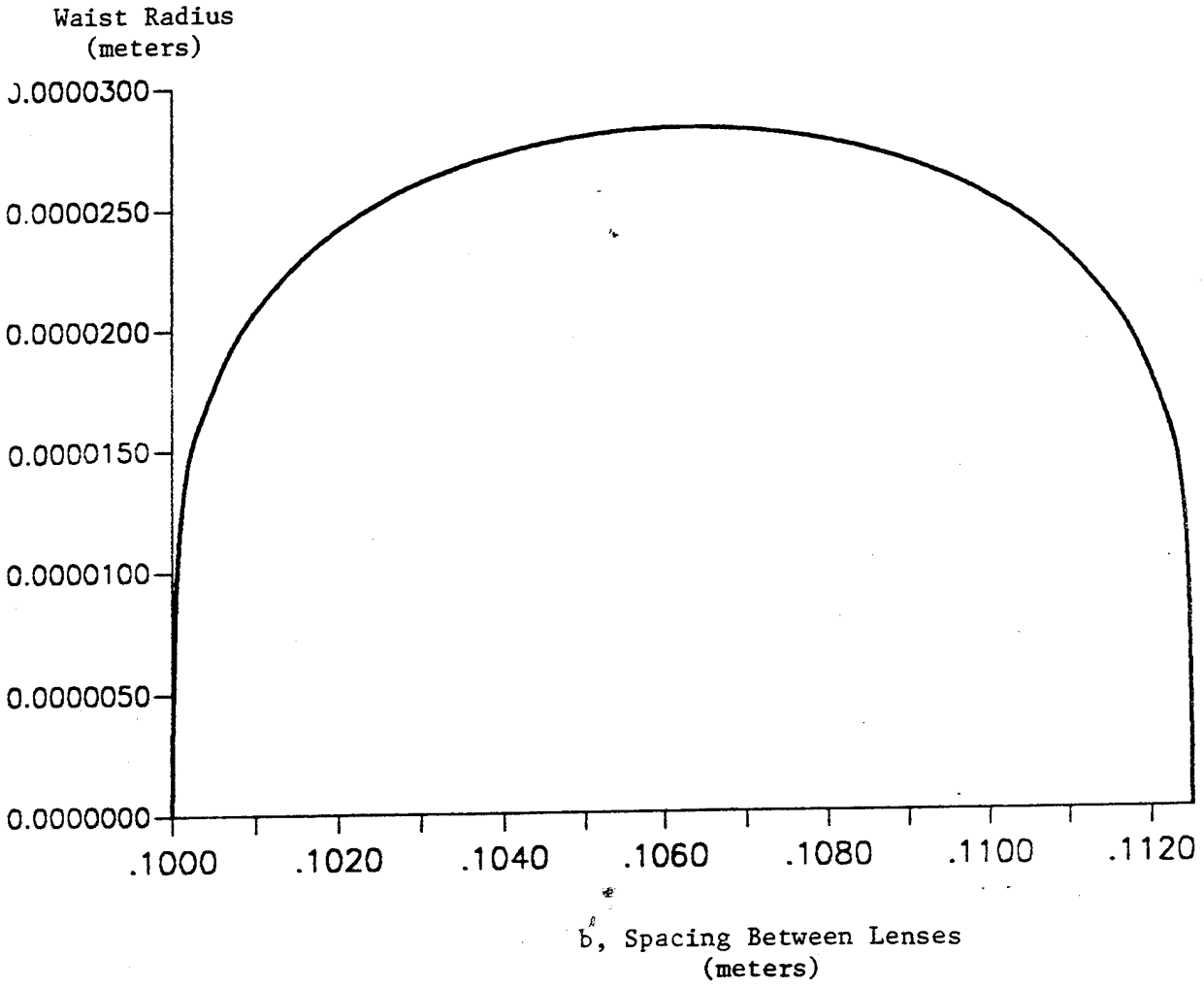

Figure 52. Dependence of Waist Size upon Spacing Between Lenses. f = 0.05 m.

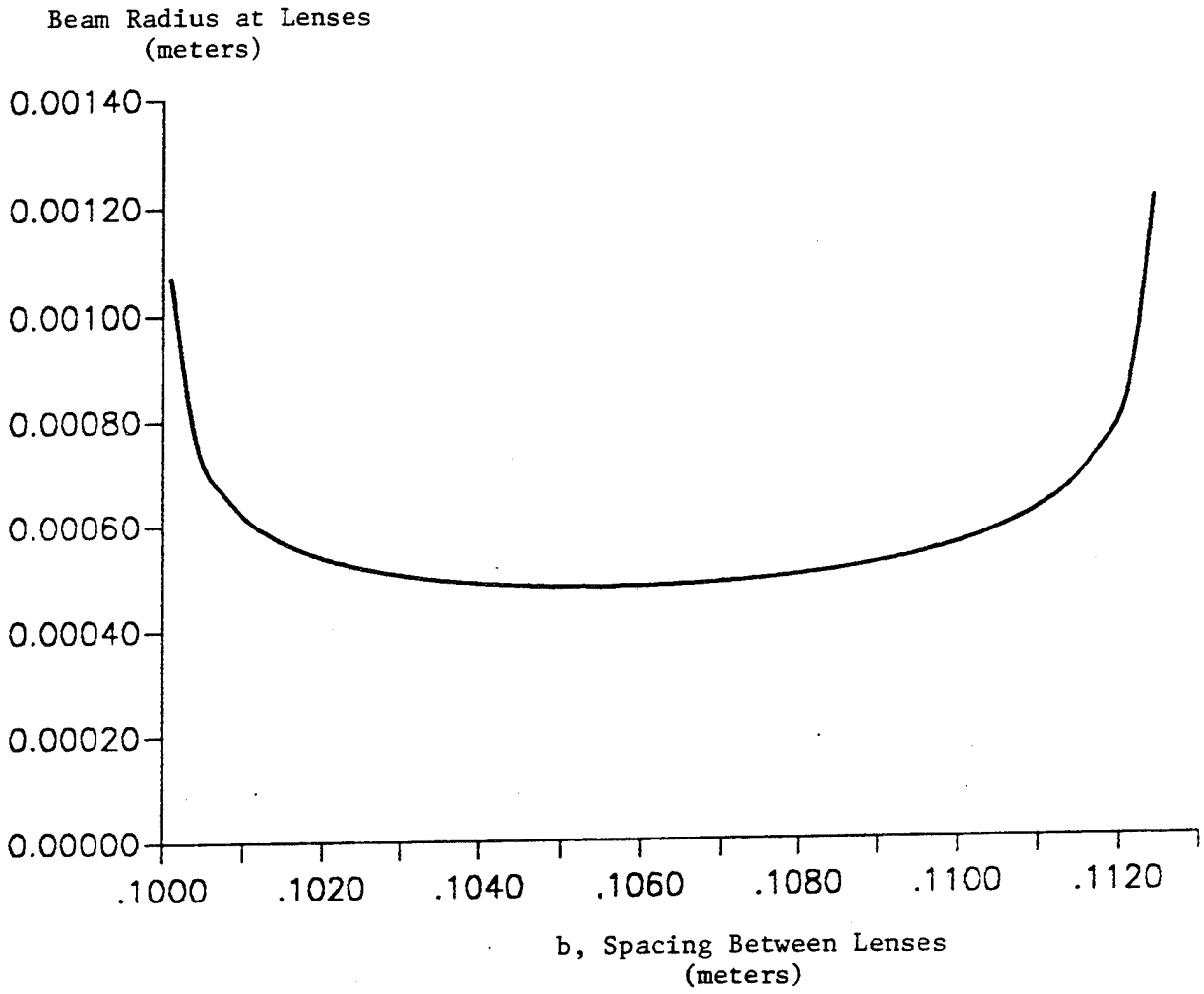

Figure 53. Dependence of Beam Radius at Lenses upon Spacing Between Lenses. f = 0.05 m.

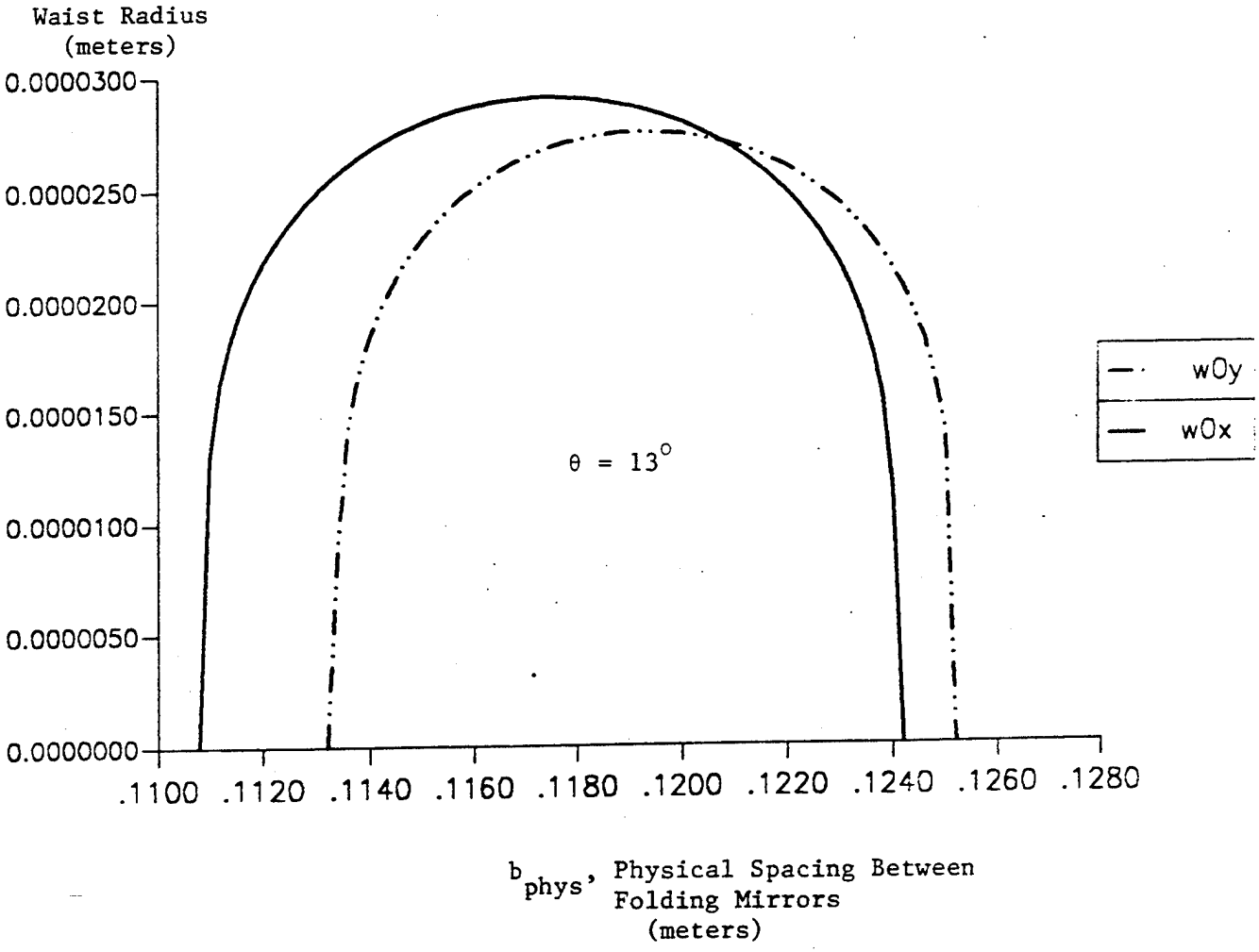

Figure 54. Dependence of Waist Radius in xz and yz Planes upon the Physical Spacing Between Folding Mirrors. f = 0.05 m. Folding Angle $\theta = 13^{\circ}$.

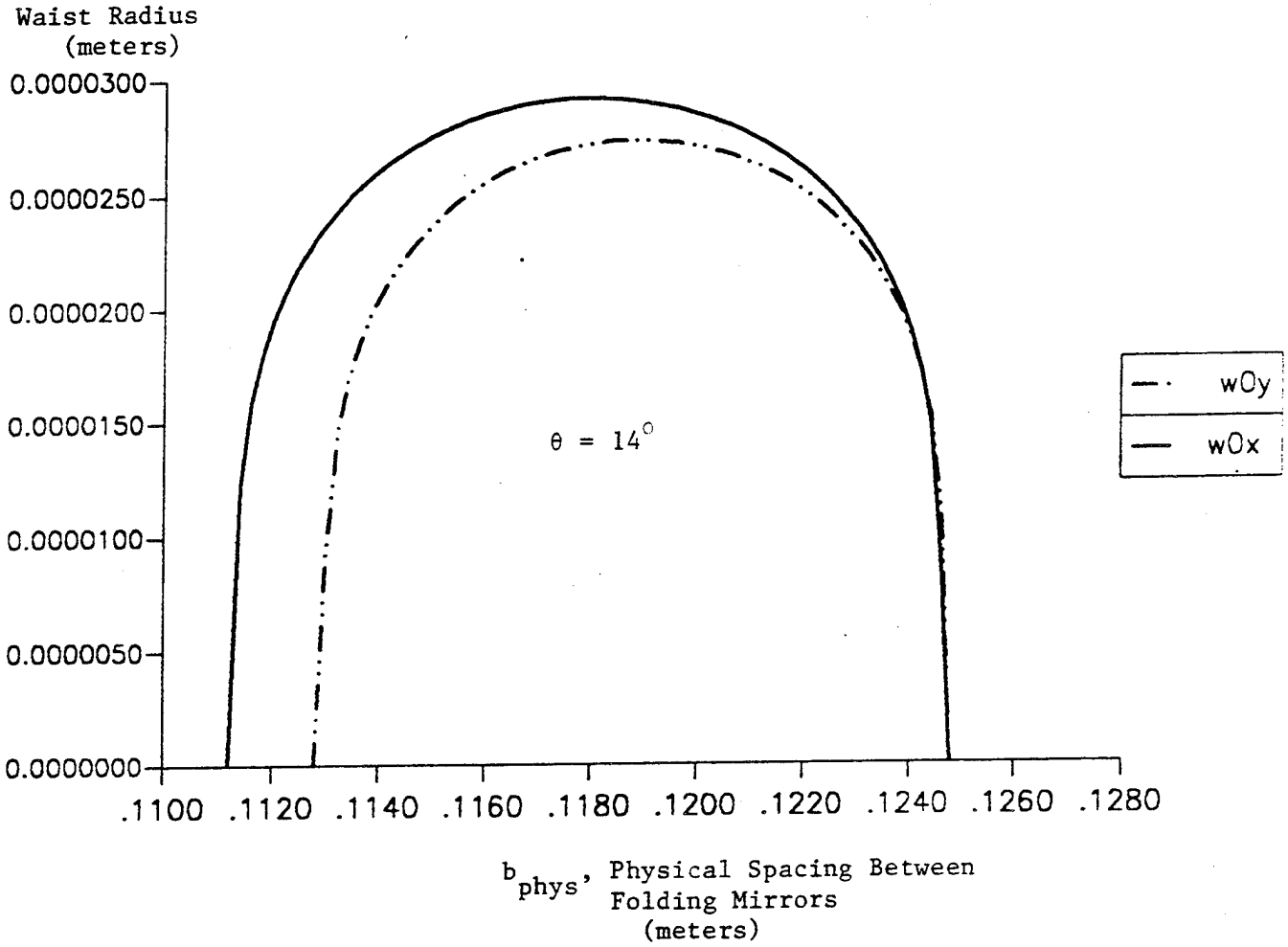

Figure 55. Dependence of Waist Radius in xz and yz Planes upon the Physical Spacing Between Folding Mirrors. f = 0.05 m. Folding Angle $\theta = 14^{\circ}$.

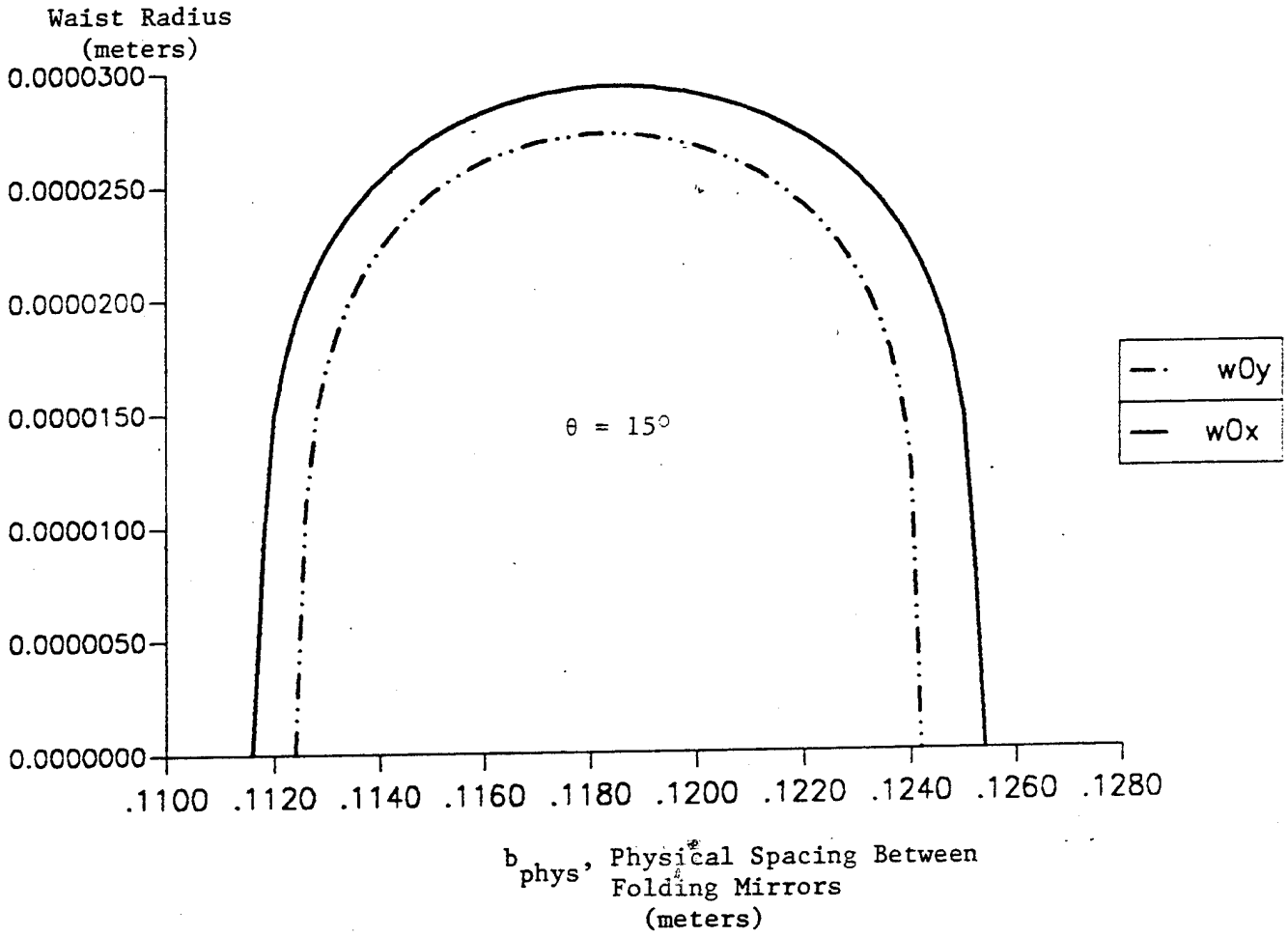

Figure 56. Dependence of Waist Radius in xz and yz Planes upon the Physical Spacing Between Folding Mirrors. f = 0.05 m. Folding Angle $\theta = 15^{\circ}$.

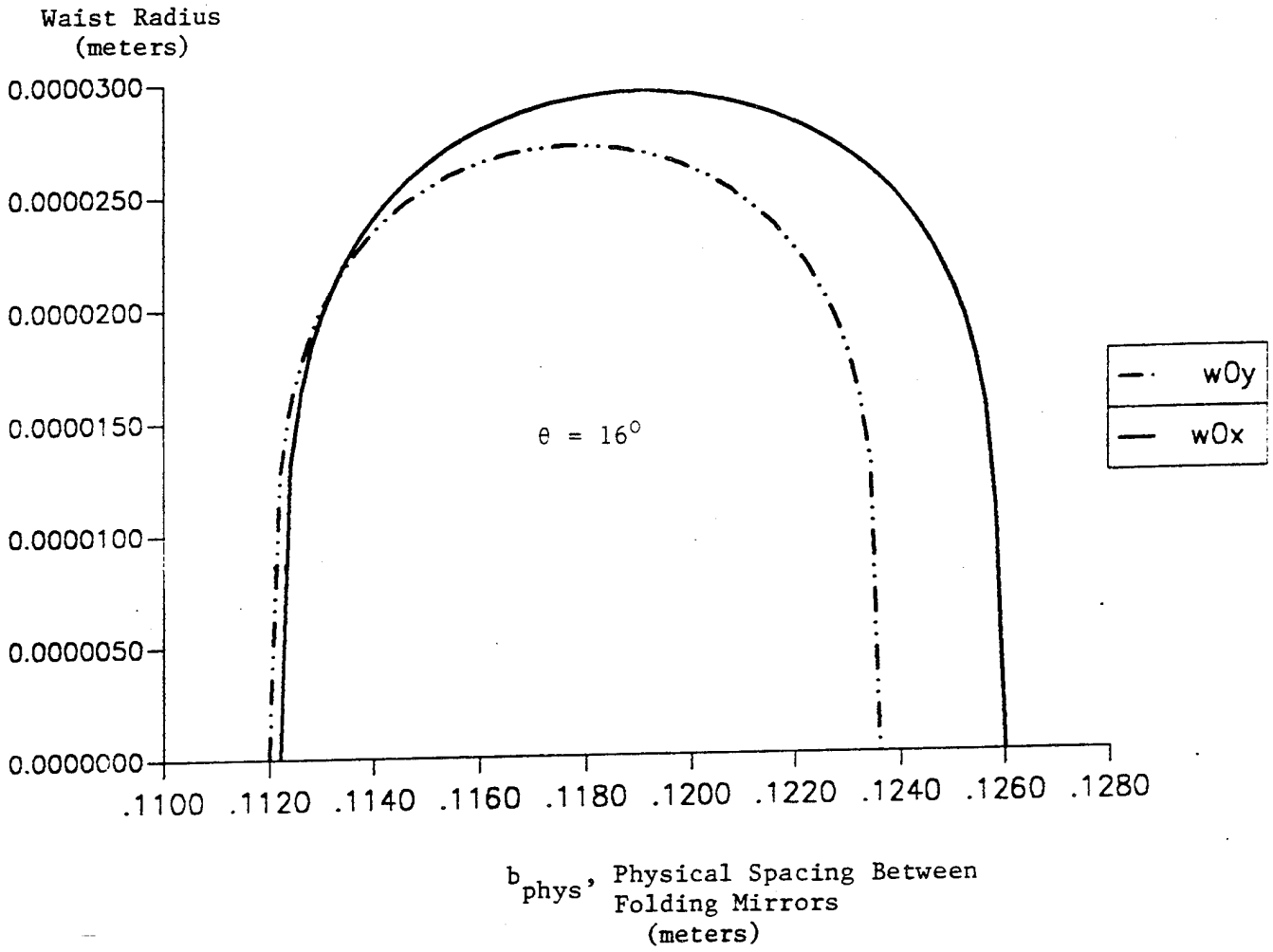

Figure 57. Dependence of Waist Radius in xz and yz Planes upon the Physical Spacing Between Folding Mirrors. f = 0.05 m. Folding Angle $\theta = 16^{\circ}$.

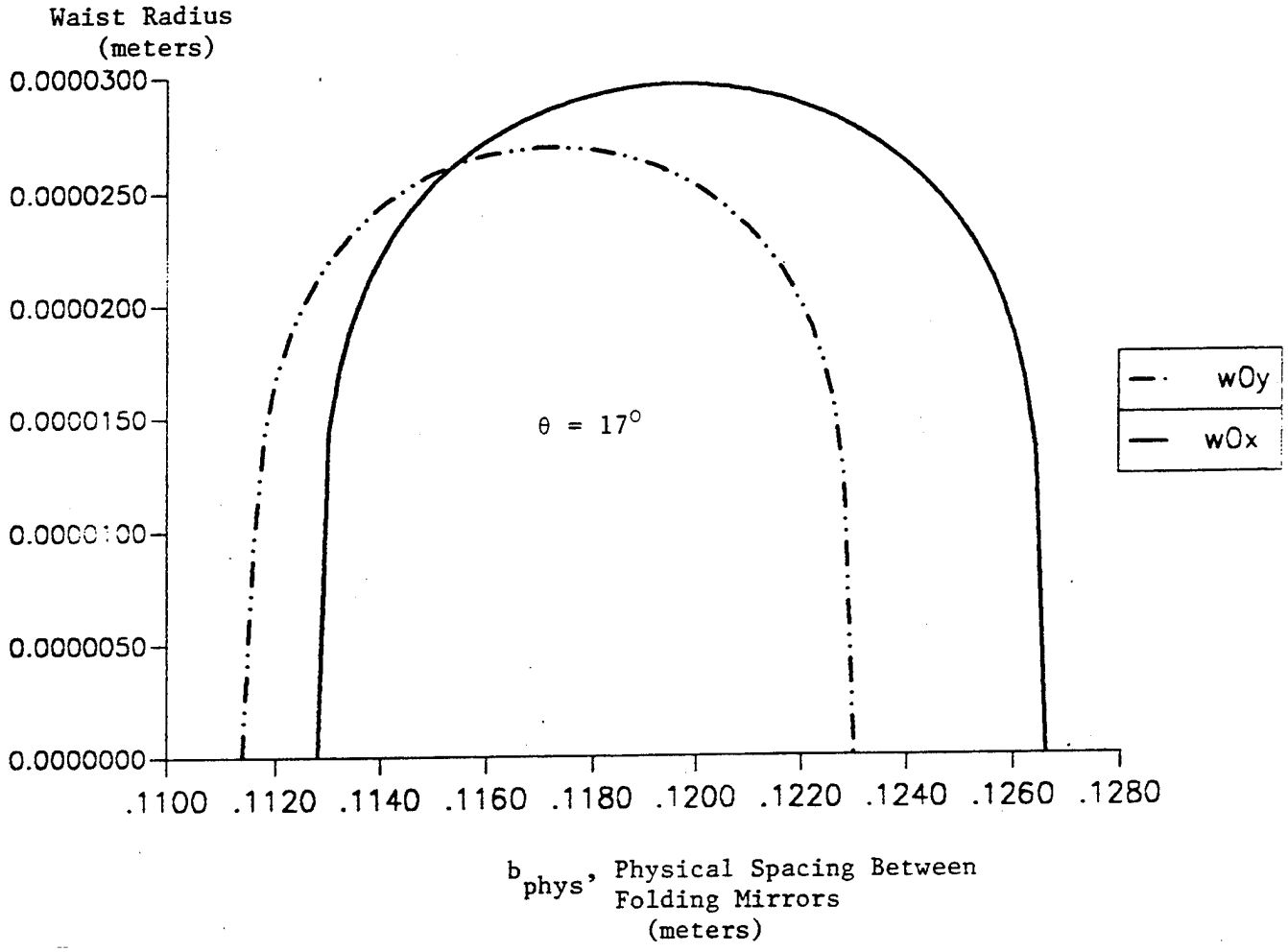

Figure 58. Dependence of Waist Radius in xz and yz Planes upon the Physical Spacing Between Folding Mirrors. f = 0.05 m. Folding Angle $\theta = 17^{\circ}$.

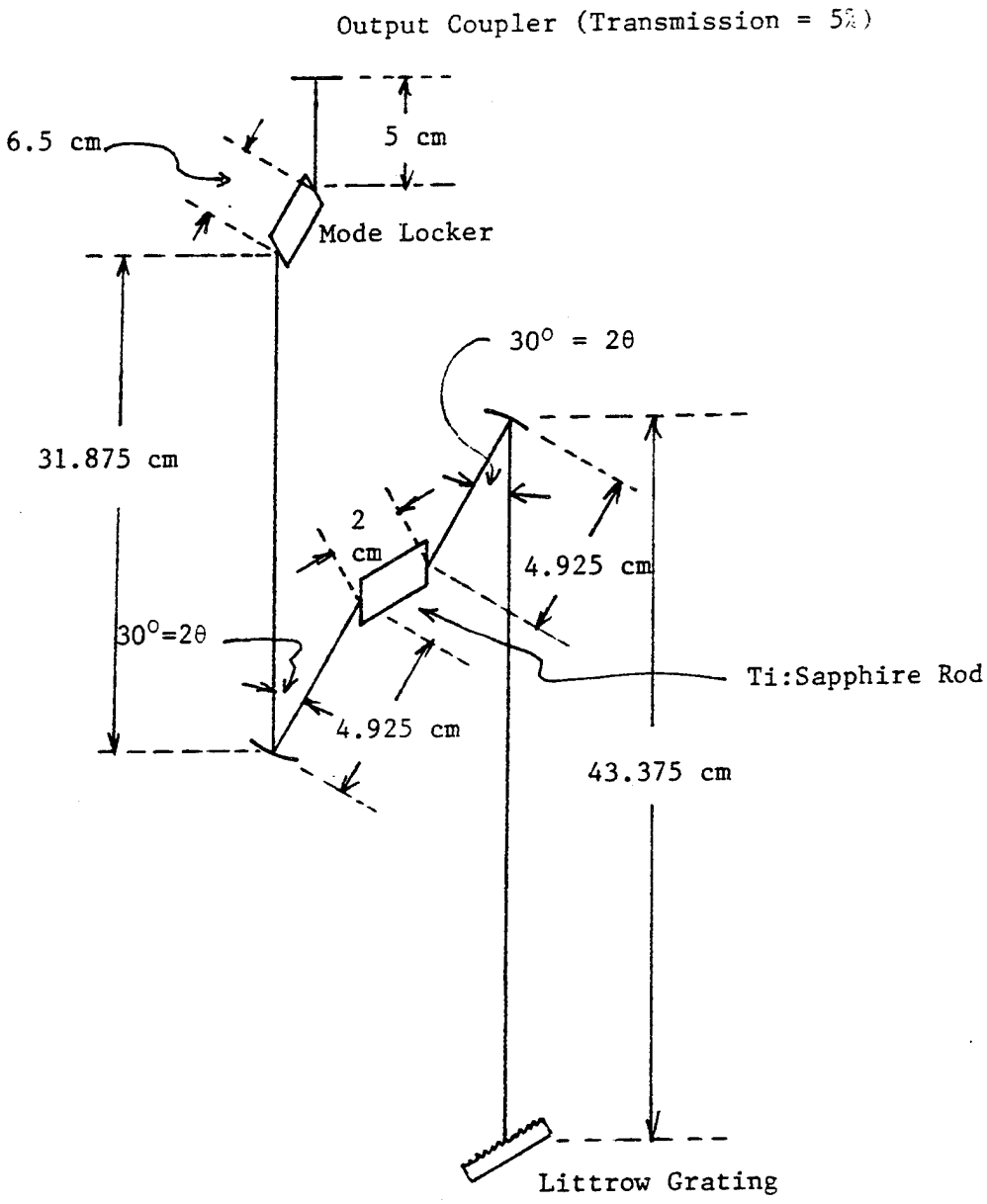

Figure 59. Cavity Layout (not to scale)

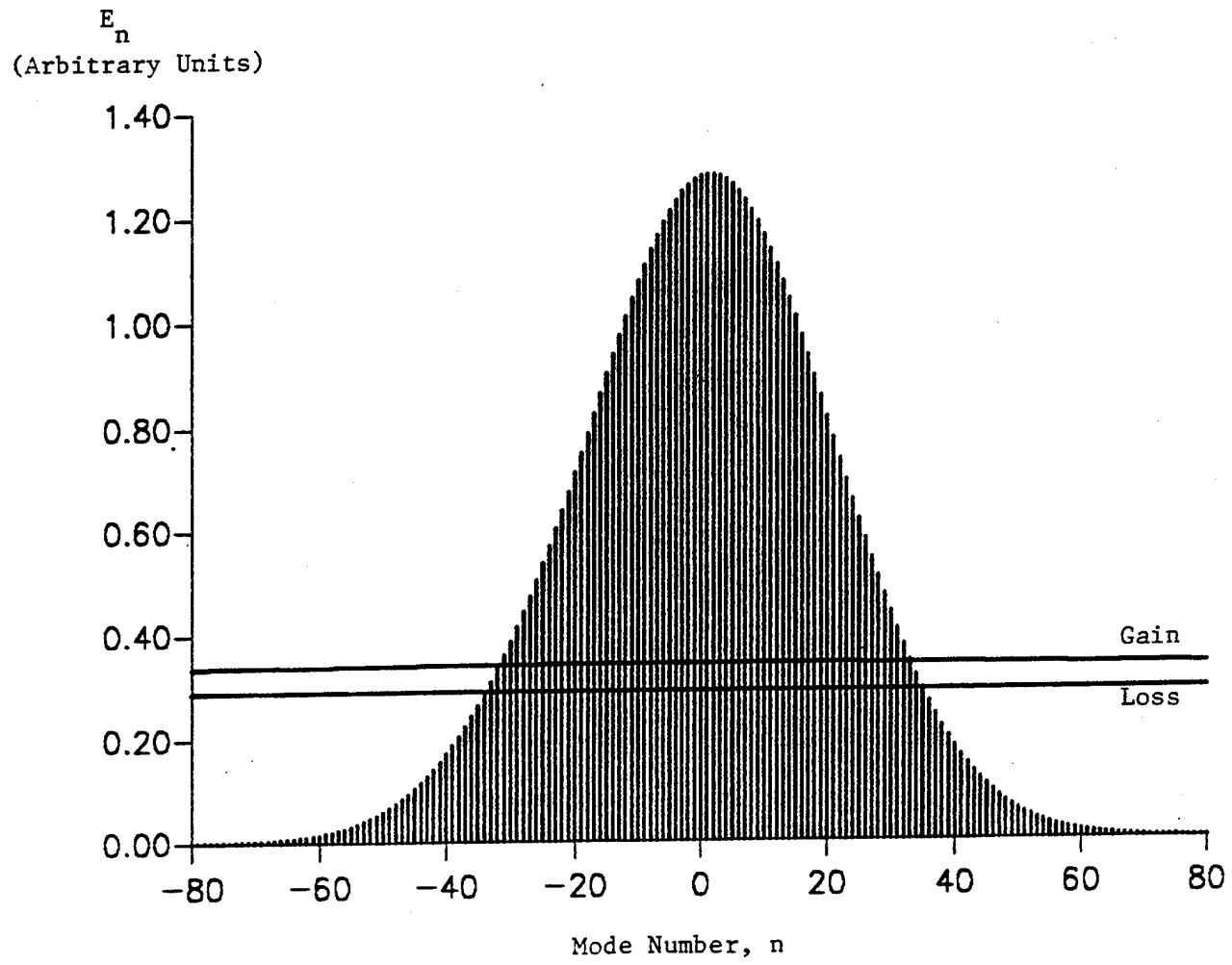

Figure 60. Mode Amplitudes for Pump Peak Power = 75 watts and Grating in Cavity. $\alpha_c = 0.50$.

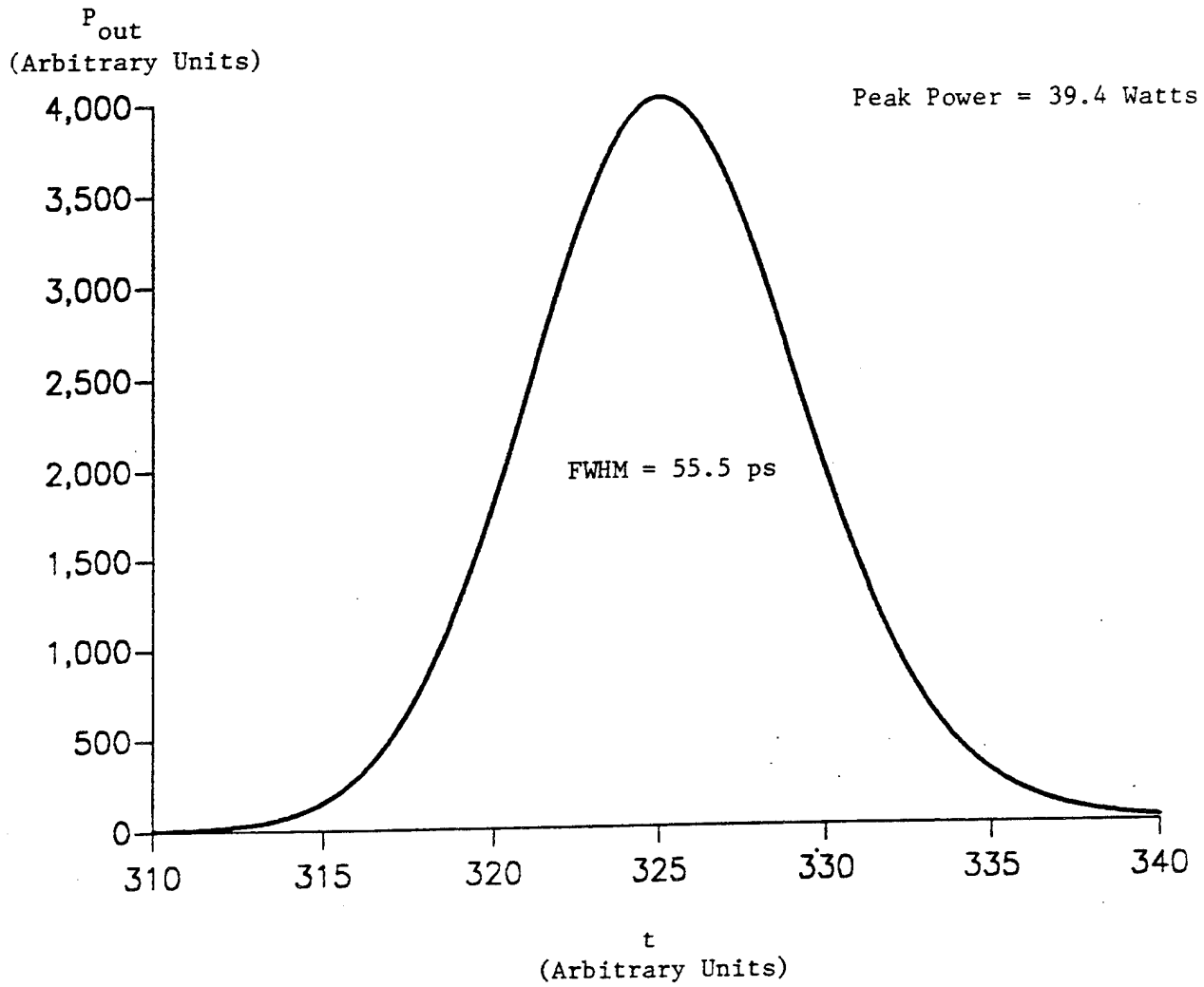

Figure 61. Output Pulse Shape for Pump Peak Power = 75 Watts and Grating in Cavity. $\alpha_c = 0.50$.